

**On the Interface between two Coexisting Phases  
and  
Reptation Models for Electrophoresis**

**André Kooiman**

1900-1901

THE UNIVERSITY OF CHICAGO  
LIBRARY  
CHICAGO, ILL.  
1900-1901

THE UNIVERSITY OF CHICAGO

**On the Interface between two Coexisting Phases  
and  
Reptation Models for Electrophoresis**

*Proefschrift*

ter verkrijging van de graad van Doctor  
aan de Rijksuniversiteit te Leiden, op gezag  
van de Rector Magnificus Dr. J. L. L. van  
der Pijl, tevens in de landelijke wetenschappelijke  
raad van het College van Dilectoren  
te verdedigen op woensdag 22 maart 1995  
te 10.30 uur

*door*

**Adrianus Kociman**

geboren te Rotterdam op 1963



**On the Interface between two Coexisting Phases  
and  
Reptation Models for Electrophoresis**

**Proefschrift**

ter verkrijging van de graad van Doctor  
aan de Rijksuniversiteit te Leiden, op gezag  
van de Rector Magnificus Dr. L. Leertouwer,  
hoogleraar in de faculteit der godgeleerdheid,  
volgens besluit van het College van Dekanen  
te verdedigen op woensdag 17 maart 1993  
te klokke 16.15 uur

door

**Adrianus Kooiman**

geboren te Barendrecht in 1963



Promotiecommissie:

Promotor	Prof.dr. J.M.J. van Leeuwen
Overige leden:	Prof.dr. C.W.J. Beenakker
	Prof.dr. H.J. Habing
	Prof.dr. H.J. Hilhorst
	Prof.dr.ir. W. van Saarloos
	Prof.dr. R.K.P. Zia



# Contents

1	General Introduction	1
1.1	Introduction	1
1.2	Renormalization approaches	3
1.3	Outline of the thesis	4
2	The Interface in a One-Dimensional System	8
2.1	Introduction	8
2.2	The general recursion relations	9
2.3	The $r = 0$ solution	13
2.4	The capillary wave solution	14
2.5	The scaling regime	16
2.6	The local field regime	18
2.7	The cross-over regime	19
2.8	The surface tension	20
2.9	The Fisk-Widom approximation	23
2.10	Concluding remarks	29
	Appendix	29
2A	The surface tension for $r \ll 1$	30
3	Finite-Size Effects and Capillary Waves in Solid-on-Solid Models	32
3.1	Introduction	32
3.2	The finite-size partition function	33
3.3	The interfacial profile	37
3.4	The capillary wave model	39
3.5	Summary and discussion	41
	Appendices	42
3A	The magnetization profile	42



3B	Finite-size effects in the 2-d Ising model . . . . .	44
4	Free Fermion Approximation for the Ising Model with Further-Neighbor Interactions on a Triangular Lattice . . . . .	51
4.1	Introduction . . . . .	51
4.2	The model . . . . .	52
4.3	The zero temperature phase diagram . . . . .	56
4.4	The free fermion conditions . . . . .	59
4.5	The free fermion solution/approximation . . . . .	63
4.6	The critical surface . . . . .	66
4.7	The surface free energy . . . . .	67
4.8	Summary . . . . .	70
	Appendices . . . . .	70
4A	Consistency relations between the numbers of vertex-pairs . . . . .	71
4B	The groundstates . . . . .	73
4C	The topological theorem . . . . .	79
5	The Drift Velocity in Reptation Models for Electrophoresis . . . . .	82
5.1	Introduction . . . . .	82
5.2	The Rubinstein-Duke model . . . . .	85
5.3	The master equation . . . . .	88
5.4	The drift velocity . . . . .	90
5.5	The solution of the master equation for the boson case . . . . .	92
5.6	The diffusion constant . . . . .	96
5.7	The scaling function . . . . .	98
5.8	The RD-model with free endpoint motion . . . . .	99
5.9	Summary . . . . .	104
	Appendices . . . . .	105
5A	Expansion of the drift velocity in power of $\epsilon$ . . . . .	105
5B	Open chains . . . . .	107
	Samenvatting . . . . .	111
	Curriculum vitae . . . . .	115
	List of publications . . . . .	116

210	Relativistic effects in the E-B field model	210
211	New Form of Approximation for the E-B Model with Relativistic Effects	211
212	Introduction	212
213	The model	213
214	The new approximate E-B field	214
215	on the E-B field	215
216	on the E-B field	216
217	on the E-B field	217
218	on the E-B field	218
219	on the E-B field	219
220	on the E-B field	220
221	on the E-B field	221
222	on the E-B field	222
223	on the E-B field	223
224	on the E-B field	224
225	on the E-B field	225
226	on the E-B field	226
227	on the E-B field	227
228	on the E-B field	228
229	on the E-B field	229
230	on the E-B field	230
231	on the E-B field	231
232	on the E-B field	232
233	on the E-B field	233
234	on the E-B field	234
235	on the E-B field	235
236	on the E-B field	236
237	on the E-B field	237
238	on the E-B field	238
239	on the E-B field	239
240	on the E-B field	240
241	on the E-B field	241
242	on the E-B field	242
243	on the E-B field	243
244	on the E-B field	244
245	on the E-B field	245
246	on the E-B field	246
247	on the E-B field	247
248	on the E-B field	248
249	on the E-B field	249
250	on the E-B field	250
251	on the E-B field	251
252	on the E-B field	252
253	on the E-B field	253
254	on the E-B field	254
255	on the E-B field	255
256	on the E-B field	256
257	on the E-B field	257
258	on the E-B field	258
259	on the E-B field	259
260	on the E-B field	260
261	on the E-B field	261
262	on the E-B field	262
263	on the E-B field	263
264	on the E-B field	264
265	on the E-B field	265
266	on the E-B field	266
267	on the E-B field	267
268	on the E-B field	268
269	on the E-B field	269
270	on the E-B field	270
271	on the E-B field	271
272	on the E-B field	272
273	on the E-B field	273
274	on the E-B field	274
275	on the E-B field	275
276	on the E-B field	276
277	on the E-B field	277
278	on the E-B field	278
279	on the E-B field	279
280	on the E-B field	280
281	on the E-B field	281
282	on the E-B field	282
283	on the E-B field	283
284	on the E-B field	284
285	on the E-B field	285
286	on the E-B field	286
287	on the E-B field	287
288	on the E-B field	288
289	on the E-B field	289
290	on the E-B field	290
291	on the E-B field	291
292	on the E-B field	292
293	on the E-B field	293
294	on the E-B field	294
295	on the E-B field	295
296	on the E-B field	296
297	on the E-B field	297
298	on the E-B field	298
299	on the E-B field	299
300	on the E-B field	300

# Chapter 1

## General Introduction

### 1.1 Introduction

Many systems separate into two coexisting phases below a certain temperature. The interface region between the coexisting phases can be characterized by a number of properties such as the surface tension, the profile of the order parameter and the correlation functions. It is the task of statistical physics to calculate these properties from the microscopic interactions between the constituting particles. We study the problem in the context of a simple classical spin system (the Ising model) that already exhibits much of the essentials of the problem. For instance, the Ising model falls into the same universality class as liquid-vapor system and therefore has the same critical behavior. For low dimensional systems a field is needed to keep the interface from wandering too much, since otherwise it would average out completely [1]. For the liquid-vapor system this would be the gravitational field and for the Ising model it is a linearly varying magnetic field.

As yet, there are only two partial solutions to the problem, which start with certain assumptions on a level where already much of the microscopic details have been integrated out. The oldest, due to van der Waals [2, 3], assumes that it is meaningful to define a local free energy density. For the local free energy density one takes the bulk free energy density of a homogeneous system in a field, which is equal to the local field. In addition there is a squared gradient term that accounts for the free energy associated with a gradient in the system. The solution is obtained by minimizing the total free energy. Thus the solution for the system with an interface is constructed out of the bulk solution and the width of the interface is determined by the bulk correlation length.

In this approach one encounters the following problem. In the interface region the

order parameter (the density for a fluid or the magnetization for the Ising model) runs through a continuous set of values, which the homogeneous system cannot assume without violating the stability criteria. The 'loop' in the van der Waals equation of state nevertheless provides such a continuous transition from the liquid to the vapour phase. A similar loop occurs in the mean field equation of state for the Ising model. Using these equations of state, the surface tension and magnetization profile can be derived. The status of the loop remains unclear because in a correct derivation, within the context of equilibrium statistical mechanics, the loop should be absent [4].

The validity of the theory is restricted to the region close to the critical point because the approximation is only justified when the system is nearly locally homogeneous, that is, when the gradient in the interface region is small. In the critical region however, the mean field nature of the van der Waals solution is not adequate, as it leads to the wrong critical exponents. Fisk and Widom [5] have adjusted the theory to yield the correct critical behavior and van Leeuwen and Sengers [6] have extensively studied this modified version of the theory in the presence of a gravitational field.

The most serious shortcoming of the van der Waals theory is that the fluctuations connected to the interface, which are waves on the interface surface, are not incorporated in the theory. The surface or capillary waves are soft (Goldstone) modes connected to the breaking of the translation symmetry in the direction perpendicular to the interface. They will smooth out the interface and cause the width to diverge as the pinning field goes to zero. But in the van der Waals theory the interface width remains finite i.e. the interface is intrinsic.

In the other partial solution, the full problem of two coexisting bulk phases is replaced by an hamiltonian that accounts only for the capillary waves. The full problem will indeed reduce such a capillary-wave theory when all the microscopy details up to the bulk correlation length have been integrated out [7]. The problem with this approach is that the constants entering in the capillary-wave hamiltonian cannot be easily related to the full microscopic hamiltonian [8, 9, 10, 11]. These constants are, the surface tension, which is the amount of free energy that is associated with enlarging the surface area, and the minimum wave length cutoff for the capillary waves. The capillary-wave theory shows that in the thermodynamic limit, the mean-squared displacement of the interface diverges as  $g^{(d-3)/2}$  for dimensions  $d < 3$  and as  $\ln(g)$  for  $d = 3$ , when the field gradient  $g$  goes to zero.

The two partial solutions have later been combined. The van der Waals theory, in the modified form of Fisk and Widom, yields an intrinsic interface on which capillary



waves, on a length scale larger than the bulk correlation length, are superimposed [9, 10, 11].

We conclude that the main physical features, relevant to the interface problem, are well understood and that it allows one to calculate, for instance, the interface profile in a reasonably satisfactory way. But a complete theory starting from the first principles of statistical mechanics, which would incorporate the above mentioned partial solutions and shows how they supplement c.q. merge into one another, is still lacking. The problem is difficult because the bulk and interface fluctuations, cannot be separated from one another on all length scales. On a length scale larger than the bulk correlation length only the capillary waves remain (capillary-wave theory) while on a shorter length scale the fluctuations are predominantly bulk like (van der Waals theory). But on the scale of the bulk correlation length the two types of fluctuations merge and can no longer be distinguished.

## 1.2 Renormalization approaches

The method of renormalization has been used to calculate interfacial profiles, starting from the Landau-Ginsburg-Wilson hamiltonian (which confines the validity of the results to the critical region) [12, 13]. The famous  $\epsilon$ -expansion ( $d = 4 - \epsilon$ ) can be carried out which allows one to incorporate, in a systematic way, the effects of the fluctuations around the mean field theory of van der Waals. In principle it includes the capillary waves, but since they are suppressed in an intermediate stage in the calculation, the divergence in the interfacial width is not recovered for  $d = 3$  ( $\epsilon = 1$ ) [13].

We have studied the possibility to obtain the constants, entering in the capillary-wave hamiltonian, by integrating out the microscopic details up to the bulk correlation length, by means of well known real-space renormalization techniques. This supplement would complete the capillary wave description. The idea is to start at some temperature  $T$  below the critical temperature  $T_c$ , carry out the renormalization up to a length scale beyond the bulk correlation length where the capillary wave description is valid and then lead the capillary-wave solution back along the renormalization trajectory to the starting temperature [14]. In principle this can be done for any interface property, the surface tension, magnetization profile or correlation functions.

We encountered two difficulties in these attempts. First, in any real-space renormalization procedure one must locally decouple the dynamical variables to some



extent. In many renormalization schemes, like that by Migdal [15, 16] and Kadanoff [17, 16] where bonds are relocated (moved), this will damage the coherence along the interface. At very low temperatures a sharp interface should remain sharp under renormalization. If not, the interface keeps broadening at very low renormalized temperatures and the resulting interface width depends on the length of the renormalization trajectory. Second, in the Ising model the surface tension  $\sigma(\theta)$  is angle dependent and the free energy associated with the deformations of the interface is determined by the stiffness  $s(\theta) = \sigma(\theta) + d^2\sigma(\theta)/d\theta^2$  [18]. Thus one is forced to consider tilted interfaces. It follows from simple scaling arguments that the surface tension scales as  $\sigma(\theta) = b^{-(d-1)}\sigma'(\theta)$  where the accent indicates the renormalized value and  $b$  is the factor by which the system has been rescaled. So the surface tension increases by factors of  $b^{d-1}$  along the renormalization trajectory but the angular dependence is preserved. This is consistent with the invariance of the equilibrium crystal shape under renormalization, which is related to the angle dependent surface tension via the Wulff construction or a Legendre transformation. At low temperatures where the entropy is unimportant, so that the free energy can be approximated by the energy of the groundstate, the surface free energy of an interface with tilt angle  $\theta$  is given by  $\sigma(\theta) \simeq 2K(|\cos\theta| + |\sin\theta|)$ . For reasonable renormalization transformations the coupling constant  $K$  indeed transforms as  $K \simeq b^{-(d-1)}K'$  which implies the correct scaling behavior for the magnitude of the surface tension. The angle dependence however is different from that close to  $T_c$  where the surface tension is isotropic. Thus, for the angle dependence of the surface tension to be invariant under renormalization, one cannot stay within the simple Ising model. The proliferation of coupling constants, which is usually cut short one way or another in order to keep the problem tractable, seems therefore to be essential.

### 1.3 Outline of the thesis

Because the renormalization approach failed, the full interface problem in dimension  $d = 2, 3$  is not solved in this thesis. In chapter 2 we present an exact solution of the interface problem in the presence of a pinning field, for the 1D-Ising model. For the one-dimensional chain the point, temperature  $T = 0$  and magnetic field gradient  $g = 0$ , behaves as a critical point, in the sense that near it, the usual critical scaling behavior applies (the scaling regime). Because the critical point is located at  $T = 0$ , the system will never spontaneously separate into two coexisting phases, and the separation must be induced by the linearly varying magnetic field. In the scaling

regime the scaled temperature variable  $r = \exp(-4K)/g$  controls a cross-over from a local ( $r \gg 1$ ) to a non-local ( $r \ll 1$ ) field regime. In the local-field regime the width of the interface is proportional to  $\sqrt{r}$ . But as  $r$  decreases the correlation length increases and starts to resist the rapid variation of the magnetization in the interface region. Therefore the profile becomes flatter than it would be in the local-field approximation. This is described well by the Fisk-Widom theory, where the non-local behavior is accounted for by a squared gradient term. Its results are exact up to second order in  $r^{-1}$  and accurate for all  $r \geq 1$ . When the correlation length exceeds the width in the local-field approximation (that is when  $r \simeq 1$ ), we enter a new regime where the profile is determined by capillary-wave fluctuations. Here the Fisk-Widom theory fails, but now the capillary-wave theory becomes applicable.

For dimension  $d = 2$  the full problem proved to be too difficult. But for the 2D-Ising model without a pinning field, the angle dependent surface tension [19] and the magnetization profile for an interface with a zero tilt angle [20] can be calculated exactly. Quite surprisingly, the zero-angle magnetization profile is simply the capillary-wave solution, depending only on the microscopic details of the model through the stiffness  $s(0)$  [18]. In chapter 3 we study a general Solid-on-Solid model (SOS model), which is an implementation of the capillary-wave model on a microscopic level. We show that also for this model the interface profile and the finite-size corrections can be traced to the stiffness alone.

For the 2D-Ising model the zero-angle surface tension  $\sigma_{\text{Ising}}(0)$  is equal to the free energy density  $f_{\text{SOS}}(0)$  of the SOS model [21]. In this approximate interface model, overhangs and bubbles are excluded so that each configuration can be specified by a set of height variables. That nevertheless the exact surface free energy of the Ising model results, is due to a fortuitous cancellation between the contribution of the overhangs and bubbles in the Ising model [22, 23]. To understand this one has to consider Vdovichenko's combinatorial solution to the 2D-Ising model. In Vdovichenko's approach, the set of configurations that make up the surface free energy can be separated from the bulk configurations. This is only possible at the expense of introducing additional non-existing configurations, which can have negative as well as positive Boltzmann weights. It has been shown for a finite strip of Ising spins, that all the configurations that contribute to the surface free energy of an interface, starting at the left side of the strip at a fixed height  $h_l = 0$  and ending on the right side at any possible height  $h_r$ , are exactly (after cancellation due to the different signs of the Boltzmann weights) the SOS configuration of the interface. Since in the thermodynamic limit the contribution of the configurations with

( $h_l = 0, h_r = 0$ ) dominate the other contributions ( $h_l = 0, h_r \neq 0$ ), one finds that  $\sigma_{\text{Ising}}(0) = f_{\text{SOS}}(0)$ .

In chapter 4 we explain Vdovichenko's method and apply it to the Ising model with next-nearest-neighbor interactions on a triangular lattice. We calculate the free energy and the surface tension, which are exact under certain conditions. When these conditions are not met, the results may still be considered as a good approximation for some range of coupling constants.

The last chapter treats a very different problem, namely, reptation models for electrophoresis. Electrophoresis is a widely used method in biology to separate uniformly charged polymers according to length. The idea is to pull the polymers through a gel by an applied electric field. The gel fibers effectively confine the long polymer chains to a tube so that the dominant chain motion is one-dimensional diffusion along its contour (reptation) [24]. When the polymers are not too long and the field is weak, the mobility is inversely proportional to the molecule's length. But for longer polymers or larger field strengths, the mobility becomes length independent due to the orientation of the molecules and the resolution is lost. For the reptation model of Rubinstein and Duke [25] we calculate the diffusion constant and show that the result is independent of process of tube renewal. For a full introduction to this topic we refer to the beginning of the last chapter.

## References

- [1] F. P. Buff, R. A. Lovett and F. H. Stillinger, *Phys. Rev. Lett.* **15**, 621 (1965).
- [2] J. D. van der Waals, Ph.D. thesis, University of Leiden, 1873; J. S. Rowlinson, *J. Stat. Phys.* **20**, 197 (1979).
- [3] J. S. Rowlinson and B. Widom, *Molecular Theory of Capillarity*, (Clarendon, Oxford, 1982).
- [4] J. M. J. van Leeuwen *J. Stat. Phys.* **57**, 433 (1989).
- [5] S. Fisk and B. Widom *J. Chem. Phys.* **50**, 3219 (1969).
- [6] J. M. J. van Leeuwen and J. V. Sengers, *Physica* **132A**, 207 (1985).
- [7] D. A. Huse, W. van Saarloos and J. D. Weeks *Phys. Rev. B* **32**, 233 (1985).
- [8] J. Meunier *J. Phys. (Paris)* **48**, 1819 (1987).



- [9] J. D. Weeks *J. Chem. Phys.* **67**, 3106 (1977).
- [10] R. F. Kayser, *Phys. Rev. A* **33**, 1948 (1986).
- [11] J. V. Sengers and J. M. J. van Leeuwen, *Phys. Rev. A* **39**, 6346 (1989).
- [12] D. Jasnow, *Rep. Prog. Phys.* **47**, 1059 (1984) and in *Phase Transition and Critical Phenomena*, Vol. 10, C. Domb and J. L. Lebowitz, eds. (Academic Press, New York, 1986), p. 296.
- [13] J. H. Sikkenk and J. M. J. van Leeuwen, *Physica* **137A**, 178 (1986).
- [14] G. L. M. Dassen, A. Kooiman, N. Jan and J. M. J. van Leeuwen, *Phys. Rev. B* **41**, 4593 (1990).
- [15] A. A. Migdal, *Zh. Eksp. Teor. Fiz.* **69**, 810 (1975); **69**, 1475 (1975) [*Sov. Phys. JETP* **42**, 413 (1976); **42**, 743 (1976)].
- [16] T. W. Burkhardt, in *Real-Space Renormalization*, Vol. 30, of *Topics in Current Physics* T. W. Burkhardt and J. M. J. van Leeuwen, eds. (Springer-Verlag, Berlin, 1982), p. 33.
- [17] L. P. Kadanoff, *Phys. Rev. Lett.* **34**, 1005 (1975); L. P. Kadanoff, A. Houghton and M. C. Yalabik, *J. Stat. Phys.* **14**, 171 (1976).
- [18] M. P. A. Fisher, D. S. Fisher and J. D. Weeks, *Phys. Rev. Lett.* **48**, 368 (1982).
- [19] D. B. Abraham, *Stud. Appl. Math.* **50**, 71 (1971); D. B. Abraham, in *Phase Transitions and Critical Phenomena*, Vol. 10, C. Domb and J. L. Lebowitz, eds. (Academic Press, New York, 1986), p. 1.
- [20] D. B. Abraham and P. Reed, *Commun. Math. Phys.* **49**, 35 (1976).
- [21] E. Müller-Hartmann and J. Zittartz, *Z. Phys. B* **27**, 261 (1977).
- [22] F. Calheiros, S. Johannesen and D. Merlini, *J. Phys. A* **20**, 5991 (1987).
- [23] T. Morita, *J. Phys. Soc. Japan* **59**, 2054 (1990).
- [24] P. G. de Gennes, *Scaling Concepts in Polymer Physics*, (Cornell Univ. Press, Ithaca, 1979); *J. Chem. Phys.* **55**, 572 (1971).
- [25] T. A. J. Duke, *Phys. Rev. Lett.* **62**, 2877 (1989); *J. Chem. Phys.* **93**, 9049 (1990); *J. Chem. Phys.* **93**, 9055 (1990).

## Chapter 2

# The Interface in a One-Dimensional System

### 2.1 Introduction

Very few calculations exist of interfacial profiles [1], even for models which permit an exact evaluation of the partition function. The reason is that in low dimensions ( $d \leq 3$ ) an external pinning field is necessary to localize and shape the interface, because without pinning the interface wanders away due to capillary waves and the transition zone between two coexisting phases spreads over macroscopic distances [2].

Pinning can be achieved by a field that couples to the order parameter. The most natural case is to take it linearly varying in space. For the fluid this is a gravitational field, for the Ising model it is a linearly varying magnetic field. Even the one-dimensional Ising chain in a varying magnetic field is a non-trivial problem for which the standard solution techniques as the transfer matrix method are not applicable [3]. In this paper we show however that a recursive method provides a relatively simple and transparent solution.

The only interesting region in a one-dimensional chain is the low temperature regime where a competition takes place between the energy, which tries to make the interface sharp, and the entropy which diffuses the interface. For all non-zero temperatures the entropy wins for an interface without an external pinning field. We will show that in the appropriate scaling variables the analysis can be phrased in complete analogy with the scaling to be expected near an ordinary critical point. Thus the one-dimensional model can serve as a testing ground for approximate interfacial theories. We have compared the Fisk-Widom interfacial theory [4, 5] with the exact results as a function of the scaled temperature variable which controls the cross-over from a non-local or capillary wave regime to a local-field regime. In the local-field regime the agreement is of course excellent. But the Fisk-Widom theory fails when



the profile becomes strongly non-local. It is in this regime that the effects associated with a non-zero critical exponent  $\eta$  ( $\eta = 1$  for  $d = 1$ ) become apparent.

In section 2.2 we give the recursive solution for the magnetization and surface tension, which is made explicit for the capillary wave limit in section 2.3 and 2.4, and put into a scaling form in section 2.5 and 2.8. The local-field- and cross-over regime are analysed in section 2.6 and 2.7. In the last section the results are compared with the Fisk-Widom theory and the chapter closes with a short discussion.

## 2.2 The general recursion relations

We consider a chain of Ising spins  $S_n = \pm 1$  in a magnetic field  $H_n$  which varies linearly with distance. As our interest will always be in the limit of vanishing field, its gradient is considered to be small,

$$H_n = hn \quad (h \ll 1). \quad (2.2.1)$$

The Hamiltonian, partition sum and free energy of the system are given by

$$H[S] = - \sum_n (JS_n S_{n+1} + H_n S_n) \quad (2.2.2)$$

$$Z(K, g) = \sum_{\{S\}} \exp(H[S]) = \sum_{\{S_n\}} \exp \left( \sum_n (K S_n S_{n+1} + g n S_n) \right) \quad (2.2.3)$$

and

$$F(K, g) = -k_B T \ln Z \quad (2.2.4)$$

respectively, with the parameters  $K$  and  $g$  denoting the ratios

$$K = J/k_B T, \quad g = h/k_B T. \quad (2.2.5)$$

The magnetization profile  $m_n$  is given by the canonical-ensemble average of  $S_n$ :

$$m_n = \frac{\sum_{\{S\}} S_n \exp(H[S])}{\sum_{\{S\}} \exp(H[S])}. \quad (2.2.6)$$

Far from the interface region the magnetization saturates,

$$m_n \rightarrow \pm 1, \quad n \rightarrow \pm \infty, \quad (2.2.7)$$

and

$$m_0 = 0 \quad (2.2.8)$$

by symmetry ( $m_n = -m_{-n}$ ).

We define the surface tension  $\sigma$  as an excess free energy,

$$\sigma \equiv F(K, g) - F_{LF}(K, g), \quad (2.2.9)$$

over the local-field free energy

$$F_{LF}(K, g) = \sum_n \psi_{LF}(K, gn). \quad (2.2.10)$$

Here  $\psi_{LF}(K, gn)$  is the free energy density of an Ising chain in an homogeneous magnetic field, the field being equal to the local field  $gn$  in the inhomogeneous system at site  $n$ .

When in the following we speak of the local-field regime we mean that the free energy and thus the magnetization etc. are local as we have defined it above. That is, the local value of a quantity for the inhomogeneous system is approximately equal to the value for a homogeneous system, with the field given by the local field of the inhomogeneous system. So in the local-field regime the problem of the inhomogeneous system reduces to that of an homogeneous system.

The point  $(T, g) = (0, 0)$  behaves like a critical point in the sense that in its vicinity the usual scaling behaviour holds (the scaling regime). The scaling forms for the magnetization and the surface tension are easily derived for the Ising chain in a homogeneous magnetic field  $H$ . By summing out the even spins one obtains for the renormalised magnetic field  $H'$  and temperature variable  $\alpha'$  ( $\alpha \equiv \exp(-2K)$ ), linearized around the "critical point"  $(T, H) = (0, 0)$ ,

$$H' = 2H \equiv 2^{y_H} H, \quad \alpha' = 2\alpha \equiv 2^{y_\alpha} \alpha \quad (2.2.11)$$

i.e. the exponents  $y_H$  and  $y_\alpha$  are both equal to 1. Rescaling the system with a scale factor  $b$  gives

$$m(H, \alpha) = b^{y_H-d} m(b^{y_H} H, b^{y_\alpha} \alpha) = m(1, \alpha/H) \equiv m(\alpha/H). \quad (2.2.12)$$

The appropriate scaling variable is therefore  $\alpha/H$ . Similarly, for the system with a linearly varying magnetic field we have

$$\begin{aligned} m(n, g, \alpha) &= b^{y_H-d} m(b^{-1}n, b^{y_H+1}g, b^{y_\alpha}\alpha) = m(\sqrt{g}n, 1, \alpha/\sqrt{g}) \\ &\equiv m(\sqrt{g}n, \alpha/\sqrt{g}) \end{aligned} \quad (2.2.13)$$

and

$$\sigma(g, \alpha) = b^{d-1} \sigma(b^{y_H+1}g, b^{y_\alpha}\alpha) = \sigma(1, \alpha/\sqrt{g}) \equiv \sigma(\alpha/\sqrt{g}) \quad (2.2.14)$$

It shows that in the critical regime the magnetization is only a function of the scaling variables  $t$  and  $r$  and surface tension is only a function of  $r$ , with  $t$  and  $r$  defined as

$$t = \sqrt{g}n, \quad r = \alpha^2/g \quad (2.2.15)$$

When  $T \rightarrow \infty$  or  $g \rightarrow 0$ , i.e. when  $r$  is large, the behavior of the system becomes local-field like either because the spins decouple and do not feel their neighbors or because the neighboring spins feel approximately the same field and the system is locally homogeneous. Thus the scaled temperature variable  $r$  can be viewed as a measure for whether the system is close to ( $r \gg 1$ ) or far from ( $r \ll 1$ ) the local-field regime.

Robert and Widom [1] have studied the one-dimensional Ising chain in an external magnetic field that varies with  $n$  as a stepfunction

$$H(n) = \begin{cases} -H, & n < 0 \\ 0, & n = 0 \\ +H, & n > 0 \end{cases} \quad (2.2.16)$$

In comparing our results with theirs we will take  $H \sim \sqrt{g}$  as is suggested by comparing the scaling variables of both systems.

It is not practical to calculate the magnetization profile and surface tension directly from (2.2.6) and (2.2.9). Another (indirect) strategy is to seek recursion relations by summing out the spins starting from the boundaries of the system coming either from the right or from the left. In each step the spin  $S_n$  to be eliminated feels an extra field  $H_n^r$  which is the effect of all the spins to the right of  $n$  (or similarly  $H_n^l$  for the effect of the spins left of  $n$ ). Coming from the right and eliminating the spin  $S_n$ , one has the relation

$$2\cosh(gn + H_n^r + KS_{n-1}) = \exp(G_n^r + H_{n-1}^r S_{n-1}). \quad (2.2.17)$$

Here  $H_{n-1}^r$  is the extra field which spin  $S_n$  induces from the right on its neighbor  $S_{n-1}$  and  $G_n^r$  is a spin independent quantity that builds up the free energy

$$-F/k_B T = \sum_n G_n^r. \quad (2.2.18)$$

By substituting the possible values  $\pm 1$  for  $S_{n-1}$ , (2.2.17) can be solved to give

$$\exp(2G_n^r) = \gamma^{-n} x_n + \alpha + \alpha^{-1} + \gamma^n x_n^{-1} \quad (2.2.19)$$

and

$$x_{n-1} = \frac{x_n + \alpha\gamma^n}{\alpha x_n + \gamma^n}, \quad (2.2.20)$$

where  $x_n$  is a new quantity defined as

$$x_n = \exp(2H_n^r), \quad (2.2.21)$$

and  $\alpha$  and  $\gamma$  stand for

$$\alpha = \exp(-2K), \quad \gamma = \exp(-2g). \quad (2.2.22)$$

An analogous equation is obtained by starting the elimination from the left, leading to

$$y_{n+1} = \frac{y_n + \alpha\gamma^n}{\alpha y_n + \gamma^n}, \quad (2.2.23)$$

with

$$y_n = \exp(2H_n^l). \quad (2.2.24)$$

Eliminating the spins from the right and from the left one obtains the magnetization of spin  $S_n$  as that of an effectively free spin in the field  $gn + H_n^r + H_n^l$ . Thus

$$m_n = \tanh(gn + H_n^r + H_n^l) \quad (2.2.25)$$

or

$$m_n = \frac{x_n y_n - \gamma^n}{x_n y_n + \gamma^n} \quad (2.2.26)$$

in the new variables.

With some manipulation one can dispose of the variable  $y_n$  in the foregoing equations. Our problem is then reduced to the following two recursion equations for  $n > 0$

$$z_{n-1} = \frac{z_n + \alpha^2 \gamma^n}{z_n + \gamma^n}, \quad (2.2.27)$$

$$m_{n+1} = \frac{1 + \alpha^2}{1 - \alpha^2} m_n + \frac{1}{1 - \alpha^2} \left\{ \left( z_n - \frac{\alpha^2}{z_n} \right) - m_n \left( z_n + \frac{\alpha^2}{z_n} \right) \right\}, \quad (2.2.28)$$

with  $z_n$  related to  $x_n$  by

$$z_n = \alpha x_n, \quad (2.2.29)$$

which should be solved together with the conditions on  $m_n$  given by (2.2.7) and (2.2.8). Since  $\gamma^n \rightarrow 0$  for  $n \rightarrow \infty$ ,  $z_n$  approaches

$$\lim_{n \rightarrow \infty} z_n = 1, \quad (2.2.30)$$



which is compatible with the boundary condition (2.2.7) for  $m_n$  as one sees from (2.2.28).

From (2.2.18), (2.2.19) and (2.2.29) we find for the free energy

$$-F/k_B T = \frac{1}{2} \sum_n \ln \frac{1}{\alpha} (\gamma^{-n} z_n + 1 + \alpha^2 + \alpha^2 \gamma^n z_n^{-1}) \quad (2.2.31)$$

The free energy  $F_{loc}$  is also given by (2.2.31) but then with  $z_n$  replaced by  $z_n^{LF}$ , the value obtained by setting  $z_{n-1} = z_n$  in (2.2.27), which gives

$$z_n^{LF} = e^{-\tau} \left( \sinh \tau + \sqrt{\sinh^2 \tau + \alpha^2} \right) \quad (2.2.32)$$

with

$$\tau = gn \quad (2.2.33)$$

the value of the local magnetic field. Thus the surface tension can be written as

$$-\sigma/k_B T = \frac{1}{2} \sum_n \ln \left[ \frac{\gamma^{-n} z_n + 1 + \alpha^2 + \alpha^2 \gamma^n / z_n}{\gamma^{-n} z_n^{LF} + 1 + \alpha^2 + \alpha^2 \gamma^n / z_n^{LF}} \right] \quad (2.2.34)$$

## 2.3 The $r = 0$ solution

The general solution of the recursion relations deduced in the last section cannot be given explicitly. They can be solved however if we set  $\alpha = 0$  in which case the recursion relations become

$$z_{n-1} = \frac{z_n}{z_n + \gamma^n} \quad (2.3.1)$$

and

$$m_{n+1} = m_n + (1 - m_n) z_n. \quad (2.3.2)$$

This is the limit  $T \rightarrow 0$ , while keeping  $g = h/k_B T$  fixed ( $r = \alpha^2/g \rightarrow 0$ ). The behavior of the magnetization profile in this limit, is similar to that in higher dimensions, close to  $T = 0$  where the capillary wave solution becomes exact.

Rewriting (2.3.1) in terms of the inverse of  $z_n$ ,

$$\frac{1}{z_{n-1}} = 1 + \frac{\gamma^n}{z_n}, \quad (2.3.3)$$

and using (2.2.30), one obtains after some manipulation:

$$z_n = \frac{\exp(-gn(n+1))}{\sum_{j=n}^{\infty} \exp(-gj(j+1))}. \quad (2.3.4)$$



By introducing the difference  $\Delta m_n = m_{n+1} - m_n$  we can solve (2.3.2) rather easily,

$$\Delta m_n = \frac{\exp(-gn(n+1))}{\sum_{j=0}^{\infty} \exp(-gj(j+1))}, \quad (2.3.5)$$

obtaining for the magnetization

$$m_n = \sum_{j=0}^{n-1} \Delta m_j = \sum_{j=0}^{n-1} \exp(-gj(j+1)) / \sum_{j=0}^{\infty} \exp(-gj(j+1)) \quad (n \geq 0) \quad (2.3.6)$$

and  $m_{-n} = -m_n$ .

For later use we will also give here the continuum version of these expressions

$$m_n = \sqrt{\frac{4}{\pi}} \int_0^t \exp(-x^2) dx = \text{erf}(t) \quad (2.3.7)$$

and

$$z_n = \sqrt{g} \frac{\exp(-t^2)}{\int_t^{\infty} \exp(-x^2) dx} \quad (2.3.8)$$

to lowest order in  $\sqrt{g}$ .

The important features of the above results are, firstly, that the interface is not intrinsic, which means that it broadens and finally becomes infinite (disappears) as the field gradient  $g$  goes to zero. Thus the interface must be maintained by a non-zero field gradient. Secondly, the magnetization and other site-dependent variables depend on the combination  $t = \sqrt{gn}$  as expected from scaling and not on the combination  $\tau = gn$ , the expression for the local field.

## 2.4 The capillary wave solution

Because the interface is zero dimensional there are no other capillary waves possible, than a shift of the location of the interface as a whole (the wavenumber  $q$  is zero mode for higher dimensional interfaces). The capillary wave approximation for the one-dimensional Ising chain therefore consists in allowing only the one-kink configurations. (A kink is a pair of neighbor spins with opposite signs i.e a broken  $K$  bond.) The only configurations that play a role in the limit  $T \rightarrow 0$  and  $g$  fixed are these one-kink configurations and the magnetization profile in the capillary wave approximation is just the above obtained  $r = 0$  solution. We will rederive this  $r = 0$  solution here in the capillary wave formulation and, more importantly, the capillary wave description allows also for a simple derivation of the surface tension in the limit  $r \rightarrow 0$ .

We will label the one-kink configurations by an index  $l$  that specifies the position of the kink which is between the spins  $S_l$  and  $S_{l+1}$  for  $l > 0$  and between the spins  $S_{l-1}$  and  $S_l$  for  $l < 0$ . The energy of a configuration, given by the hamiltonian (2.2.2), is written as

$$E_l = E_R + \epsilon_l \quad (2.4.1)$$

with  $E_R$  the reference energy

$$E_R = - \sum_n (K + |gn|) \quad (2.4.2)$$

and  $\epsilon_l$  the energy of the configuration relative to the reference energy

$$\epsilon_l = 2K + 2 \sum_{n=0}^l gn = 2K + gl(l+1) \quad (l > 0) \quad (2.4.3)$$

and  $\epsilon_l = \epsilon_l$ . For the partition sum we have

$$Z = \exp(-E_R) \sum_{l=-\infty}^{\infty} \exp(-\epsilon_l) \quad (2.4.4)$$

and for the magnetization

$$m_n = \frac{\partial \ln Z}{\partial gn} = 1 - 2 \frac{\sum_{l=n}^{\infty} \exp(-\epsilon_l)}{\sum_{l=-\infty}^{\infty} \exp(-\epsilon_l)} \quad (n \geq 0) \quad (2.4.5)$$

Substituting the above expression for  $\epsilon_l$  and using that  $\epsilon_{-l} = \epsilon_l$  we find again the  $r = 0$  result

$$m_n = \sum_{j=0}^{n-1} \exp(-gj(j+1)) / \sum_{j=0}^{\infty} \exp(-gj(j+1)) \quad (n \geq 0) \quad (2.4.6)$$

The surface tension is also easily obtained. From (2.4.4) we have for the free energy

$$F/k_B T = E_R - \ln \sum_l e^{-\epsilon_l} \quad (2.4.7)$$

Because for  $T \rightarrow 0$ ,  $F_{loc}/k_B T$  is just  $E_R$ , the surface tension (2.2.9) becomes

$$\sigma/k_B T = -\ln \sum_l e^{-\epsilon_l} \quad (2.4.8)$$

By substituting the above expression for  $\epsilon_l$  we obtain

$$\sigma/k_B T \simeq -\ln \left[ \alpha \int_{-\infty}^{\infty} dl \exp(-gl^2) \right] = -\frac{1}{2} \ln(\pi r). \quad (g \ll 1) \quad (2.4.9)$$

Since the capillary wave solution corresponds to the limit  $r \rightarrow 0$  ( $T \rightarrow 0$  and  $g$  fixed), we see that in this limit the surface tension diverges logarithmically.

## 2.5 The scaling regime

In the last section we have deduced an exact expression for the magnetization in the limit  $T \rightarrow 0$  and  $g$  fixed, which is the "capillary wave" limit. In this section we will derive an approximate solution for the whole scaling regime.

In order to do so we first introduce the rescaled variable

$$w_n \equiv z_n / \sqrt{g}, \quad (2.5.1)$$

so that close to  $r = 0$ ,  $w_n$  is of order 1 (see 2.3.8)) and we write (2.2.27) as

$$w_{n-1} = \frac{w_n + r\sqrt{g}\exp(-2\sqrt{g}t)}{\sqrt{g}w_n + \exp(-2\sqrt{g}t)}, \quad (2.5.2)$$

with  $r$  and  $t$  the scaling variables given in (2.2.15). We see that if  $r$  is considered fixed,  $w_n$  depends only on the parameter  $\sqrt{g}$  and an expansion in this parameter should be adequate. In accordance with the  $r = 0$  solution we take  $w_n$  as a function of  $t = \sqrt{g}n$ , considered as a continuous variable. Thus we write

$$w_n = w(\sqrt{g}n) = w(t) = w_0(t) + \sqrt{g}w_1(t) + gw_2(t) + \dots \quad (2.5.3)$$

and

$$w_{n-1} = w_0 + \sqrt{g}(w_1 - \dot{w}_0) + g\left(\frac{1}{2}\ddot{w}_0 - \dot{w}_1 + w_2\right) + \dots \quad (2.5.4)$$

The dot means differentiation with respect to the argument  $t = \sqrt{g}n$ . Substitution of these two expressions into the recursion relation (2.5.2) and equating powers of  $\sqrt{g}$  results to lowest order in

$$\dot{w}_0 - w_0^2 + 2tw_0 + r = 0 \quad (2.5.5)$$

and to first order in

$$\dot{w}_1 - 2(w_0 - t)w_1 = t\dot{w}_0 + (2t^2 - 1)w_0 + 2rt. \quad (2.5.6)$$

The magnetization is expanded in the same way. First we write (2.2.28) in terms of  $w_n$  and  $r$ :

$$m_{n+1} = m_n + \sqrt{g} \left\{ \left( w_n - \frac{r}{w_n} \right) - m_n \left( w_n + \frac{r}{w_n} \right) \right\}. \quad (2.5.7)$$

where we have neglected  $\alpha^2$  as compared to 1 as is appropriate in the scaling regime. Substituting the expansions for  $m_n$  and  $m_{n+1}$ , similar to (2.5.3) and (2.5.4) for  $w_n$ , in (2.5.7) we find to lowest order in  $\sqrt{g}$

$$\dot{m}_0 = \left( w_0 - \frac{r}{w_0} \right) - m_0 \left( w_0 + \frac{r}{w_0} \right) \quad (2.5.8)$$

and to first order in  $\sqrt{g}$

$$\dot{m}_1 + \left(w_0 + \frac{r}{w_0}\right) m_1 = w_1 \left\{ \left(1 + \frac{r}{w_0^2}\right) - m_0 \left(1 - \frac{r}{w_0^2}\right) \right\} - \frac{1}{2} \dot{m}_0. \quad (2.5.9)$$

One sees that it is possible to determine successively higher powers, first  $w$  and then  $m$ , through linear, inhomogeneous first order differential equations after first having solved (2.5.5) which is non-linear. It is a Riccati type differential equation and can be transformed into a linear, homogeneous second order equation through the substitution:

$$w = -\dot{v}/v, \quad (2.5.10)$$

with the result

$$v'' + 2tv - rv = 0. \quad (2.5.11)$$

This is a Hermite type differential equation with non-integer coefficients, so the solution will be an infinite series rather than the well known Hermite polynomials. We will not solve the equation here, because later we shall present some general numerical solutions of our problem using the exact discrete recursion relations from section 2.2. An important check however, can be carried out. From (2.5.5) our earlier capillary wave solution should be retained (at least in its continuum version) in the limit  $r \rightarrow 0$ . From (2.3.8) we have

$$w_0 = \frac{z_n}{\sqrt{g}} = \frac{\exp(-t^2)}{\int_0^\infty \exp(-x^2) dx} \quad (2.5.12)$$

and it is easy to show that this expression satisfies (2.5.5) with  $r = 0$ . Also, with  $r = 0$ , (2.5.8) becomes

$$\dot{m}_0 = w_0(1 - m_0), \quad (2.5.13)$$

which is indeed satisfied by relation (2.3.7), using (2.5.12). Thus we conclude that for any fixed  $r$  the magnetization can be expanded in powers of  $\sqrt{g}$  where the coefficients of this expansion are functions of  $t = \sqrt{g}n$ . For  $r = 0$  the capillary wave solution of the previous section is recovered by this expansion method. The higher terms in the expansion in  $\sqrt{g}$  correspond, for  $r = 0$ , to the deviation of the exact form (2.3.6) from the continuum expression (2.3.7).



## 2.6 The local field regime

When  $r \gg 1$ , the behavior of the system should become local-field like, that is, the magnetization profile becomes a function of  $\tau = gn$ . In this section we derive a solution for the local-field regime from the general recursion relations obtained in section 2.2.

Writing (2.2.27) as

$$z_{n-1} = \frac{z_n + r g \exp(-2\tau)}{w_n + \exp(-2\tau)} \quad (2.6.1)$$

we see that an expansion in  $g$  should be adequate. We put

$$z_n = z_0(\tau) + g z_1(\tau) + g^2 z_2(\tau) + \dots \quad (2.6.2)$$

and thus

$$z_{n-1} = z_0(\tau) + g\{z_1(\tau) - \dot{z}_0(\tau)\} + g^2\{z_2(\tau) - \dot{z}_1(\tau) + \frac{1}{2}\ddot{z}_0(\tau)\} + \dots \quad (2.6.3)$$

Substitution in the basic recursion relation (2.6.1) yields after some manipulation and selection in powers of  $g$

$$z_0(\tau) = e^{-\tau}(\sinh \tau + \sqrt{\sinh^2 \tau + \alpha^2}) \quad (2.6.4)$$

(see also (2.2.32)) and

$$z_1(\tau) = \frac{(z_0 + e^{-2\tau})^2 \dot{z}_0}{(z_0 + e^{-2\tau})(z_0 + e^{-2\tau} - 1) + z_0 + \alpha^2 e^{-2\tau}} \quad (2.6.5)$$

For the magnetization we proceed in an analogous way, putting

$$m_n = M_0(\tau) + g M_1(\tau) + g^2 M_2(\tau) + \dots \quad (2.6.6)$$

Using this expansion in (2.2.28) together with (2.6.2), we obtain

$$M_0 = \frac{1 + \alpha^2}{1 - \alpha^2} M_0 + \frac{1}{1 - \alpha^2} \left\{ \left( z_0 - \frac{\alpha^2}{z_0} \right) - M_0 \left( z_0 + \frac{\alpha^2}{z_0} \right) \right\} \quad (2.6.7)$$

and

$$M_1 = \frac{(1 - \alpha^2) \dot{M}_0 - z_1 \{ (1 - M_0) + (1 + M_0) \alpha^2 / z_0^2 \}}{2\alpha^2 - z_0(1 + \alpha^2 / z_0^2)} \quad (2.6.8)$$

The first equation is easily solved for  $M_0$  with the aid of (2.6.4):

$$M_0 = \frac{\sinh \tau}{\sqrt{\sinh^2 \tau + \alpha^2}} \quad (\tau = gn). \quad (2.6.9)$$



As expected this result is indeed the so-called "local-field approximation", i.e. the magnetization at site  $n$  is equal to the magnetization, which we would have if there existed a constant field in all space, its value being that of the actual field at site  $n$ . This solution follows from (2.2.27) and (2.2.28) when we put  $z_{n-1} = z_n$  and  $m_{n+1} = m_n$ . It shall be clear that in principle the procedure sketched above can be pushed forward to obtain corrections on the local field  $M_0$  up to any desired order in  $g$ .

## 2.7 The cross-over regime

In the foregoing sections we have analysed two essentially different regimes, the scaling regime and the local-field regime. In this section we give an  $1/r$  expansion for the solution in the scaling regime and show that in the limit  $r \rightarrow \infty$  the local-field solution results.

In the scaling regime we had

$$\dot{w}(t) = w(t)^2 + 2tw(t) - r \quad (2.7.1)$$

and

$$\dot{m}(t) = w(t) - \frac{r}{w(t)} - m(t) \left\{ w(t) + \frac{r}{w(t)} \right\}, \quad (2.7.2)$$

where  $t = \sqrt{gn}$  and  $r = \alpha^2/g$ . We start by assuming that for large  $r$  the solution for (2.7.1) can be written as an expansion in  $r^{-1}$ ,

$$w(q) = \sqrt{r} \left\{ \hat{w}_0(q) + \frac{\hat{w}_1(q)}{r} + \frac{\hat{w}_2(q)}{r^2} + \dots \right\} \quad (2.7.3)$$

with the argument

$$q \equiv t/\sqrt{r} \quad (2.7.4)$$

Substitution in (2.7.1) yields for successive powers of  $r^{-1}$

$$\begin{aligned} \hat{w}_0^2 - 2q\hat{w}_0 - 1 &= 0 \\ \hat{w}_0 - 2\hat{w}_0\hat{w}_1 + 2q\hat{w}_1 &= 0 \\ \hat{w}_1 - \hat{w}_1^2 - \hat{w}_0\hat{w}_2 + 2q\hat{w}_2 &= 0 \end{aligned} \quad (2.7.5)$$

and we find for  $w(q)$  up to second order in  $r^{-1}$

$$w(q) = \sqrt{r}(q + \sqrt{1+q^2}) \left\{ 1 + \frac{1}{2(1+q^2)} \frac{1}{r} + \frac{\sqrt{1+q^2} - 5q}{8(1+q^2)^{5/2}} \frac{1}{r^2} + \dots \right\}. \quad (2.7.6)$$

For the magnetization we write

$$m(q) = \hat{m}_0(q) + \frac{\hat{m}_1(q)}{r} + \frac{\hat{m}_2(q)}{r^2} + \dots \quad (2.7.7)$$

This expansion and (2.7.3) are used in (2.7.2) and after some calculation we find the following expressions for  $\hat{m}_0$  and higher coefficients:

$$\hat{m}_0 = \frac{\hat{w}_0^2 - 1}{\hat{w}_0^2 + 1}, \quad (2.7.8)$$

$$\hat{m}_1 = (\hat{w}_0^2 + 1)^{-1} \left\{ \hat{w}_0 \hat{w}_1 (1 - \hat{m}_0) + \frac{\hat{w}_1}{\hat{w}_0} (1 + \hat{m}_0) - \hat{w}_0 \hat{m}_0 \right\} \quad (2.7.9)$$

$$\hat{m}_2 = (\hat{w}_0^2 + 1)^{-1} \left\{ \hat{w}_0 \hat{w}_2 (1 - \hat{m}_0) + \frac{\hat{w}_0 \hat{w}_2 - \hat{w}_1^2}{\hat{w}_0^2} (1 + \hat{m}_0) \right. \quad (2.7.10)$$

$$\left. - \frac{\hat{w}_1}{\hat{w}_0} (1 - \hat{w}_0^2) \hat{m}_1 - \hat{w}_0 \hat{m}_1 \right\}. \quad (2.7.11)$$

It yields for the magnetization up to second order in  $r^{-1}$

$$m = \frac{q}{\sqrt{1+q^2}} \left( 1 - \frac{5}{8} \frac{1}{(1+q^2)^3} \frac{1}{r^2} + \dots \right). \quad (2.7.12)$$

The expansion up to second order will be used in section 2.9 where we compare this expression with the Fisk-Widom theory. Here we take the limit  $r \rightarrow \infty$  and obtain from the scaling regime equations the solution

$$w(q) = \sqrt{r(q + \sqrt{1+q^2})} \quad (2.7.13)$$

$$m(q) = \frac{q}{\sqrt{1+q^2}} \quad (2.7.14)$$

In order to compare with the local-field solution we remark the following. In the scaling regime formulas, the variables acquire structure when the argument  $t = \sqrt{g}\tau$  is of the order 1. Then  $\tau = gn \simeq \sqrt{g}$  and thus small. So, in the local-field expressions (2.6.4) and (2.6.9) we can approximate  $\sinh \tau \simeq \tau$  and  $\exp(-\tau) \simeq 1$ , yielding again (2.7.13) and (2.7.14). This shows that the local field regime corresponds to  $r \gg 1$ .

## 2.8 The surface tension

In the local-field regime  $z_n \simeq z_n^{\text{LF}}$  and the surface tension  $\sigma \simeq 0$ . Therefore we focus on the scaling regime and start by rewriting the expression for the surface tension (2.2.34) in the appropriate scaling form.

The tails of the chain ( $|n| \gg 1$ ) are always in the local-field regime because there  $g \ll \tau = gn$  and the local field can be considered as uniform over large distances.

Therefore we divide the chain into a central region A and the outer parts B. The border between the two regions is chosen to be at a very small magnetic field value  $|\tau| = \delta$ , but such that  $|t|$  is already large:

$$\sqrt{g} \ll |\delta| \ll 1 \quad (|t| = \frac{|\delta|}{\sqrt{g}} \gg 1) \quad (2.8.1)$$

We will first show that around  $|\tau| \simeq \delta$  the solution already becomes local-field like. The local-field solution for  $w(t)$  at this point in the chain can be written as (see (2.2.32))

$$w(t) = \frac{z_n^{\text{LF}}}{\sqrt{g}} \simeq t + \sqrt{t^2 + r} = \begin{cases} -r/2t, & t \ll -1 \\ 2t, & t \gg 1 \end{cases} \quad (2.8.2)$$

Note that  $w(t)$  is unsymmetric. For  $t \ll -1$ ,  $w(t)$  is small, while for  $t \gg 1$ ,  $w(t)$  is large.

In general, the solution of  $w(t)$  is given by (2.7.1). Because  $w(t)$  is unsymmetric we distinguish the cases  $t < 0$  and  $t > 0$ . For  $t \simeq -\delta/\sqrt{g} \ll -1$  we see from (2.8.2) that  $w^2(t) \ll 2tw(t)$ ,  $r$  and (2.7.1) becomes

$$2tw(t) + r \simeq 0, \quad (2.8.3)$$

that is,  $w(t)$  assumes its local field value  $-r/2t$ .

For  $t \simeq \delta/\sqrt{g} \gg 1$  we have  $w(t), r \ll w(t)$ ,  $2tw(t)$  and (2.7.1) becomes

$$w^2(t) - 2tw(t) \simeq 0 \quad (2.8.4)$$

and again  $w(t)$  is seen to attain its local field value  $2t$  already at the boundary between regions A and B.

We conclude that the contribution to the surface tension from region B is negligible because there  $z_n \simeq z_n^{\text{LF}}$ . Thus, to a high degree of accuracy, the surface tension is given by

$$-\sigma/k_B T = \frac{1}{2} \sum_{n \in A} \ln \left[ \frac{\gamma^{-n} z_n + 1 + \alpha^2 \gamma^n / z_n}{\gamma^{-n} z_n^{\text{LF}} + 1 + \alpha^2 \gamma^n / z_n^{\text{LF}}} \right] \quad (2.8.5)$$

where we have also neglected  $\alpha^2$  as compared to 1, appropriate in the scaling regime. Since  $z_n = \sqrt{g}w(t)$  and for  $n \in A$ ,  $\gamma^n \simeq 1$  and  $z_n^{\text{LF}} \simeq \sqrt{g}(t + \sqrt{t^2 + r})$ , we can further simplify the expression for the surface tension and write

$$\begin{aligned} -\sigma/k_B T &\simeq \frac{1}{2} \sum_{n \in A} \ln \left[ \frac{1 + \sqrt{g}(w(t) + r/w(t))}{1 + 2\sqrt{g}\sqrt{t^2 + r}} \right] \\ &\simeq \frac{1}{2} \int_A dt \left[ w(t) + \frac{r}{w(t)} - 2\sqrt{t^2 + r} \right] \end{aligned} \quad (2.8.6)$$

where in the last equation we consider  $t = \sqrt{g}n$  as a continuous variable ( $g \ll 1$ ).

From this expression we see that the surface tension has the correct scaling form (see (2.2.14)). For  $r \ll 1$  the expression is well approximated by the capillary wave solution (2.4.9) although this is not readily seen. In appendix 2A we will show that a rough estimate of (2.8.6) for  $r \ll 1$  also gives the  $\ln(r)$  dependence.

For  $r \gg 1$ , the local-field regime, the surface tension is easily evaluated. We substitute the  $1/r$  expansion (2.7.6) for  $w(q)$  into (2.8.6) and obtain

$$-\sigma/k_B T \simeq \frac{1}{8r} \int_A dq \frac{1 - 4q^2}{(1 + q^2)^{5/2}} \simeq -\frac{1}{6r} \quad (2.8.7)$$

In the second equation we have extended the range of the integral to run from  $-\infty$  to  $\infty$  since the integral falls off as  $1/q^3$  for large  $q$ .

Robert and Widom [1] obtain for the surface tension, in the case that the magnetic field profile is a stepfunction, the exact expression

$$-\sigma/k_B T = -\frac{1}{2} \ln \left[ 1 + \frac{\sinh^2(H)}{\alpha^2} \right] \quad (2.8.8)$$

$$\simeq -\frac{1}{2} \ln[1 + (H/\alpha)^2] \quad (H \ll 1) \quad (2.8.9)$$

In accordance with scaling (see section 2.2) we should take  $H \sim \sqrt{g}$  when comparing their results with ours. Thus  $(H/\alpha)^2 \sim g/\alpha^2 = r^{-1}$ . This suggests that the surface tension in our case is given by

$$\begin{aligned} -\sigma/k_B T &= -\frac{1}{2} \ln[1 + (ar)^{-1}] \\ &\simeq \begin{cases} 1/2 \ln(ar), & r \ll 1 \\ -(2ar)^{-1}, & r \gg 1 \end{cases} \end{aligned} \quad (2.8.10)$$

This agrees with our results if we take  $a = \pi$  for  $r \ll 1$  and  $a = 3$  for  $r \gg 1$ .

In Fig. 2.1 we have plotted the surface tension as given by (2.8.10) with  $a = 3, \pi$  together with the exact values obtained numerically from (2.2.27) and (2.2.34). The curves coincide over the entire range of  $r$  values and we conclude that the surface tension is indeed given by (2.8.10) with  $a \simeq 3, \pi$ .

The surface tension as defined by (2.2.9) can also be regarded as measuring the extent to which the solution is local-field like. The local-field regime corresponds to  $\sigma \simeq 0$  and the solution becomes more and more non-local as the surface tension increases. Thus we see again that  $r \gg 1$  corresponds to the local-field regime since then  $\sigma$  vanishes as  $1/r$ .



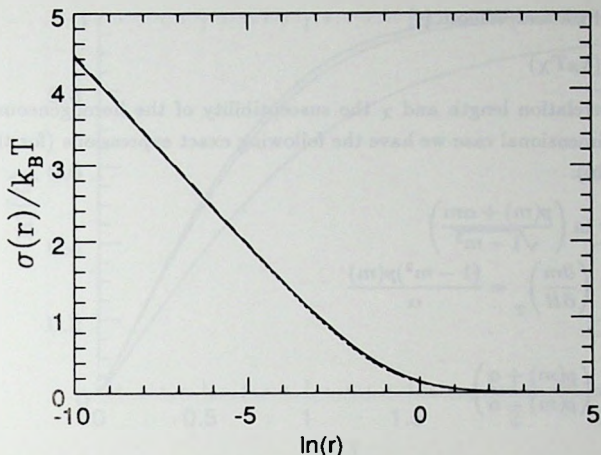


Fig. 2.1. The surface tension  $\sigma$  as given by (2.8.10) with  $a = 3$  (dashed line) and  $a = \pi$  (dotted line) together with the exact solution (solid line), obtained numerically from the general recursion relations given in section 2.2.

## 2.9 The Fisk-Widom approximation

The basic assumption of the Fisk-Widom approximation [4] is the existence of a local free energy density  $\psi(z)$  whose dependence on the position  $z$  in the chain is given by

$$\psi(z) = \psi(m(z)) + \frac{1}{2}A(m(z))(\dot{m}(z))^2 - H(z)m(z). \quad (2.9.1)$$

where we have absorbed a factor  $1/k_B T$  in  $\psi$ ,  $A$  and  $H$ . The first term on the rhs,  $\psi(m(z))$ , is the free energy density of a uniform chain with magnetization equal to the local magnetization  $m(z)$ . The second is a Landau type contribution that accounts for the free energy associated with the gradient in the system, while the third is the usual Zeeman energy with  $H(z) = gz$ , the local magnetic field. In the local-field regime this assumption is of course correct. Away from the local-field regime the squared gradient term will account for the non-local behavior. The extent to which this term is capable of handling the non-locality is studied in this section.

From (2.9.1) one deduces the variational equation

$$A\ddot{m}(z) = H(m(z)) - H(z) - \frac{1}{2}\frac{\partial A}{\partial m}(\dot{m}(z))^2. \quad (2.9.2)$$

According to Fisk and Widom [4]

$$A = \xi^2 / (k_B T \chi) \quad (2.9.3)$$

with  $\xi$  the correlation length and  $\chi$  the susceptibility of the homogeneous system. For the one-dimensional case we have the following exact expressions (for the homogeneous system):

$$H(m) = \ln \left( \frac{p(m) + \alpha m}{\sqrt{1 - m^2}} \right) \quad (2.9.4)$$

$$k_B T \chi = \left( \frac{\partial m}{\partial H} \right)_T = \frac{(1 - m^2)p(m)}{\alpha} \quad (2.9.5)$$

and

$$\xi^{-1} = \ln \left( \frac{p(m) + \alpha}{p(m) - \alpha} \right). \quad (2.9.6)$$

with

$$p(m) = \sqrt{1 - (1 - \alpha^2)m^2} \quad (2.9.7)$$

In higher dimensions  $A$  is only weakly dependent on  $m$  and is usually taken as  $m$  independent ( $A(m) \equiv A(0)$ ), neglecting thus the third term on the rhs of (2.9.2). For  $d = 1$ , this is not the case and we compare the exact solution with the full Fisk-Widom equation as well as with the further approximated form for which  $A(m) \equiv A(0)$ .

Before confronting the numerical solutions of the FW-equation with the exact ones, we compare the  $1/r$  expansion for  $m$ , given by (2.7.12), with the same expansion in the FW-approximation. When  $\alpha \ll 1$  we can expand  $A(m)$  and  $H(m)$  to first order in  $\alpha$  and putting the resulting expressions into the FW-equation we obtain the scaling form

$$\tilde{m}(q) = 4r^2[m(q) - q\sqrt{1 - m^2(q)}] - \frac{m(q)\dot{m}^2(q)}{2(1 - m^2(q))} \quad (2.9.8)$$

with  $r = \alpha^2/g$  and  $q = t/\sqrt{r}$ . Substituting the  $1/r$  expansion (2.7.7) for  $m$  into the above equation we find for the local-field regime again

$$m_{\text{FW}} = m_{\text{LF}} \left( 1 - \frac{5}{8} \frac{1}{(1 + q^2)^3} \frac{1}{r^2} + \dots \right). \quad (2.9.9)$$

with  $m_{\text{LF}} = q/\sqrt{1 + q^2}$  the local-field solution.

Similarly, we obtain for the FW-equation with  $A(m) \equiv A(0)$

$$m_{\text{FW}} = m_{\text{LF}} \left( 1 - \frac{6}{8} \frac{1}{(1 + q^2)^{7/2}} \frac{1}{r^2} + \dots \right). \quad (2.9.10)$$

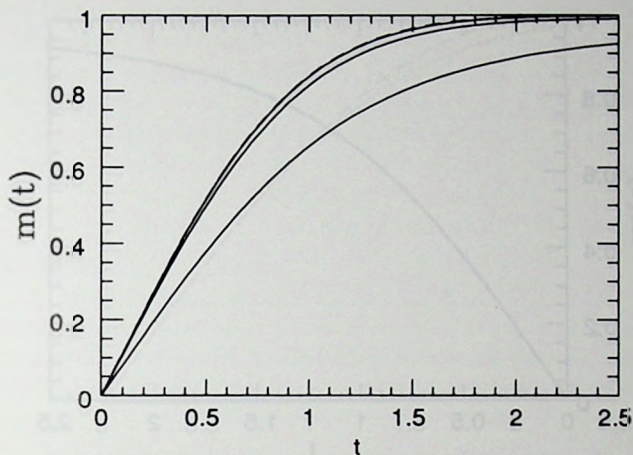


Fig. 2.2. Exact magnetization profiles for  $g = 1 \times 10^{-6}$  and  $r = 0$  (dashed line), 0.01, 0.1 and 1 (solid lines). As  $r \rightarrow 0$ , the curves become steeper, the limiting curve of which is the analytically obtained capillary wave solution.

From the above expressions we conclude that FW-theory describes the non-locality well for  $r \gg 1$

For smaller values of  $r$ , that is away from the local-field regime, we have calculated the magnetization profile numerically. In Fig. 2.2 we plotted the profile as obtained from the recursion relations (2.2.27) and (2.2.28), showing the approach to the capillary wave solution as  $r \rightarrow 0$ . For  $r = 0.01$  the profile has already reached its asymptotic shape. The Figs. 2.3, 2.4 and 2.5 show the exact and FW-solution for  $g = 1.0 \times 10^{-6}$  and  $r = 1, 0.1$  and  $0.01$ . We see that, for  $r = 1$ , the FW-profile is still a good approximation. For  $r = 0.1$  the two solutions start to deviate and only for  $r = 0.01$ , the most non-local case, the FW-solution is beginning to flatten out, with an initial slope smaller than the exact profile, which has almost reached its final shape of the  $r = 0$  solution. In the limit  $r \rightarrow 0$  the FW-solution becomes infinitely broad. We conclude that the FW-equation is remarkably good in handling the non-local behavior for  $r \geq 1$ .

The reason that the approximation deviates from the exact solution for  $r < 1$  is that the coefficient of the squared gradient term  $A \sim 1/\alpha$  diverges as  $r \rightarrow 0$ . As is shown by Fisk and Widom [4],  $A \sim \xi^\eta$  with  $\eta$  the critical exponent, defined by the

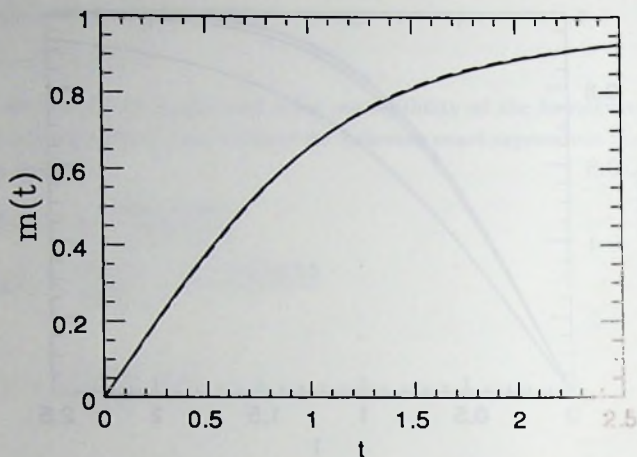


Fig. 2.3. The exact- and FW-magnetization profiles for  $g = 1 \times 10^{-6}$  and  $r = 1$ . The solid line is the exact solution, the dotted line the solution of the full FW-equation and the dashed line the FW-approximation for which  $A(m) \equiv A(0)$ . For this and higher values of  $r$  three curves coincide.

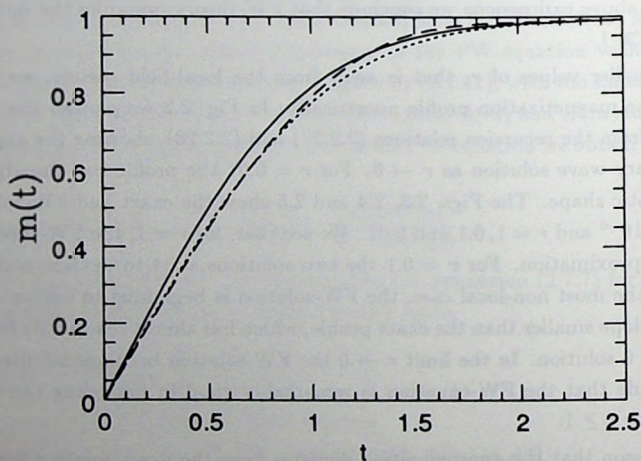


Fig. 2.4. The exact- and FW-magnetization profiles for  $g = 1 \times 10^{-6}$  and  $r = 0.1$ . The meaning of the lines is the same as in Fig. 2.3



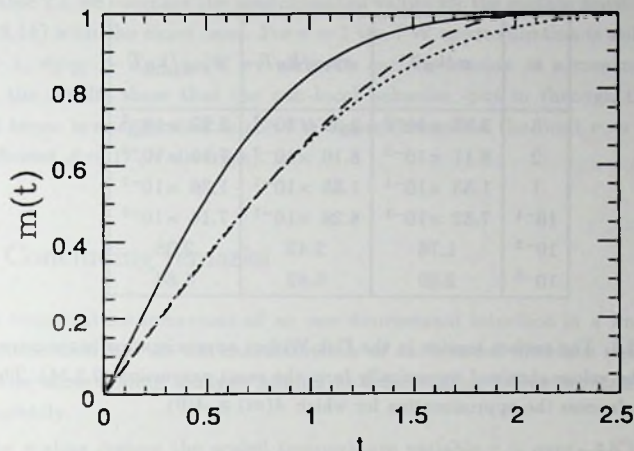


Fig. 2.5. The exact- and FW-magnetization profiles for  $g = 1 \times 10^{-6}$  and  $r = 0.01$ . The meaning of the lines is the same as in Fig. 2.3

decay rate of the correlation function at the critical point. For  $\alpha \ll 1$  the correlation length (2.9.6) is approximately

$$\xi \simeq \frac{\sqrt{1-m^2}}{2\alpha} \sim \frac{1}{\alpha} \quad (2.9.11)$$

and

$$A \simeq [4\alpha\sqrt{1-m^2}]^{-1} \sim \frac{1}{\alpha} \quad (2.9.12)$$

We see that  $A \sim \xi$  and thus the exponent  $\eta = 1$  for  $d = 1$ . In the limit  $T \rightarrow 0$  and  $r$  fixed the behavior is similar to that in higher dimensions in the limit  $T \rightarrow T_c$ . But in higher dimensions  $\eta$  is closer to zero ( $\eta = 1/4$  for  $d = 2$  and  $\eta = 0.03$  for  $d = 3$ ) and we expect the range of validity of the Fisk-Widom theory to increase for  $d > 1$  since  $A$  is less strongly divergent.

Next we compare the FW-approximation for the surface tension with the solution obtained from the exact expression (2.2.34) together with (2.2.27). We start from the definition (2.2.9) where the free energy of the inhomogeneous system is now approximated by the FW-expression

$$F/k_B T = \int dz \psi(z) \quad (2.9.13)$$

$r$	$\sigma/k_B T$	$\sigma_{FW}/k_B T$	$\sigma'_{FW}/k_B T$
5	$3.32 \times 10^{-2}$	$3.37 \times 10^{-2}$	$2.93 \times 10^{-2}$
2	$8.11 \times 10^{-2}$	$8.16 \times 10^{-2}$	$7.16 \times 10^{-2}$
1	$1.53 \times 10^{-1}$	$1.55 \times 10^{-1}$	$1.36 \times 10^{-1}$
$10^{-1}$	$7.52 \times 10^{-1}$	$8.28 \times 10^{-1}$	$7.14 \times 10^{-1}$
$10^{-2}$	1.76	2.42	2.08
$10^{-3}$	2.89	5.62	4.84

Table 2.1. The surface tension in the Fisk-Widom approximation is compared with the values obtained numerically from the exact expression (2.234). The accent denotes the approximation for which  $A(m) \equiv A(0)$ .

with  $\psi(z)$  given by (2.9.1). By integrating the expression for  $\sigma$  in parts we obtain

$$\sigma_{FW}/k_B T = \int_{-\infty}^{\infty} dz \left[ A(m)(\dot{m}(z))^2 + gz (m(z) - m_{LF}(z)) \right] \quad (2.9.14)$$

with  $m_{LF}(z)$  as in (2.6.9)

$$m_{LF}(z) = \frac{\sinh gz}{\sqrt{\sinh^2 gz + \alpha^2}} \quad (2.9.15)$$

For  $\alpha \ll 1$  the coefficient  $A(m)$  is given by (2.9.12) and we can write  $\sigma_{FW}$  in a scale invariant form:

$$\sigma_{FW}/k_B T = \frac{1}{r} \int_{-\infty}^{\infty} dq \left[ \frac{1}{4\sqrt{(1-m^2)}} (\dot{m}(q))^2 + r^2 q (m(q) - m_{LF}(q)) \right] \quad (2.9.16)$$

When we put the  $r^{-1}$  expansion (2.9.9) for  $m(q)$  into the above expression we find

$$\sigma_{FW}/k_B T = \frac{1}{6r} + O\left(\frac{1}{r^3}\right) \quad (2.9.17)$$

which should be compared with (2.8.7). Similarly we obtain for  $\sigma'_{FW}/k_B T$  with  $A(m) \equiv A(0)$ ,

$$\sigma'_{FW}/k_B T = \frac{3\pi}{64r} + O\left(\frac{1}{r^3}\right) \quad (2.9.18)$$

We see from (2.9.9) and (2.9.17) that the full FW-equation is exact up to second order in  $r^{-1}$ .

In Table 2.1 we compare the approximated values for the surface tension obtained from (2.9.14) with the exact ones. For  $r = 1$  the FW-approximation is still excellent. For  $r < 1$ ,  $\sigma_{FW} > \sigma_{\text{exact}}$ . If we view the surface tension as a measure for non-locality, the results show that the non-local behavior - put in through the squared gradient term - is exaggerated in the FW-approximation in the limit  $r \rightarrow 0$  (because the coefficient  $A \sim 1/\sqrt{r}$  diverges).

## 2.10 Concluding remarks

The low temperature behaviour of an one-dimensional interface in a linearly varying magnetic field has all the characteristics of an induced interface near a critical point. The same scaling analysis applies and the scaling behaviour can be worked out completely.

In the scaling regime the scaled temperature variable  $r = \exp(-4K)/g$  controls a cross-over from a local ( $r \gg 1$ ) to a non-local ( $r \ll 1$ ) field regime. In the local-field regime the width of the interface is proportional to  $\sqrt{r}$ . But as  $r$  decreases the correlation length  $\sqrt{g}\xi \sim 1/\sqrt{r}$  - measured in the scaled distance variable  $t = \sqrt{g}n$  - increases and starts to resist the rapid variation of the magnetization around  $t = 0$ . Therefore the profile becomes flatter than it would be in the local-field approximation. When the correlation length exceeds the width in the local-field approximation (that is when  $r \simeq 1$ ) we enter a new regime where the profile is determined by capillary wave fluctuations. In the capillary wave regime the width remains of order 1 (measured in  $t$ ) as  $r \rightarrow 0$ , i.e. the real width (measured in  $n$ ) diverges as  $1/\sqrt{g}$ .

The Fisk-Widom interfacial theory is an extension of the local-field approximation, where the non-local behavior is accounted for by a squared gradient term. Its results are exact up to second order in the  $r^{-1}$  expansion and accurate for all  $r \geq 1$ . For  $r \ll 1$  the width of the magnetization profile becomes proportional to the correlation length and thus proportional to  $1/\sqrt{r}$ . In the limit  $r \rightarrow 0$  the profile becomes infinitely broad because there is no cross-over to a capillary wave regime in this theory.

The surface tension is defined as the excess free energy over the local-field approximation. It goes to zero as  $r^{-1}$  in the local-field limit ( $r \rightarrow \infty$ ) and diverges logarithmically in the capillary wave limit ( $r \rightarrow 0$ ). For  $r \geq 1$  the Fisk-Widom theory gives accurate values for the surface tension, but for  $r < 1$  the values obtained are too high.

## Appendix

### 2A The surface tension for $r \ll 1$

In this appendix we give a rough estimate for the surface tension for  $r \ll 1$  to show how the  $\ln(r)$  dependence results from the expression

$$-\sigma/k_B T \simeq \frac{1}{2} \int_A dt \left[ w(t) + \frac{r}{w(t)} - 2\sqrt{t^2 + r} \right] \quad (2A.1)$$

with  $w(t)$  the solution of

$$\dot{w}(t) = w(t)^2 - 2tw(t) - r \quad (2A.2)$$

We treat separately the cases  $t > 0$  and  $t < 0$ . For  $t > 0$ ,  $w(t) \gg r$  and we can neglect  $r$  in (2A.2). Then  $w(t)$  is given by the capillary wave solution

$$w(t) = \frac{\exp(-t^2)}{\int_t^\infty \exp(-x^2) dx} \quad (2A.3)$$

We rewrite the integral by changing the integration variable to  $y = 2t(x - t)$ :

$$\int_t^\infty dx \exp(-x^2) = \frac{\exp(-t^2)}{2t} \int_0^\infty dy \exp(-y(1 + y/4t^2)) \simeq \frac{\exp(-t^2)}{2t} \quad (2A.4)$$

for  $t \gg 1$ . In this approximation  $w(t) \simeq 2t$ , the local field value, which cancels the local field term  $-2\sqrt{t^2 + r} \simeq -2t$  in (2A.1). The contribution from region A with  $t > 0$  is therefore of order 1.

For  $t < 0$ ,  $w(t)$  becomes small and we neglect  $w^2(t)$  as compared to  $2tw(t)$ . In this approximation the solution of (2A.2) is given by

$$w(t) = C(r)e^{-t^2} + re^{-t^2} \int_0^{-t} dx \exp(x^2) \quad (2A.5)$$

with  $C(r)$  some amplitude. According to the capillary solution (2.3.8),  $C(0) = 2/\sqrt{\pi}$ . Again we estimate the value of the integral by changing the integration variable to  $y = 2t(x + t)$ :

$$\int_0^{-t} dx \exp(x^2) = -\frac{\exp(t^2)}{2t} \int_0^{2t^2} dy \exp(-y(1 - y/4t^2)) \simeq -\frac{\exp(t^2)}{2t} \quad (2A.6)$$

for  $t \ll -1$ . Thus

$$w(t) \simeq C(r)e^{-t^2} - \frac{r}{2t} \quad (t \ll -1) \quad (2A.7)$$



The second term is the local field value for  $t < 0$ . For  $t < -\sqrt{-\ln r}$  this term starts to dominate over the other and the term  $r/w(t)$  in (2A.1) will cancel the local field term  $-2\sqrt{t^2 + r} \simeq 2t$ . But when  $-\sqrt{-\ln r} < t < 0$  the local field term  $-2\sqrt{t^2 + r}$  is not compensated and we have the order of magnitude estimate

$$-\sigma/k_B T \simeq \frac{1}{2} \int_{-\sqrt{-\ln r}}^0 dt - 2\sqrt{t^2 + r} \simeq \int_{-\sqrt{-\ln r}}^0 dt \, t = \frac{1}{2} \ln r \quad (2A.8)$$

## References

- [1] M. Robert and B. Widom, *J. Stat. Phys.* **37**, 419 (1984).
- [2] F. P. Buff, R. A. Lovett and F. H. Stillinger, *Phys. Rev. Lett.* **15**, 621 (1965).
- [3] J. K. Percus, *J. Stat. Phys.* **16**, 299 (1977).
- [4] S. Fish and B. Widom, *J. Chem. Phys.* **50**, 3219 (1969).
- [5] J. V. Sengers and J. M. J. van Leeuwen, *Physica A* **116**, 345 (1982).

## Chapter 3

# Finite-Size Effects and Capillary Waves in Solid-on-Solid Models

### 3.1 Introduction

Many systems phase-separate below a certain temperature, creating an interface between two bulk phases. The interface between the coexisting phases is deformed by thermally excited capillary waves [1]. The resulting fluctuations in the order parameter smear out the interface. The interface is called "smooth" if the width remains finite and "rough" if it diverges (in the limit of infinite system size and no pinning field present). Generally for dimensions  $d \leq 3$  the interface is rough.

In lattice models the capillary waves are hindered by the fact that there is a minimum amount of energy associated with each deformation. Therefore, in  $d=3$ , the interface can be either rough or smooth. For high temperatures it is rough and (for certain orientations) a roughening temperature  $T_R$  exists below which the interface becomes smooth [2, 3, 4]. In the rough phase the discreteness of the energy spectrum becomes irrelevant and the interface fluctuations can be well described by a continuous capillary-wave picture.

The distinction between capillary-wave excitations of the interface and what may be called intrinsic fluctuations is difficult. In lattice models one can introduce the solid-on-solid (SOS) condition, which allows only wave like excitations. Bubbles and overhangs can be considered as the excluded intrinsic excitations, certainly at low temperatures. In spite of this simplification the general SOS interface problem has not been solved for  $d=3$ , with a few notable exceptions [5, 6, 7, 8]. In contrast, for  $d=2$ , the SOS model is generally solvable by the transfer matrix method [9, 10, 11].

The capillary-wave model describes the long wavelength fluctuations of an inter-

face. The constants entering in the capillary wave hamiltonian however, cannot be related easily to the microscopic hamiltonian of the model [12]. The SOS model permits this connection for  $d=2$ , as we shall see below, for a general microscopic hamiltonian and for any orientation of the interface. Recently Švrakić, Privman and Abraham [13] have performed such a calculation for a SOS model of an interface, making only infinitesimally small angles with the crystal axes and controlled by the specific interaction :  $K|h_i - h_j|$ .

In this chapter we want to link explicitly the finite-size effects with the capillary waves for a general  $d=2$  SOS model. In fact, by keeping the model general it displays this connection more transparently than by considering a specific SOS hamiltonian. In section 3.2 we derive the finite-size correction to the surface tension, linking these to the surface stiffness of the model. In section 3.3, the interface profile of a tilted interface is derived in terms of the stiffness and in the last section we derive the capillary-wave hamiltonian for this model, which again only depends on the microscopic details of the model via the surface stiffness.

## 3.2 The finite-size partition function

Consider a strip of a planar square lattice of width  $l$  (see figure 3.1). On every lattice point, labelled by  $i = 0, \dots, l$  and  $j = \pm\frac{1}{2}, \pm\frac{3}{2}, \pm\frac{5}{2}, \dots$ , there is an Ising spin  $s_{ij} = \pm 1$ . Only nearest neighbour spins interact. In the SOS approximation, overhangs and bubbles are excluded so that each configuration can be specified by a set of height variables  $h_i = 0, \pm 1, \pm 2, \pm 3 \dots$  with  $i = 0, \dots, l$ . Let the energy of a configuration, with boundary conditions  $h_0 = 0$  and  $h_l = n$  as indicated in Fig. 3.1, be given by

$$E_l(n) = \sum_{i=1}^l V(|h_{i-1} - h_i|). \quad (3.2.1)$$

Here  $V$  is any positive valued function. Typically, we consider functions which diverge as the argument goes to infinity, e.g. a linear or quadratic function. The partition sum,

$$Z_l(n) = \sum_{\{h_i\}} \exp[-\sum_{i=1}^l V(|h_{i-1} - h_i|)/k_B T], \quad (3.2.2)$$

can be rewritten in terms of the transfer matrix,

$$\langle h|T|h' \rangle \equiv \exp[-V(|h - h'|)/k_B T], \quad (3.2.3)$$

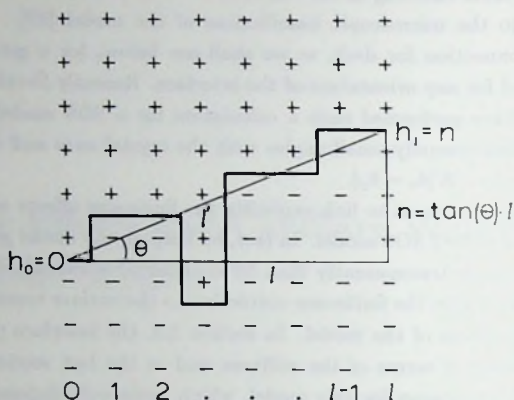


Fig. 3.1. A two-dimensional strip of Ising spins of width  $l$  with boundary conditions  $h_0 = 0$  and  $h_l = n$ , forcing an interface into the system of length  $l' = l/\cos\theta$  between the endpoints  $(0,0)$  and  $(l,n)$ . The average inclination angle is given by  $\tan\theta = n/l$ . Only solid-on-solid configurations are allowed.

yielding

$$Z_l(n) = \langle 0|T^l|n \rangle \quad (3.2.4)$$

in Dirac notation.

The system has translational invariance in the vertical direction of the strip, so that

$$\sum_{h'} \langle h|T|h' \rangle e^{iqh'} = e^{iqh} \sum_m \langle 0|T|m \rangle e^{iqm} \quad (3.2.5)$$

with  $m = h' - h$ . Thus the eigenvectors of the transfer matrix are  $e^{iqh}$  with the eigenvalues

$$\lambda(q) \equiv \sum_{m=-\infty}^{\infty} \exp[-V(|m|) + imq] \quad (3.2.6)$$

where  $q$  is limited to the first Brillouin zone:  $-\pi \leq q < \pi$ . So a fourier transform of the height variables

$$\langle q|h \rangle \equiv \frac{1}{\sqrt{2\pi}} e^{iqh}, \quad (3.2.7)$$



diagonalizes the transfer matrix,

$$\langle q|T|q' \rangle = \lambda(q)\delta(q - q'), \quad (3.2.8)$$

and the partition sum is simply given by

$$Z_l(n) = \frac{1}{2\pi} \int_{-\pi}^{\pi} dq \lambda^l(q) e^{iqn}. \quad (3.2.9)$$

For large  $l$  one can evaluate this expression with the steepest descent method. First we write (3.2.9) in the form

$$Z_l(t) = \frac{1}{2\pi} \int_{-\pi}^{\pi} dq \exp[-lf(q, t)] \quad (3.2.10)$$

with

$$f(q, t) = -\ln(\lambda(q)) - iqt \quad (3.2.11)$$

and

$$t = l\tau; \theta = \frac{n}{l}. \quad (3.2.12)$$

The partition sum can also be transformed to an integral over the unit circle in the complex  $z$ -plane by changing the integration variable to  $z = e^{iq}$ . One may deform the integration contour in such a way that it runs through the saddle point where the real part of  $f(q, t)$  assumes its maximum value. When  $l$  is large the complete integral is well approximated by the contribution coming from the immediate vicinity of the saddle point. The location of the saddle point  $q_0(t)$  is determined by the steepest descent condition

$$\partial_q f(q_0, t) = -\left[\frac{\lambda'(q_0)}{\lambda(q_0)} + it\right] = 0. \quad (3.2.13)$$

The accent in  $\lambda'(q)$  denotes the derivative with respect to  $q$ . Returning again to an integration over  $q$  instead of  $z$  and extending it from  $-\infty$  to  $+\infty$ , one obtains to second order in the expansion around the saddle point:

$$\begin{aligned} Z_l(t) &\cong \frac{\exp[-lf(q_0(t), t)]}{2\pi} \int_{-\infty}^{\infty} dq \exp\left[-\frac{l}{2} \partial_{qq} f(q_0(t), t)(q - q_0(t))^2\right] \\ &= \frac{\exp[-lf(q_0(t), t)]}{\sqrt{2\pi l \partial_{qq} f(q_0(t), t)}} \end{aligned} \quad (3.2.14)$$

Because later we will also need the other partial derivatives of  $f(q, t)$ , we give them here :

$$\partial_t f(q, t) = -iq, \quad (3.2.15)$$

$$\partial_{iq}f(q, t) = -i, \quad (3.2.16)$$

$$\partial_{qq}f(q_0(t), t) = i(q'_0(t))^{-1}. \quad (3.2.17)$$

In the last equation we have used the steepest descent condition. The accent in  $q'_0(t)$  denotes the derivative with respect to the argument. Thus we find for the angle dependent surface tension  $\sigma$  of the tilted interface, which is the free energy per unit "length" associated with the interface,

$$\sigma(l', \theta) \equiv -\frac{\ln[Z_l(t)]}{l'} \quad (3.2.18)$$

$$= \cos\theta f(q_0(t), t) + \frac{1}{2l'} \ln[2\pi l' \cos\theta \partial_{qq}f(q_0(t), t)], \quad (3.2.19)$$

with

$$l' = \frac{l}{\cos\theta}. \quad (3.2.20)$$

If we take the limit  $l' \rightarrow \infty$ , we obtain the full angle dependent surface tension for the infinite system :

$$\sigma(\infty, \theta) = \cos\theta f(q_0(t), t) \quad (3.2.21)$$

Note that this expression is valid for a SOS model with an arbitrary interaction  $V(|h_i - h_j|)$ .

Next we consider the angle dependent stiffness  $s(\infty, \theta)$  for the infinite system, defined by [14]

$$s(\infty, \theta) \equiv \sigma(\infty, \theta) + \frac{\partial^2 \sigma(\infty, \theta)}{\partial \theta^2}. \quad (3.2.22)$$

(Since we will not consider the finite-size effect of the stiffness, we simply write  $s(\theta)$  from now on.) When we insert (3.2.21) into (3.2.22) and use (3.2.13) and (3.2.15) we have

$$s(\theta) = -\frac{i}{\cos^3\theta} q'_0(t). \quad (3.2.23)$$

Substituting (3.2.17) we get the final expression:

$$s(\theta) = \frac{1}{\cos^3\theta \partial_{qq}f(q_0, t)}. \quad (3.2.24)$$

Again, this is the stiffness for an infinite SOS model with arbitrary interaction  $V(|h_i - h_j|)$ . Comparing (3.2.19) and (3.2.24) we see that we can write the finite-size correction to the surface tension in terms of the stiffness :

$$\sigma(l', \theta) = \sigma(\infty, \theta) + \frac{1}{2l'} \ln\left(\frac{2\pi l'}{\cos^2\theta s(\theta)}\right). \quad (3.2.25)$$

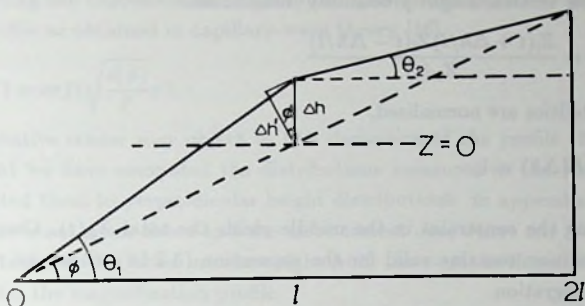


Fig. 3.2. An interface with an overall inclination angle  $\phi$ , and a fixed height  $z = \Delta h$  in the middle, so that the inclination angle is  $\theta_1$  in the first part and  $\theta_2$  in the second part.

Let us emphasize that this equation, which expresses all the finite-size effects of the surface tension up to  $O(1/l)$  in terms of the stiffness of an infinite system, is a consequence of a number of features of the model. We will discuss these points more fully in the discussion, within the context of other models such as the 2-d Ising and the 3-d SOS model.

Finally we use (3.2.18) and rewrite (3.2.25) to obtain the finite-size partition sum in terms of the surface tension and the stiffness of the infinite system :

$$Z_l(\theta) = \sqrt{\frac{s(\theta)\cos^2\theta}{2\pi l'}} \exp[-l'\sigma(\infty, \theta)]. \quad (3.2.26)$$

### 3.3 The interfacial profile

To study the profile of a tilted interface we consider a bent one, as depicted in Fig. 3.2. Here we show an interface of length  $2l'$  under an angle  $\phi$ , while the middle is fixed at height  $l \tan\phi + \Delta h$ . This situation can be viewed as the result of appending two strips of width  $l$ , similar to the one in Fig. 3.1. For each strip, we use expression (3.2.14) for the partition sum with  $\tan\theta_1 = (t + \frac{\Delta h}{l})$  and  $\tan\theta_2 = (t - \frac{\Delta h}{l})$ , and  $t = \tan\phi$

The magnetization profile  $m_l(z)$  is defined as

$$m_l(z) = \sum_{\Delta h=-\infty}^{z-1/2} P(\Delta h) - \sum_{\Delta h=z+1/2}^{\infty} P(\Delta h) = \sum_{\Delta h=-(z-1/2)}^{z-1/2} P(\Delta h), \quad (3.3.1)$$

in terms of the vertical-height probability distribution

$$P(\Delta h) = \frac{Z_l(t + \Delta h/l) Z_l(t - \Delta h/l)}{Z_{2l}(t)}. \quad (3.3.2)$$

These probabilities are normalised,

$$\sum_{\Delta h=-\infty}^{\infty} P(\Delta h) = 1, \quad (3.3.3)$$

since removing the constraint in the middle yields the total  $Z_{2l}(t)$ . One may check that this condition remains valid for the expression (3.2.14) when one replaces the sum by an integration.

Since  $\Delta h$  is expected to be of the order  $\sqrt{l}$  (because of the random walk like nature of the problem [15]) we may expand in  $\Delta h/l$ . If we use the expressions (3.2.13) up to (3.2.17) for the partition sum and for the derivatives of  $f(q_0(t), t)$ , we get up to order  $O(l^{(0)})$  in the exponent

$$Z_l(t \pm \frac{\Delta h}{l}) = \frac{\exp - l \{ f(q_0(t), t) \mp i q_0(t) (\Delta h/l) + [2\partial_{qq} f(q_0(t), t)]^{-1} (\Delta h/l)^2 \}}{\sqrt{2\pi l \partial_{qq} f(q_0(t), t)}} \quad (3.3.4)$$

To this order the denominator does not require expansion. Notice that in (3.3.2) the linear terms drop out. Using (3.2.24) for the stiffness and (3.2.25) for the surface tension, we find

$$P(\Delta h) = \sqrt{\frac{\cos^3 \phi s(\phi)}{\pi l}} \exp[-\frac{1}{l} \cos^3 \phi s(\phi) (\Delta h)^2]. \quad (3.3.5)$$

For the tilted interface, the natural variables to use are :  $l' = l/\cos \phi$ ,  $\Delta h' = \Delta h \cos \phi$  and  $z' = z \cos \phi$ , and the perpendicular height distribution  $P'(\Delta h')$  defined by

$$P'(\Delta h') \Delta h' \equiv P(\Delta h) \Delta h. \quad (3.3.6)$$

Rewriting expression (3.3.1) for the magnetization profile, using the last two equations (and approximating the sum by an integration) we obtain

$$m'_\mu(z') \equiv m_l(z) \cong \int_{-z'}^{z'} d(\Delta h') P'(\Delta h') \quad (3.3.7)$$

with

$$P'(\Delta h') = \sqrt{\frac{s(\phi)}{\pi l'}} \exp[-\frac{1}{l'} s(\phi) (\Delta h')^2]. \quad (3.3.8)$$



When inserting the expression for  $P'(\Delta h')$  into (3.3.7) one arrives at the usual error function profile as obtained in capillary-wave theory [16]:

$$m'_p(z') = \text{erf}\left(\sqrt{\frac{s(\phi)}{l'}} z'\right). \quad (3.3.9)$$

The attentive reader may object to this derivation of the profile (3.3.9), on the grounds that we have computed the distributions measured in the vertical heights and translated them to perpendicular height distributions. In appendix 3A we show that the derivation given above and the more correct one, where one works with the natural variables of the tilted interface right from the start, both result in the same expression for the magnetization profile.

### 3.4 The capillary wave model

To derive a continuous capillary-wave description for the SOS model, we join together  $m$  strips of width  $l$ . From (3.2.4) one can see that the partition sum for the SOS model on a strip of size  $l$  is just a matrix element of  $T^l$ . Starting with a strip of size  $L = ml$  ( $m = 2, 3, 4, \dots$ ), one can group the product of  $L$  transfer matrices into strings of length  $l$  and sum over all heights within each string. The resulting  $Z_l$  for each string can be regarded as the renormalised transfer matrix on a length scale  $l$  times larger. The total  $Z_L$  for an interface with an overall inclination angle  $\phi$  is therefore

$$Z_L(t) = \sum_{x_1 \dots x_{m-1}} Z_l\left(t + \frac{x_1 - x_0}{l}\right) \dots Z_l\left(t + \frac{x_m - x_{m-1}}{l}\right) \quad (3.4.1)$$

with  $x_i = \Delta h_{il}$  and  $t = \tan \phi$  and boundary conditions  $x_0 = x_m = 0$ .

Substituting (3.3.4) for  $Z_l$  we find that

$$Z_L(t) = (Z_l(t))^m Z_{cw}(\phi), \quad (3.4.2)$$

with the capillary-wave partition function given by

$$Z_{cw}(\phi) = \int_{-\infty}^{\infty} dx_1 \dots \int_{-\infty}^{\infty} dx_{m-1} \exp\left[-\frac{l}{2\partial_{qq}f(q_0(t), t)} \sum_{i=1}^m \left(\frac{x_i - x_{i-1}}{l}\right)^2\right], \quad (3.4.3)$$

where we have replaced the sums by integrations. Next we use expression (3.2.24) to eliminate  $\partial_{qq}f(q_0(t), t)$ , and change to the variables  $l' = l/\cos \phi$  and  $x' = x \cos \phi$ , obtaining

$$Z_{cw}(\phi) = \left(\frac{1}{\cos \phi}\right)^{m-1} \int_{-\infty}^{\infty} dx'_1 \dots \int_{-\infty}^{\infty} dx'_{m-1} \exp\left[-\frac{s(\phi)}{2l'} \sum_{i=1}^m (x'_i - x'_{i-1})^2\right] \quad (3.4.4)$$

Finally, we take the continuum limit by the substitution

$$x'_i = x'(r') \quad (3.4.5)$$

$$x'_i - x'_{i-1} = l' \frac{dx'(r')}{dr'} \quad (3.4.6)$$

with  $r' = l'i$ . Then partition function (3.4.4) becomes

$$Z_{cw} = \left(\frac{1}{\cos\phi}\right)^{m-1} \int_{-\infty}^{\infty} D\{x'\} \exp[-H_{L'}(\{x'\})] \quad (3.4.7)$$

with the capillary-wave hamiltonian given by

$$H_{L'} = -\frac{s(\phi)}{2} \int_0^{L'} dr' \left| \frac{d}{dr} x'(r') \right|^2 \quad (3.4.8)$$

Alternatively one can write  $Z_{cw}$  explicitly in terms of waves :

$$x'_i = \frac{1}{\sqrt{m}} \sum_{n=1}^{m-1} \tilde{x}'(k_n) \sin(k_n r_i) \quad (3.4.9)$$

where  $k_n = \pi n/m l'$ ,  $r_i = l'i$  and  $\tilde{x}'(k_n)$  is the amplitude of the wave  $k_n$ . Inserting (3.4.9) into (3.4.4) yields

$$\begin{aligned} Z_{cw}(\phi) &= \left(\frac{1}{\cos\phi}\right)^{m-1} \int_{-\infty}^{\infty} d\tilde{x}'(k_1) \cdots \int_{-\infty}^{\infty} d\tilde{x}'(k_{m-1}) \\ &\times \exp\left[-\frac{s(\phi)}{2l'} \sum_{n=1}^{m-1} (1 - \cos k_n l') (\tilde{x}'(k_n))^2\right] \end{aligned} \quad (3.4.10)$$

Doing the gaussian integrals we get for the capillary wave contribution to the surface tension :

$$\sigma_{cw}(\phi) \equiv -\frac{1}{L'} \ln[Z_{cw}(\phi)] = \frac{1}{2L'} \sum_{n=1}^{m-1} \ln\left[\frac{s(\phi) \cos^2\phi (1 - \cos k_n l')}{\pi l'}\right]. \quad (3.4.11)$$

Working this out gives, of course,

$$\sigma_{cw} = -\frac{1}{2l'} \ln\left(\frac{2\pi l'}{s(\phi) \cos^2\phi}\right) + \frac{1}{2L'} \ln\left(\frac{2\pi L'}{s(\phi) \cos^2\phi}\right) \quad (3.4.12)$$

Comparing this with (3.2.25) shows that the finite-size correction to the surface tension is equal to the contribution of the capillary waves which are released when the restrictions at the boundaries are removed. Since the capillary waves are determined by the stiffness alone, the same holds for the finite-size correction.

We note that the standard capillary-wave hamiltonian (3.4.8) and the corresponding partition function (3.4.7) are only approximately equivalent to the exact expression (3.4.11). When  $\cos k_n l'$  is expanded to order  $k_n^2$  in (3.4.11) the result (3.4.7) is recovered. One could say that (3.4.11) displays a wavelength dependent stiffness but the dispersion found in (3.4.11) is a typical reflection only of the nearest neighbour character of the interaction of the SOS model, and is not sensitive to the detailed form of the function  $V(|\Delta h|)$ .

### 3.5 Summary and discussion

We considered a solid-on-solid model for interfaces in a 2-d (bulk) system. The site and height variables are both integer, with the former restricted to the range  $[0, l]$ . For nearest-neighbour interactions of arbitrary form  $V(|\Delta h|)$ , we find the surface tension  $\sigma(l', \theta)$  as a function of both the tilt angle  $\theta$  and the length of the interface,  $l' = l/\cos\theta$ . Though one may not be inclined to take this function seriously for large angles, it does have a thermodynamic limit,  $\sigma(\infty, \theta)$ , which is analytic for all  $\theta \in (-\pi/2, \pi/2)$ . Thus, the stiffness [14] for an infinite system is well defined by  $s(\theta) \equiv \sigma(\infty, \theta) + \sigma''(\infty, \theta)$ .

The leading  $l' < \infty$  correction to  $\sigma(l', \theta)$  is the universal [17],  $\ln(l')/2l'$ , being independent of both  $\theta$  and  $V(|\Delta h|)$ . The next order,  $O(1/l')$ , has a "universal" form, in that it depends only on  $s(\theta)\cos^2(\theta)$ . We find it reasonable to interpret the first factor as the result of capillary waves and the  $\cos^2\theta$  as an end point effect.

We further found that the interface profile, exact to leading order, can also be expressed in term of  $s(\theta)$  alone, as in equation (3.3.9). This fact is again consistent with a description of the systems fluctuations by a capillary-wave picture with the effective hamiltonian given by expression (3.4.8), in which the only manifestation of the microscopic model is the parameter  $s(\theta)$ . Note that the end point effect is absent, as it should, from the expression for the profile far from the system boundaries.

Unfortunately, there are limitations to the capillary-wave picture, especially for describing the finite-size effect of the surface tension. Of course, the leading order,  $\ln(l')/2l'$ , will emerge from the capillary-wave picture. But this term is so universal that hardly any detail of the capillary-wave hamiltonian comes through. In this sense, only a Goldstone-like character of an effective hamiltonian is needed to produce such a term. At the next order,  $O(1/l')$ , one expects contributions both from the end points and from the capillary waves. For our model, we believe it is possible to untangle the two in the following sense. For  $\theta = 0$ , the SOS condition forbids all configurations of the interface which go "beyond" the end points. In this case, only  $s(\theta = 0)$  enters. However for  $\theta \neq 0$ , many configurations go outside the range  $[0, l']$ , though they are restricted to  $[0, l]$ . Since these can be ascribed to "geometry" alone, we argue that they are responsible for the factor  $\cos^2\theta$ . That this factor is completely insensitive to the microscopic hamiltonian further strengthens our argument to dissociate it from the fluctuations of the interface inside the system.

Note that it is meaningful to speak of the interface going through the point  $i$  at height  $h$ , since we have a SOS condition. Thus we recall the example in section 3.3.

There, the full partition sum over all interfaces from  $(0,0)$  to  $(2l, 2l \tan\theta)$ , can be done by first finding two partial sums, over interfaces from  $(0,0)$  to  $(l, h)$  and from  $(l, h)$  to  $(2l, 2l \tan\theta)$ , and then summing over  $h$ . In contrast, for the 2-d Ising model, where overhangs and bubbles proliferate, the full sum associated with an interface is not simply related to those associated with its segments. Thus, we are unable to untangle the finite-size effects due to capillary waves from those due to the end points. Therefore the  $O(1/l')$  finite-size effect of the surface tension cannot be used to support the capillary wave theory. We will discuss this point in detail in appendix 3B for two different definitions of the finite-size surface tension.

To test the capillary wave theory for the 2-d Ising model beyond the universal  $\ln(l')/2l'$  term, we must look towards an exact calculation, similar to the work done by Abraham and Reed [18], of the magnetization profile associated with an interface at arbitrary angles. If capillary-wave theory is correct, that profile should depend only on  $s(\theta)$ .

Finally we recall that for  $d > 2$  the capillary-wave picture gives finite-size corrections to the surface tension at a higher order than the boundary effects. The latter always appears at  $O(1/l')$  while capillary-wave contributions are  $O(\ln(l')/(l')^{d-1})$ . Thus, in higher dimensions, we can expect to check the validity of the capillary wave theory only via the magnetisation profile.

## Appendices

### 3A The magnetization profile

In this appendix we will do the calculation of section 3.3 again, but now we work with the variables of the tilted interface right from the start. In Fig. 3.3 we have drawn an interface with an inclination angle  $\phi$ . The length of the interface is  $2l'$  and in the middle it has a fixed height  $\Delta h'$ . Most of the notation we use in this appendix is explained in the figure. To calculate the partition sum for this situation we use expression (3.2.14) for the triangles 123 and 345 so we have  $Z_{l_0}(t_0)$  with  $t_0 \equiv \tan\theta_0$  for the first triangle and  $Z_{l_1}(t_1)$  with  $t_1 \equiv \tan\theta_1$  for the second. We want to expand these partition sums in  $\Delta h'/l'$ . Basic geometry leads to the following equalities

$$l_0 = l' \cos\phi \left[ 1 - t \left( \frac{\Delta h'}{l'} \right) \right] \quad (3A.1)$$



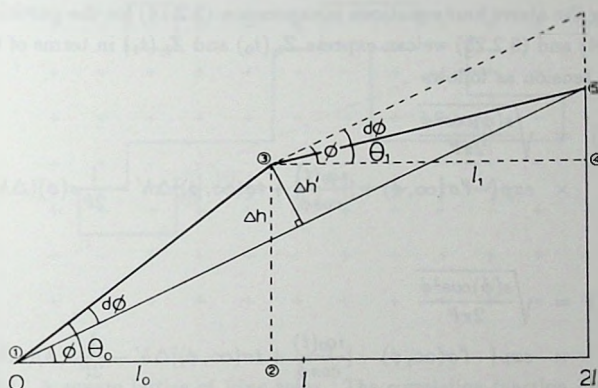


Fig. 3.3. An interface with an overall inclination angle  $\phi$ , and a fixed height  $z' = \Delta h'$  in the middle. The average inclination angle is  $\theta_0 = \phi + d\phi$  in the first part, where the triangle 123 is used for the calculation of the partition sum. In the second part, the average inclination angle is  $\theta_1 = \phi - d\phi$  and the triangle 345 is used.

and

$$l_1 = l' \cos \phi \left[ 1 + t \left( \frac{\Delta h'}{l'} \right) \right] \quad (3A.2)$$

with  $t \equiv \tan \phi$ . Expanding  $t_0$  and  $t_1$  to second order, we have

$$t_0 \cong t + (1 + t^2) \left( \frac{\Delta h'}{l'} \right) + t(1 + t^2) \left( \frac{\Delta h'}{l'} \right)^2 \quad (3A.3)$$

and

$$t_1 \cong t - (1 + t^2) \left( \frac{\Delta h'}{l'} \right) + t(1 + t^2) \left( \frac{\Delta h'}{l'} \right)^2 \quad (3A.4)$$

Substituting the above four equations in expression (3.2.14) for the partition sum and using (3.2.24) and (3.2.25) we can express  $Z_{l_0}(t_0)$  and  $Z_{l_1}(t_1)$  in terms of the stiffness and surface tension as follows

$$\begin{aligned} Z_{l_0}(t_0) &= \sqrt{\frac{s(\phi) \cos^2 \phi}{2\pi l'}} \\ &\times \exp \left\{ -l' \sigma(\infty, \phi) + \left[ \frac{i q_0(t)}{\cos \phi} + t \sigma(\infty, \phi) \right] \Delta h' - \frac{1}{2l'} s(\phi) (\Delta h')^2 \right\} \end{aligned} \quad (3A.5)$$

and

$$\begin{aligned} Z_{l_1}(t_1) &= \sqrt{\frac{s(\phi) \cos^2 \phi}{2\pi l'}} \\ &\times \exp \left\{ -l' \sigma(\infty, \phi) - \left[ \frac{i q_0(t)}{\cos \phi} + t \sigma(\infty, \phi) \right] \Delta h' - \frac{1}{2l'} s(\phi) (\Delta h')^2 \right\} \end{aligned} \quad (3A.6)$$

The magnetization profile is again given by (3.3.7) with the probability  $P'(\Delta h')$  as defined by (3.3.6) and

$$P(\Delta h) = \frac{Z_{l_0}(t_0) Z_{l_1}(t_1)}{Z_{2l}(t)} \quad (3A.7)$$

Putting everything together we retrieve (3.3.9) for the magnetization profile. The only difference between (3A.6) and (3A.7), and the more intuitive approach in section 3.3 lies in the terms linear in  $\Delta h'$ . But this is inconsequential since the linear terms cancel.

### 3B Finite-size effects in the 2-d Ising model

Here we consider the finite-size correction to the surface tension for the 2-d Ising model. There are two ways to define the finite-size surface tension.

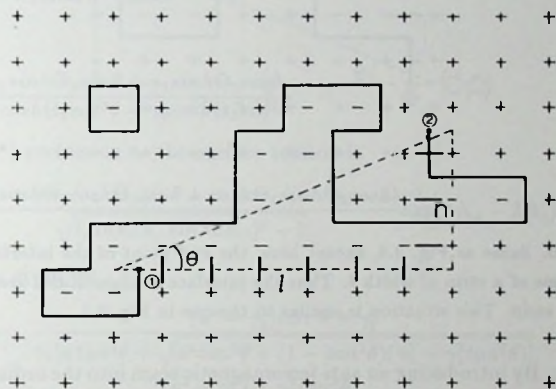


Fig. 3.4. A square lattice of Ising spins. The correlation function between the points 1 and 2 on the dual lattice corresponds with  $Z_{seam}/Z_{no\ seam}$  on the original lattice, where  $Z_{seam}$  is the partition sum when there is a seam (a series of negative bonds along an arbitrary path between the points 1 and 2, indicated by the little thick lines) in the lattice. This forces an interface into the system between  $(0,0)$  and  $(l,n)$ . Since these end points are imbedded in an infinite lattice, the interface configurations are free to go beyond them.

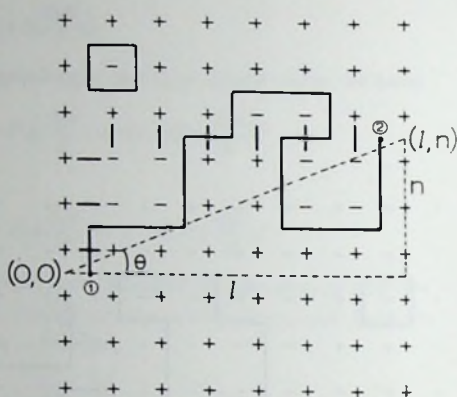


Fig. 3.5. Same as Fig. 3.4, except here, the end point of the interface lie on the edges of a strip of width  $l$ . Thus the interface configurations are confined to this strip. This situation is similar to the one in Fig. 3.1.

definition 1 : By introducing an anti-ferromagnetic seam into the ordinary Ising model between  $(0,0)$  and  $(l, l \tan \theta)$ , thereby allowing the interface to make arbitrarily large excursions beyond the end points (see Fig. 3.4)

definition 2 : By introducing an anti-ferromagnetic seam on a strip of Ising spins of width  $l$ , between  $(0,0)$  and  $(l, l \tan \theta)$ , and with all spins up at the strip boundaries, creating a situation analogous to the one in section 3.2 for the SOS model. Now the interface is confined to the strip (see Fig. 3.5).

Because the behaviour of the interface around the end points is very different for these two cases, we expect different end point effects, but the capillary wave contribution should be the same.

First, we translate both definitions to the dual form [19, 20, 21, 22, 23], in terms of the two spin correlation function, by the relation

$$\sigma(l', \cos \theta) = -\frac{1}{\nu} \ln [\exp(-2K_2) \langle \sigma(\frac{1}{2}, 0) \sigma(l - \frac{1}{2}, l \tan \theta) \rangle_{free boundaries}^*] \quad (3B.1)$$

where  $K_2 = \beta J_2$  is the reduced vertical bond strength (and  $K_1$ , the horizontal). The star indicates that the correlation function is defined on the dual lattice where the



reduced coupling constants  $K_i^*$  are given by  $\exp(-2K_i^*) = \tanh(K_i)$  for  $i=1,2$ . The factor  $\exp(-2K_2)$  is needed to put the expression on an equal footing with the SOS definition, it accounts for the extra broken  $K_2$ -bond at one of the end points. Notice that the free energy for an interface of length  $l$  compares with a correlation function between spins, only (a horizontal) distance  $l-1$  apart.

For definition 1 we use a result of H. Cheng and T. T. Wu [24, 25] to obtain

$$\sigma(\infty, \theta) = \Theta_1 \sin \theta + \Theta_2 \cos \theta \quad (3B.2)$$

and

$$s(\theta) = \frac{\gamma_1 \sinh \Theta_1 \sin \theta + \gamma_2 \sinh \Theta_2 \cos \theta}{\gamma_1 \cosh \Theta_1 \cos^2 \theta + \gamma_2 \cosh \Theta_2 \sin^2 \theta} \quad (3B.3)$$

while the  $O(1/l')$  correction to the surface tension is

$$\frac{1}{2l'} \ln \left[ \frac{2\pi (\sinh \Theta_1 \cosh \Theta_2 \sin \theta + \cosh \Theta_1 \sinh \Theta_2 \cos \theta)}{\sqrt{(\sinh 2K_1 \sinh 2K_2)^2 - 1}} \exp(4K_2 - 2\Theta_2) \right], \quad (3B.4)$$

with  $\Theta_1$  and  $\Theta_2$  given by

$$\cosh \Theta_1 = \frac{(a^2 - \gamma_2^2) \tan^2 \theta + \gamma_1^2}{\gamma_1 [a \tan^2 \theta + \sqrt{a^2 \tan^2 \theta + (1 - \tan^2 \theta)(\gamma_1^2 - \gamma_2^2 \tan^2 \theta)}]} \quad (3B.5)$$

$$\cosh \Theta_2 = \frac{(a^2 - \gamma_1^2) + \gamma_2^2 \tan^2 \theta}{\gamma_2 [a + \sqrt{a^2 \tan^2 \theta + (1 - \tan^2 \theta)(\gamma_1^2 - \gamma_2^2 \tan^2 \theta)}]} \quad (3B.6)$$

and

$$a = (1 + \exp(-4K_1))(1 + \exp(-4K_2)) \quad (3B.7)$$

$$\gamma_1 = 2\exp(-2K_1)(1 - \exp(-4K_2)) \quad (3B.8)$$

$$\gamma_2 = 2\exp(-2K_2)(1 - \exp(-4K_1)) \quad (3B.9)$$

Since expression (3B.4) can be written as

$$\frac{1}{2l'} \ln \left( \frac{2\pi}{\cos^2 \theta s(\theta)} \right) + \frac{1}{2l'} \ln \left[ \frac{\sinh(2K_1)}{\sinh(2K_2)} \frac{\exp(4K_2 - 2\Theta_2) \sinh^2 \Theta_2}{\sqrt{[\sinh(2K_1) \sinh(2K_2)]^2 - 1}} \right] \quad (3B.10)$$

one can interpret the second term as an angle dependent end point effect. In the SOS limit  $K_2 \rightarrow \infty$  the endpoint effect vanishes.

For definition 2, D. B. Abraham found [4, 26]

$$Z_l(n) = \frac{1}{2\pi} \int_{-\pi}^{\pi} dq \frac{\exp(iqn)}{[\cosh(l\gamma(q)) + \sinh(l\gamma(q)) \cos \delta^*(q)]} \quad (3B.11)$$

where  $\gamma(q)$  and  $\delta^*(q)$  are elements of Onsager's hyperbolic triangle [1]

$$\cosh \gamma(q) = \frac{\cosh(2K_1)\cosh(2K_2) - \sinh(2K_2)\cos(q)}{\sinh(2K_1)} \quad (3B.12)$$

$$\cos \delta^*(q) = \frac{\cosh(2K_1)\sinh(2K_2) - \cosh(2K_2)\cos(q)}{\sinh(2K_1)\sinh(\gamma(q))} \quad (3B.13)$$

For large  $l$  we may approximate  $Z_l$  by

$$Z_l(t) \simeq \frac{1}{2\pi} \int_{-\pi}^{\pi} dq \frac{\exp(-lg(q, t))}{(1 + \cos \delta^*(q))/2} \quad (3B.14)$$

with

$$g(q, t) = \gamma(q) - iqt \quad (3B.15)$$

This form is very similar to expression (3.2.10) for the SOS model and can be treated in the same way, resulting in

$$Z_l(t) \simeq \left( \frac{1}{1 + \cos \delta^*(q_0)} \right) \frac{\exp[-lg(q_0(t), t)]}{\sqrt{2\pi} \partial_{q_0} g(q_0(t), t)} \quad (3B.16)$$

with  $q_0(t)$ , the solution of the steepest descent condition  $\partial_{q_0} g(q_0(t), t) = 0$ , given by

$$q_0(t) = i\Theta_1, \quad (3B.17)$$

and thus

$$\gamma(q_0) = \Theta_2 \quad (3B.18)$$

and

$$\cos \delta^*(q_0) = \sqrt{1 + (t/\sinh(2K_2))^2} \quad (3B.19)$$

Using equation (3.2.23) one gets again expression (3B.3) for the stiffness while the  $O(1/l')$  correction to the surface tension becomes

$$\frac{1}{2l'} \ln \left( \frac{2\pi}{\cos^2 \theta_s(\theta)} \right) + \frac{1}{l'} \ln \left( \frac{1 + \sqrt{1 + (t/\sinh 2K_2)^2}}{2} \right) \quad (3B.20)$$

The first term is the contribution one expects from the capillary waves. But the second term cannot be interpreted so easily, making it again impossible to untangle the end point effects from the finite-size effects due to the capillary waves. In the SOS limit  $K_2 \rightarrow \infty$  this last term vanishes.

## References

- [1] F. P. Buff, R. A. Lovett and F. H. Stillinger, *Phys. Rev. Lett.* **15**, 621 (1965).
- [2] J. D. Weeks, G. H. Gilmer and H. J. Leamy, *Phys. Rev. Lett.* **31**, 549 (1973).
- [3] H. van Beijeren and I. Nolden, in *Topics in Current Physics*, Vol. 43, W. Schommers and P. von Blanckenhagen, eds. (Springer, Berlin, 1987), p. 259.
- [4] D. B. Abraham, in *Phase Transitions and Critical Phenomena*, Vol. 10, C. Domb and J. L. Lebowitz, eds. (Academic Press, New York, 1986), p. 1.
- [5] H. van Beijeren, *Phys. Rev. Lett.* **38**, 993 (1977).
- [6] D. R. Nelson, *Phys. Rev. B* **26**, 269 (1982).
- [7] H. W. J. Blöte and H. J. Hilhorst, *J. Phys. A* **15**, L631 (1982).
- [8] B. Nienhuis, H. J. Hilhorst and H. W. J. Blöte, *J. Phys. A* **17**, 3559 (1984).
- [9] S. T. Chui and J. D. Weeks, *Phys. Rev. B* **23**, 2438 (1981).
- [10] T. W. Burkhardt, *J. Phys. A* **14**, L63 (1981).
- [11] H. J. Hilhorst and M. J. M. van Leeuwen, *Physica* **107A**, 319 (1981).
- [12] R. F. Kayser, *Phys. Rev. A* **33**, 1948 (1986).
- [13] N. M. Švrakić, V. Privman and D. B. Abraham, *J. Stat. Phys.* **53**, 1041 (1988).
- [14] M. P. A. Fisher, D. S. Fisher and J. D. Weeks, *Phys. Rev. Lett.* **48**, 368 (1982).
- [15] M. E. Fisher, *J. Stat. Phys.* **34**, 667 (1984).
- [16] D. Jasnow, *Rep. Prog. Phys.* **47**, 1059 (1984) and in *Phase Transition and Critical Phenomena*, Vol. 10, C. Domb and J. L. Lebowitz, eds. (Academic Press, New York, 1986), p. 296.
- [17] V. Privman, *Phys. Rev. Lett.* **61**, 183 (1988).
- [18] D. B. Abraham and P. Reed, *Commun. Math. Phys.* **49**, 35 (1976).
- [19] H. A. Kramers and G. K. Wannier, *Phys. Rev.* **60**, 252 (1941).
- [20] A. E. Ferdinand, PhD Thesis (University of London, 1967) unpublished.

- [21] P. G. Watson, *J. Phys. C* **1**, 575 (1968).
- [22] M. E. Fisher, *J. Phys. Soc. Japan (suppl.)* **26**, 87 (1969).
- [23] R. K. P. Zia, *Phys. Lett. A* **64**, 345 (1978).
- [24] H. Cheng and T. T. Wu, *Phys. Rev.* **160**, 719 (1967), see equation (5.1).
- [25] B. M. McCoy and T. T. Wu, *The Two-Dimensional Ising Model*, (Harvard University Press, Cambridge, 1973), p.305.
- [26] D. B. Abraham, *Stud. Appl. Math.* **50**, 71 (1971), see equation (4.27).
- [27] L. Onsager, *Phys. Rev.* **65**, 117 (1944).



## Chapter 4

# Free Fermion Approximation for the Ising Model with Further-Neighbor Interactions on a Triangular Lattice

### 4.1 Introduction

Since Onsagers solution of the 2D-Ising model [1], many efforts have been made to extend the solution to include further-neighbor interactions. Such solutions would allow for a better modelling of real magnetic systems [2] and of course of all other systems that can be mapped onto the Ising model such as e.g. recent models for microemulsions [3, 4]. The only generalisations along this line that have led to exact solutions are the free fermion models (models that can be rewritten as free fermion field theories [5]), where still certain restrictions have to be imposed on the allowed values of the coupling constants. But for a large range of values, where these conditions are not met, simply ignoring them still provides a good approximation to the real solution (the so called free fermion approximation [6]). Of the different methods that can be employed to solve these models, Vdovichenko's method [7, 8, 9, 10] has the advantage that it can easily be extended to yield the surface tension [11, 12, 13], as well as the corresponding equilibrium crystal shape [12, 13].

In this chapter we present the free fermion solution/approximation for the Ising model with first- and second neighbor interactions and a four-spin interaction on a triangular lattice, using the method of Vdovichenko [8]. In section 4.2 we define the model and rewrite it as a vertex-pair model on the dual lattice. The zero temperature phase diagram of the isotropic model is given in section 4.3. In section 4.4 we derive the free fermion conditions for which the solution will be exact and in section 4.5 we calculate the, in general approximate, partition sum and discuss the accuracy of the

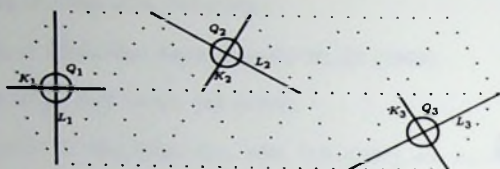


Fig. 4.1. The lattice is seen as built up out of overlapping diamonds. We assign to each diamond a first- and second neighbor interaction and a four-spin interaction, with coupling constants  $K_i, L_i$  and  $Q_i$  respectively, whose values are different for each orientation  $i$ .

approximation. The approximate critical surface of the model is derived in section 4.6 and in section 4.7 we study the surface free energy.

## 4.2 The model

Consider a triangular lattice consisting of  $N$  sites with periodic boundary conditions. On every site there is an Ising spin  $\sigma = \pm 1$ . The interactions between the spins are as follows. Any two neighboring elementary triangles of the lattice form a diamond. To each diamond we assign three interactions (see Fig. 4.1), a first- and second neighbor interaction  $K_i$  and  $L_i$  (along the two diagonals of the diamond) and a four-spin interaction  $Q_i$ , with different values for each orientation  $i=1,2$  or  $3$ . In the interaction constants we have already absorbed a factor  $1/k_B T$  for later convenience. Note that each triangle is part of three diamonds (the diamonds overlap), one in each possible orientation.

A diamond can occur in eight different configurations  $q$ , which are depicted in Fig. 4.2. The energy  $E$  of a configuration of the total system is given by

$$E = \sum_{i=1}^3 \sum_{q=1}^8 n_i(q) \epsilon_i(q) \quad (4.2.1)$$

with

$$\epsilon_i(q) = -(K_i \sigma_1 \sigma_3 + L_i \sigma_2 \sigma_4 + Q_i \sigma_1 \sigma_2 \sigma_3 \sigma_4), \quad (4.2.2)$$

the energy of a diamond of type  $(i, q)$  and with  $n_i(q)$  the number of times this diamond occurs in the configuration. Thus the partition sum becomes

$$Z = \sum_{\{\text{configurations}\}} \prod_{i=1}^3 \prod_{q=1}^8 [\omega_i(q)]^{n_i(q)} \quad (4.2.3)$$



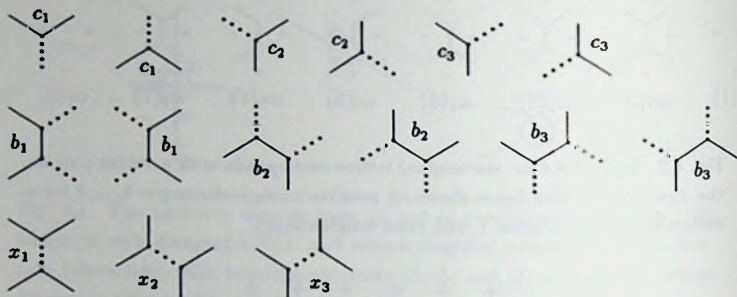


Fig. 4.4. Weights assigned to corners, bends and close encounters.

original lattice (see Fig. 4.3). Only 0 or 2 bonds meet at every dual lattice site, forming closed loops that cannot cross. A set of loops belonging to one configuration is called a graph. When there is no bond between two nearest neighbor sites on the dual lattice, we speak of an hole.

With every diamond on the triangular lattice corresponds a vertex-pair on the dual lattice (see Fig. 4.2). In appendix 4A we derive all independent relations that exist between the numbers of vertex-pairs  $n_i(q)$  and show that, as a result, the partition sum can be written as

$$Z = [\omega_1(1)\omega_2(1)\omega_3(1)]^N \sum_{\{\text{configurations}\}} \prod_{i=1}^3 a_i^{n_i(2)} b_i^{n_i(5)+n_i(6)} c_i^{n_i(7)+n_i(8)} \quad (4.2.8)$$

with

$$a_i = \frac{\omega_i(2)\omega_{i+1}(3)\omega_{i+2}(4)}{\omega_i(1)\omega_{i+1}(1)\omega_{i+2}(1)} \quad (4.2.9)$$

$$b_i = \left( \frac{\omega_i(5)\omega_i(6)}{\omega_i(3)\omega_i(4)} \right)^{1/2} \quad (4.2.10)$$

$$c_i = \left( \frac{\omega_i(7)\omega_i(8)\omega_{i+1}(3)\omega_{i+2}(4)}{[\omega_i(1)]^2\omega_{i+1}(1)\omega_{i+2}(1)} \right)^{1/2} \quad (4.2.11)$$

and  $i = i \pmod{3}$ .

For the application of the method of Vdovichenko, a more appropriate formulation of the partition sum is [8]

$$Z = \left[ \prod_i \omega_i(1) \right]^N \sum_G I_G \quad (4.2.12)$$





Fig. 4.5. An example of a graph. The Boltzmann weight of this graph is given by  $I_G = c_1^6 c_2^2 c_3^2 b_1^2 b_2^2 b_3^2 x_1$ .

where the sum is over all graphs  $G$  on the dual lattice and  $I_G$  is the Boltzmann weight of the configuration specified by graph  $G$ , which is given by

$$\begin{aligned} I_G &= \prod_{i=1}^3 a_i^{n_i(2)} b_i^{n_i(5)+n_i(6)} c_i^{n_i(7)+n_i(8)} \\ &= \prod_{i=1}^3 c_i^{n_{c_i}} b_i^{n_{b_i}} x_i^{n_{x_i}} \end{aligned} \quad (4.2.13)$$

with the weight

$$x_i = \frac{a_i}{c_i^2} = \frac{\omega_i(1)\omega_i(2)}{\omega_i(7)\omega_i(8)} \quad (4.2.14)$$

and

$$n_{c_i} = 2n_i(2) + n_i(7) + n_i(8) \quad (4.2.15)$$

the total number of corners (single turns) with orientation  $i$  in graph  $G$ , to each of which a weight  $c_i$  is assigned,

$$n_{b_i} = n_i(5) + n_i(6) \quad (4.2.16)$$

the total number of bends (two successive turns in the same direction) with orientation  $i$  in graph  $G$ , to each of which a weight  $b_i$  is assigned and

$$n_{x_i} = n_i(2) \quad (4.2.17)$$

the total number of close encounters with orientation  $i$  in graph  $G$ , to each of which a weight  $x_i$  is assigned (see Fig. 4.4). The factor in front of the sum rescales  $I_G$  so that  $I_G = 1$  for  $G = \emptyset$  (the empty graph representing the configuration with all spins parallel). As an example, the Boltzmann weight for the graph in Fig. 4.5 is given by

$$I_G = c_1^6 c_2^2 c_3^2 b_1^2 b_2^2 b_3^2 x_1 \quad (4.2.18)$$

Expressing the corner, bend and close encounter weights in the original language of coupling constants, using (4.2.2) and (4.2.4), we obtain

$$c_i = \exp[-2(L_i + Q_i) - (K_{i+1} + L_{i+1} + K_{i+2} + L_{i+2})] \quad (4.2.19)$$

$$b_i = \exp[2(L_i - Q_i)] \quad (4.2.20)$$

$$x_i = \exp[4(L_i + Q_i)] \quad (4.2.21)$$

For the nearest-neighbor Ising model the coupling constants  $L_i$  and  $Q_i$  are zero so that  $c_i = \exp(-K_{i+1} - K_{i+2})$  and  $x_i = b_i = 1$  for  $i = 1, 2, 3$ .

### 4.3 The zero temperature phase diagram

The groundstate for arbitrary coupling constants may be very complicated since the various tendencies compete and disorder can exist down to zero temperature. Therefore we restrict ourselves to the isotropic case:  $K_i = K$ ,  $L_i = L$  and  $Q_i = Q$  for  $i = 1, 2, 3$ . A superficial inspection readily shows that the configurations A to F as shown in Fig. 4.6 are the groundstate in some part of the phase diagram. As the energies of the configurations are given by

$$\begin{aligned} E_A &= -N \ln\left(\prod_i^3 \omega_i(1)\right) \\ E_B &= E_A - N \ln(c^2 x) \\ E_C &= E_A - N \ln(b^2 c^2 x) \\ E_D &= E_A - (3N/2) \ln(bc) \\ E_E &= E_A - N \ln(c) \\ E_F &= E_A - (N/2) \ln(b^2 c^3) \end{aligned} \quad (4.3.1)$$

we can also find the domains for these groundstates, if they are the only contenders. In the Figs. 4.7 and 4.8 we give these domains for  $Q > 0$  and  $Q < 0$ . We prove in appendix 4B that the groundstates A - E are indeed the groundstates of the system in their domain. For state F the arguments presented are not sufficient to rule out possible other groundstates. We indicate why we find it plausible that F is indeed the groundstate in its domain. We have not further investigated this case as it involves an examination of the lattice on a larger scale than a hexagon (which is sufficient for A - E) and as the free fermion approximation is inaccurate in this region of the phase diagram anyway.



Configuration A



Configuration B



Configuration C



Configuration D



Configuration E



Configuration F

Fig. 4.6. The groundstates for the isotropic model.

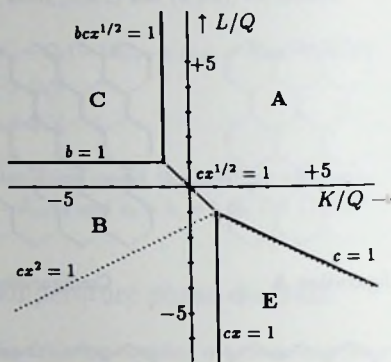


Fig. 4.7. The zero temperature phase diagram for the isotropic model with  $Q > 0$ . The letters A, B, C and E refer to the groundstates as given in Fig. 4.6. The boundary equations follow from equating their weights.

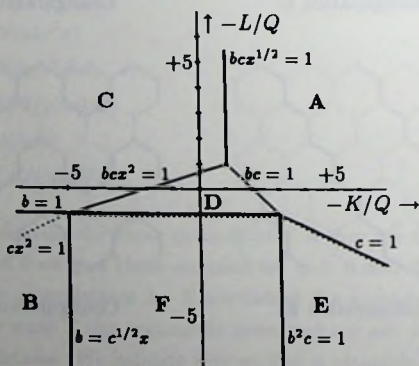


Fig. 4.8. The zero temperature phase diagram for the isotropic model with  $Q < 0$ . The letters A up to F refer to the groundstates as given in Fig. 4.6.



## 4.4 The free fermion conditions

A graph consists of a number of closed loops. These loops are not independent because they avoid each other and because weights are assigned to close encounters. When  $x_i = b_i = 1$  (the nearest neighbor Ising model) the loops can be made independent by a trick. This can be expressed in the form of a topological theorem, which was first conjectured by Feynman [7] and later proven by Sherman [15, 16]:

$$\sum_G I_G = \prod_p (1 + W_p) \quad (4.4.1)$$

On the lhs (left hand side) we have essentially the partition sum of (4.2.12), while on the rhs (right hand side) there is a product over all closed non-periodic paths  $p$  (any closed non-periodic trajectory that can be traced out by a random walker).  $W_p$ , the weight of path  $p$ , is given by

$$W_p = (-1)^{n_p} I_p = -(-1)^{t_p} I_p \quad (4.4.2)$$

with  $n_p$  the number of selfcrossings,  $t_p$  the winding number and  $I_p$  the Boltzmann weight of path  $p$ . Similar to (4.2.13) we have ( $x_i = b_i = 1$ )

$$I_p = \prod_{i=1}^3 c_i^{n_{c_i}} \quad (4.4.3)$$

with  $n_{c_i}$  the number of times  $c_i$  occurs in path  $p$ . Note that the set of paths is much larger than the set of loops, because self-overlap is allowed and because expanding the rhs of the topological theorem also generates products of paths that partly overlap. The sum of all terms (=products of paths) *without* overlapping bonds gives exactly the lhs of (4.4.1). So all other terms in the expansion must cancel. The sign introduced in the path weights takes care of that [7, 16]. This is the trick that decouples the paths and because the sign is determined by the winding number, it can be locally implemented by assigning a proper phase factor ( $\exp[\pm i\pi/6]$ ) to each turn in the path. The topological theorem is the foundation on which the whole method of Vdovichenko is based.

Thus the method of Vdovichenko replaces the sum over graphs by a sum over products of independent paths. For our model two complications arise in this crucial step. First, it is evident that in the path weights no close encounter weights  $x_i \neq 1$  may occur, otherwise the path cannot be interpreted as a random walker with local transition probabilities. Therefore we put for the Boltzmann weight of path  $p$

$$I_p = \prod_{i=1}^3 b_i^{n_{b_i}} c_i^{n_{c_i}} \quad (4.4.4)$$

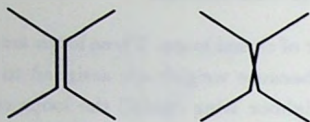


Fig. 4.9. The two new bond configurations for a vertex-pair that arise when working out the product over paths in the topological theorem (considering only the terms that do not cancel).

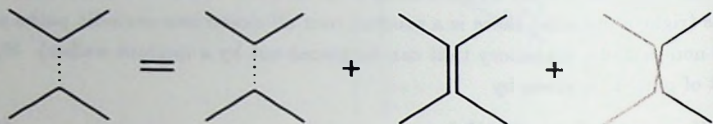


Fig. 4.10. The two new vertex-pair configurations, given in Fig. 4.9, can be considered as two additional path interpretations of a close encounter. The weight of a close encounter in a graph should be chosen equal to the sum of the weights of the three path interpretations of this close encounter, i.e. the diagram equation in this figure must hold (when close encounters have no bonds in common).

where the close encounter weights  $x_i$  have been left out. Second, when the bend weight  $b_i \neq 1$ , the trick above does not give a complete cancellation of all additional terms in the expansion of the rhs of (4.4.1). In appendix 4C we show that all terms with an overlap, consisting solely of a number of occurrences of the bond configurations, depicted in Fig. 4.9, do not cancel. So it appears that the topological theorem cannot be used for a wider class than the nearest-neighbor Ising model. But we will show below that the contributions from the additional paths can be interpreted as close encounter weights in the graphs and that under certain restrictions the topological theorem is exact even when  $x_i, b_i \neq 1$  (the two mistakes exactly compensate one another).

We will now try to establish the conditions under which the topological theorem is restored again. It is customary to speak of them as free fermion conditions because, when they apply, the model is equivalent to a free fermion field theory [5, 6]. Consider the diagram equation in Fig. 4.10. If in all graphs on the lhs of (4.4.1), each close encounter is replaced by the sum of the three diagrams, shown on the rhs of the

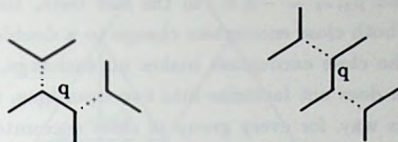


Fig. 4.11. Diagrams with two close encounters that have the bond  $q$  in common.

diagram equation, then all surviving terms of the rhs of (4.4.1) are generated. So, if there are  $k$  close encounters in a graph, there are  $3^k$  corresponding paths and the sum of their weights must be made equal to that of the graph. When the close encounters have no bonds in common we can do this by restricting the close encounter weights in the graph in accordance with the diagram equation of Fig. 4.10 :

$$c_i^2 x_i = c_i^2 + b_{i+1}^{\mu_i} b_{i+2}^{\nu_i} (c_{i+1}^2 c_{i+2}^2 b_i^2 - c_{i+1}^2 c_{i+2}^2) \quad (4.4.5)$$

with  $\mu_i, \nu_i = 0, \pm 2$  for  $i = 1, 2, 3$ . On the lhs we have the factor that the diagram, on the lhs of the diagram equation, contributes to the graph weight. Similar, the three terms on the rhs are the factors, that the corresponding diagrams on the rhs of the diagram equation, contribute to the path weights. In the term on the lhs there are two corner weights and a weight for the close encounter (only in the path weights close encounter weights are left out, not in the graphs). The first term on the rhs is  $c_i^2$  because the close encounter weight  $x_i$  cannot be incorporated in the path weights. The common factor  $b_{i+1}^{\mu_i} b_{i+2}^{\nu_i}$  in the last two terms arises because the change in bond configuration makes bends appear/disappear (for each outward bond there is an exchange, bend  $\longleftrightarrow$  no bend, because one of its neighboring bonds has changed its direction). The minus sign in the last term is due to the extra bond-crossing in the last diagram. So we obtain the free fermion conditions

$$x_i = 1 + b_{i+1}^{\mu_i} b_{i+2}^{\nu_i} z_i, \quad \mu_i, \nu_i = 0, \pm 2 \quad (4.4.6)$$

with

$$z_i = \left( \frac{c_{i+1} c_{i+2}}{c_i} \right)^2 (b_i^2 - 1) \quad (4.4.7)$$

When two close encounters share a bond (see Fig. 4.11), they interfere with each other. For instance, for the first diagram in Fig. 4.11 we have (similar to (4.4.6))

$$x_1 x_3 = 1 + b_2^{\mu_1} b_3^{\nu_1} z_1 + b_1^{\mu_2} b_2^{\nu_2} z_3 + b_1^{\mu_2} b_2^{\mu_1 + \nu_2 + 2} b_3^{\nu_1} z_1 z_3 \quad (4.4.8)$$

with  $\mu_1, \nu_2 = 0, \pm 2$  and  $\mu_2, \nu_1 = -2, 0$ . In the last term, the exponent of  $b_2$  has an extra 2 because, if both close encounters change to a double bond configuration, the bond shared by the close encounters makes no exchange, bend  $\longleftrightarrow$  no bend. Therefore the equation does not factorize into two equations, with forms similar to that of (4.4.6). In this way, for every group of close encounters lumping together, new free fermion conditions will be found. In spite of all these complications there exists a non-trivial solution. If we choose one direction as special (say direction  $i$ ) and for the other two directions we set

$$b_{i+1} = b_{i+2} = 1 \quad (4.4.9)$$

(4.4.6) becomes

$$x_i = 1 + z_i, \quad x_{i+1} = x_{i+2} = 1 \quad (4.4.10)$$

and all other free fermion conditions do factorize into products of (4.4.10), leaving a total of only five restrictions which can be satisfied in a non-trivial way. Translating (4.4.9) and (4.4.10) back to the Ising language with (4.2.19) to (4.2.21), we obtain

$$L_{i+1} = L_{i+2} = Q_{i+1} = Q_{i+2} = 0 \quad (4.4.11)$$

and

$$\exp(-4Q_i) = \frac{\cosh[2(K_i + L_i)]}{\cosh[2(K_i - L_i)]} \quad (4.4.12)$$

These are the free fermion conditions under which the topological theorem is valid. They reduce the model to the free fermion model on a square lattice, as studied by Fan and Wu [6]. This is shown in Fig. 4.12, with the non-zero coupling constants renamed as follows

$$\begin{aligned} K &= K_{i+1} & L &= K_i & Q &= Q_i \\ K' &= K_{i+2} & L' &= L_i \end{aligned} \quad (4.4.13)$$

In the dual language it means that the central bond of the vertex-pairs, depicted in Fig. 4.2, should be shrunk to a point (since they no longer correspond to a nearest neighbor interaction ( $K_i = L$ )), so that the vertex-pairs transform into the vertices of the eight-vertex model. Equation (4.4.12) can also be written as

$$\omega_i^{(1)} \omega_i^{(2)} + \omega_i^{(3)} \omega_i^{(4)} = \omega_i^{(5)} \omega_i^{(6)} + \omega_i^{(7)} \omega_i^{(8)} \quad (4.4.14)$$

which is the more usual form for the free fermion condition for this model.



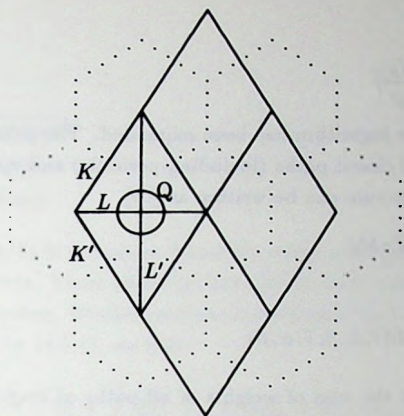


Fig. 4.12. When (4.4.11) holds and we rename the other coupling constants as in (4.4.12), the model is equivalent to the eight vertex model on a square lattice as shown in the figure for  $i = 1$ .

What are the results so far? There are no free fermion solutions in our model, other than the ones already found for the square lattice. But if the free fermion conditions are not met, wrong weights are given only to the close encounters in the graphs. So for any set of values of variables  $c_i$ ,  $b_i$  and  $x_i$  we can give an approximate solution that fully takes into account the corner- and the bend-weights, while the close encounter weights, dictated by the free fermion conditions (4.4.6), are in general different from the real close encounter weights given by (4.2.21). When the coupling constants are such (like in the ferromagnetic phase at low temperatures) that close encounters are rare, the result will be a good approximation (the free fermion approximation).

## 4.5 The free fermion solution/approximation

We will now continue with the weight (4.4.4) and use (4.4.1). On the basis of (4.4.1) it is easy to evaluate the partition sum. It is exact only when the topological theorem is exact, that is, when the free fermion conditions are satisfied. First we write the sum in a new form:

$$\sum_G I_G = \exp\left[\sum_p \ln(1 + W_p)\right]$$

$$= \exp\left[\sum_{p'} \frac{W_{p'}}{\tau_{p'}}\right] \quad (4.5.1)$$

In the second equation the logarithm has been expanded. The prime indicates that the sum now runs over *all* closed paths (including periodic) and  $\tau_{p'}$  is the period of path  $p'$ . Then the partition sum can be written as [16]

$$Z = \exp[E_0 + \sum_{l=0}^{\infty} \frac{1}{2l} \text{Tr} M_l] \quad (4.5.2)$$

with

$$\text{Tr} M_l = \sum_{\vec{r}} \sum_{\alpha} \sum_{\beta} M_l(\vec{r}, \alpha, \beta; \vec{r}, \alpha, \beta) \quad (4.5.3)$$

and  $M_l(\vec{r}, \alpha, \beta; \vec{r}, \alpha', \beta')$  is the sum of weights of all paths of length  $l$ , starting in  $\vec{r}$  where it arrives from direction  $\alpha$  and leaves in direction  $\beta$  and ending in  $\vec{r}$  where it arrives from direction  $\alpha'$  and leaves in direction  $\beta'$ . The sum in (4.5.3) is over all closed paths (also periodic) of length  $l$ , that can be traced out by a random walker. Therefore  $M_l$  can be constructed out of matrices  $M_2$  that describe a double step on the lattice. The advantage of using a two step matrix  $M_2$  as a basic building block instead of the one step matrix  $M_1$ , is that in using  $M_2$  there are only 3 directions of arrival and 2 for leaving, making  $M_2$  a  $6 \times 6$  matrix, while using  $M_1$ , there would be 6 directions of arrival, giving a  $12 \times 12$  matrix. (Note that all paths lengths are even.)

In a derivation similar to that given by Feynman [7] we find for the free energy density

$$\begin{aligned} f &\equiv -\frac{1}{N} \ln(Z) \\ &= -\sum_i (K_i + L_i + Q_i) - \frac{1}{8\pi^2} \int_0^{2\pi} dq_1 \int_0^{2\pi} dq_2 \ln[\det(I - \Lambda(\vec{q}))] \end{aligned} \quad (4.5.4)$$

with  $\Lambda$  the fourier transform of  $M_2$

$$\Lambda_{\alpha\beta, \alpha'\beta'}(\vec{q}) = \sum_{\vec{r}} \exp(i\vec{q} \cdot \vec{r}) M_2(\vec{0}, \alpha, \beta; \vec{r}, \alpha', \beta') \quad (4.5.5)$$

and  $I$  the diagonal matrix. For the matrix  $\Lambda$  we obtain

$$\Lambda_{\alpha\beta, \alpha'\beta'}(\vec{q}) = \begin{pmatrix} (\gamma\delta)^{-1}c_3^2 & (\gamma\delta)^{-1}b_1c_3\phi^{-1} & 0 & 0 & \gamma^{-1}b_2b_3\phi^2 & \gamma^{-1}b_2c_1\phi \\ \delta^{-1}b_1c_2\phi & \delta^{-1}c_2^2 & \gamma b_2b_3\phi^{-2} & \gamma b_3c_1\phi^{-1} & 0 & 0 \\ 0 & 0 & \gamma\delta c_3^2 & \gamma\delta b_2c_3\phi & \delta b_1c_2\phi^{-1} & \delta b_1b_3\phi^{-2} \\ \delta^{-1}b_1b_3\phi^2 & \delta^{-1}b_3c_2\phi & \gamma b_2c_1\phi^{-1} & \gamma c_1^2 & 0 & 0 \\ 0 & 0 & \gamma\delta b_1c_3\phi & \gamma\delta b_1b_2\phi^2 & \delta c_2^2 & \delta b_3c_2\phi^{-1} \\ (\gamma\delta)^{-1}b_2c_3\phi^{-1} & (\gamma\delta)^{-1}b_1b_2\phi^{-2} & 0 & 0 & \gamma^{-1}b_3c_1\phi & \gamma^{-1}c_1^2 \end{pmatrix} \quad (4.5.6)$$

with

$$b'_i = \sqrt{c_{i+1}c_{i+2}} b_i \quad (4.5.7)$$

$$\gamma = \exp(iq_1) \quad (4.5.8)$$

$$\delta = \exp(iq_2) \quad (4.5.9)$$

and  $\phi = \exp(-i\pi/6)$  is the phase factor for every counterclockwise turn and  $\phi^{-1}$  for every clockwise turn. These phase factors give to every path  $p$  a sign  $(-1)^{l_p}$  where  $l_p$  is the winding number. Working out the determinant that determines the free energy density, as given by (4.5.4), we find

$$\begin{aligned} \det(I - \Lambda(\vec{q})) &= \Omega_0^2 + \sum_{j=1}^3 [\Omega_j^2 - 2(\Omega_0\Omega_j - \Omega_{j+1}\Omega_{j+2})\cos(q_j) \\ &\quad + 4(\frac{\Omega_0 - 1}{b_j^2 - 1})\sin^2(q_j) \\ &\quad - 4[\Omega_j + c_j^2(\Omega_0 - 2)]\sin(q_{j+1})\sin(q_{j+2})] \end{aligned} \quad (4.5.10)$$

with

$$\Omega_0 = 1 + z_1 z_2 z_3 \quad (4.5.11)$$

$$\Omega_j = c_j^2(1 + z_j), \quad (4.5.12)$$

$q_3 = -(q_1 + q_2)$  and  $z_j$  is given by (4.4.7).

This completes the solution. It is exact only when (4.4.9) and (4.4.10) hold. But it also provides a good approximation when close encounters are rare, in the important configurations of both the exact and approximate partition sum. So we have a good low temperature approximation, for those phases, for which at least the groundstate and its lowest excitations, are free of close encounters. We consider this issue only for the isotropic case. Phase A (the phase that has configuration A as the groundstate) meets the necessary requirements. For configuration B we can use the symmetries, given by (4.2.5) to (4.2.7), to map it onto configuration A (with anisotropic coupling constants). After the symmetry transformation the free fermion approximation can be applied, and the result will be a good low temperature approximation (for the free energy) for phase B. So we conclude that in the low temperature regime, for the isotropic model, the phases A and B are described well. For high temperatures  $b_i \simeq 1$  so that  $x_i \simeq 1$  (see (4.4.6) and (4.4.7)) and the approximation will also be reasonable. For the other parts of the phase diagram, no such regions exist where the approximation is accurate for both high and low temperatures.

For the isotropic model with  $K \geq 0$  and  $L \geq Q \geq 0$  ( $b \geq 1, z \geq 0$ ) the free fermion conditions obey (see (4.4.6))

$$\begin{aligned} \prod_{j=1}^k x'_j &\leq (1 + b^4 z)^k \\ &\leq x^k [1 - (1 - x^{-1})(1 - e^{-4K-12Q})]^k \end{aligned} \quad (4.5.13)$$

with  $x$  given by (4.2.21) and  $x'_j$  the close encounter weights as they are dictated by the free fermion conditions, so that

$$1 \leq \prod_{j=1}^k x'_j \leq x^k \quad (4.5.14)$$

and the approximate partition sum is a strict lower bound.

## 4.6 The critical surface

The free energy density as given by (4.5.4) is analytic unless the determinant given by (4.5.10) is zero. In the next section we will show that for a continuous phase transitions  $q_1, q_2$  is 0 or  $\pi$  and eq(4.5.10) becomes

$$\begin{aligned} \det(I - \Lambda(\vec{q})) &= \delta_{q_1,0} \delta_{q_2,0} (\Omega_0 - \Omega_1 - \Omega_2 - \Omega_3)^2 \\ &+ \delta_{q_1,0} \delta_{q_2,\pi} (\Omega_1 - \Omega_0 - \Omega_2 - \Omega_3)^2 \\ &+ \delta_{q_1,\pi} \delta_{q_2,0} (\Omega_2 - \Omega_0 - \Omega_1 - \Omega_3)^2 \\ &+ \delta_{q_1,\pi} \delta_{q_2,\pi} (\Omega_3 - \Omega_0 - \Omega_1 - \Omega_2)^2 \end{aligned} \quad (4.6.1)$$

so that the critical surface is given by the condition that the largest  $\Omega$  is equal to the sum of the three others or

$$\Omega_0 + \Omega_1 + \Omega_2 + \Omega_3 = 2 \max(\Omega_0, \Omega_1, \Omega_2, \Omega_3) \quad (4.6.2)$$

This is the usual form for the critical condition of free fermion models [17]. For the exact free fermion solution, when (4.4.11) and (4.4.12) hold, (4.6.2) reduces to the critical condition for the free fermion solution of the square lattice as derived by Fan and Wu [6].

Part of the critical surface is clearly an artefact of the approximation. When we set  $z_i = -1$  for  $i=1,2,3$ , all  $\Omega$ 's are zero and (4.6.2) is satisfied. But then, according to (4.4.6), the weights  $x_i$  of close encounters with  $\mu_i = \nu_i = 0$  will be zero. So all configurations with close encounters of this type will have their weights reduced to



zero. This dramatic effect is solely due to the approximation since the real weights for these close encounters are always larger than zero.

If, for the isotropic case, we substitute (4.5.11) and (4.5.12) into the critical condition (4.6.2) we find for the critical surface

$$1 + z = \pm \sqrt{3} bc \quad (4.6.3)$$

(or  $z = -1$  which we have already exposed as an artefact of the approximation).

To find the singular behaviour of the free energy we expand it about  $q_i = 0, \pi (i = 1, 2)$ . For instance, when  $q_1 = q_2 = 0$  we have

$$f \sim \int_0^1 dq_1 \int_0^1 dq_2 \ln[(\Omega_0 - \Omega_1 - \Omega_2 - \Omega_3)^2 + uq_1^2 + vq_1q_2 + wq_2^2] \quad (4.6.4)$$

and close to the critical point  $(\Omega_0 - \Omega_1 - \Omega_2 - \Omega_3)$  is of the order  $O(T - T_c)$ . Performing the integration yields [18]

$$f \sim |T - T_c|^2 \ln |T - T_c| \quad (4.6.5)$$

and the specific heat will diverge logarithmically, unless  $(v^2 - 4uw) \rightarrow 0$  as  $T \rightarrow T_c$ , then a different critical behaviour will be found.

## 4.7 The surface free energy

The topological theorem is also valid when an interface contour, separating two coexisting phases, is present in the system [11]. The interface contour becomes just another path, decoupled from all others. Thus the surface free energy can be calculated between two coexisting phases (one of the phases A - F, coexisting with its opposite phase, for which the groundstate has all its spins reversed). In the argumentation below, we specialize to the case of phase A. For the other phases the argumentation would be analogous.

At  $T=0$  a mixed boundary condition, as depicted in Fig. 4.13, forces the two degenerate groundstates to coexist, separated by an interface contour. At  $0 < T < T_c$  a typical graph will consist of a number of closed paths and an additional interface contour, running all the way across the system. The proof of Calheiros et al. [11], that the topological theorem can also be applied in this situation, is roughly the following. The two bonds on the dual lattice that mark the change from (+) to (-) boundary spins are connected through a new bond (with weight 1, and no bend weight at this bond) outside the existing lattice (see Fig. 4.13). Applying the topological theorem to the lattice with the extra bond, gives rise to a new class of closed paths, that

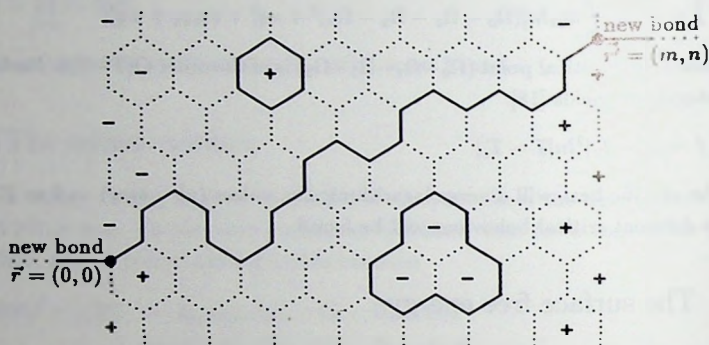


Fig. 4.13. A typical configuration for the ferromagnetic phase at  $0 < T < T_c$  when the boundary condition is chosen such that the spin up phase is forced to coexist with the spin down phase. An interface contour runs from  $\vec{r} = (0,0)$  on the left side of the system to  $\vec{r}' = (m,n)$  on the right side. The average tilt angle  $\theta$  of the interface is given by  $\tan\theta = n/m$ . The points  $\vec{r}$  and  $\vec{r}'$  are connected through a new bond, of which only the end parts are shown.

make use of this bond. All paths that use the new bond more than ones cancel each other, leaving as an additional set of paths all random walks starting in  $\vec{r} = (0, 0)$  and ending in  $\vec{r}' = (m, n)$ . Since all paths are decoupled [12] the partition sum  $Z_{+-}$ , with mixed boundary conditions as Fig. 4.13, can be written as

$$Z_{+-}(m, n) = Z_{++} \sum_{p'} W_{p'} \quad (4.7.1)$$

with  $Z_{++}$  the partition sum with an all (+) boundary. The sum runs over all paths  $p'$  (the interface contours) that start in  $(0, 0)$  and end in  $(m, n)$ . Then the surface free energy is [12, 13]

$$F_s(m, n) \equiv -\ln\left(\frac{Z_{+-}(m, n)}{Z_{++}}\right) = -\ln\left(\sum_{p'} W_{p'}\right) \quad (4.7.2)$$

Similar to the way we obtained the bulk free energy, the random walk formalism will give for the angle dependent free energy density in the thermodynamic limit

$$f_s(\theta) = -\frac{1}{\sqrt{1 + \tan^2(\theta)}} \lim_{m \rightarrow \infty} \frac{1}{m} \ln \left[ \int_0^{2\pi} \frac{dq_1}{2\pi} \int_0^{2\pi} \frac{dq_2}{2\pi} \exp(-i\vec{q} \cdot \vec{r}) \text{Tr}(I - \Lambda(\vec{q}))^{-1} \right] \quad (4.7.3)$$

with  $\vec{r} = (m, n)$  and  $\tan(\theta) = n/m$ . This expression can be evaluated with the steepest descend method. Note that the saddle point does not change (in the thermodynamic limit) when  $\text{Tr}(I - \Lambda(\vec{q}))^{-1}$  is replaced by  $[\det(I - \Lambda(\vec{q}))]^{-1}$  because

$$\text{Tr}(I - \Lambda(\vec{q}))^{-1} = \sum_{i=1}^6 (1 - \lambda_i)^{-1} = \frac{c(\vec{q})}{\det(I - \Lambda(\vec{q}))} \quad (4.7.4)$$

with  $\lambda_i$  the eigenvalues of the matrix  $\Lambda$  and

$$c(\vec{q}) = \sum_{i=1}^6 \prod_{j \neq i} (1 - \lambda_j(\vec{q})) \quad (4.7.5)$$

which is harmless at the saddle point. The steepest descent method yields [13]

$$f_s(\theta) = k_1 \cos(\theta) + k_2 \sin(\theta) \quad (4.7.6)$$

with

$$\begin{aligned} k_1 &= -i[q_1(\text{mod}\pi)] \\ k_2 &= -i[q_2(\text{mod}\pi)] \end{aligned} \quad (4.7.7)$$

and  $\vec{q}$  is the imaginary solution of  $\det(I - \Lambda(\vec{q})) = 0$  for which

$$\tan(\theta) = \frac{\partial_{\vec{q}_2} \det(I - \Lambda(\vec{q}))}{\partial_{\vec{q}_1} \det(I - \Lambda(\vec{q}))} \quad (4.7.8)$$

Note that the determinant that gives the bulk partition sum also completely determines the angle dependent free energy density.

For a continuous transition  $f_s \rightarrow 0$  as  $T \rightarrow T_c$ . Therefore  $k_1, k_2 \rightarrow 0$  which justifies putting  $q_1, q_2$  equal to 0 or  $\pi$  in our search for the critical surface.

Finally, we remark that the equilibrium crystal shape can be obtained as a Legendre transformation of the surface free energy [12, 13]. If  $Y(X)$  is the equilibrium crystal shape in cartesian coordinates then

$$X = \lambda k_y \quad (4.7.9)$$

$$Y = \lambda k_x \quad (4.7.10)$$

with  $k_x$  and  $k_y$  given by (4.7.7) and  $\lambda$  a constant controlling the volume of the crystal.

## 4.8 Summary

We have derived an approximate expression for the partition function of an Ising model on a triangular lattice with further-neighbor interactions, by extending the method of Vdovichenko which is based on an equivalence between a summations over graphs and a summation over products of unrestricted paths with only local weights. The equivalence is exact only when the free fermion conditions are satisfied and is approximate outside the free fermion region. For the general solution, the path sum gives approximate weights to the close encounters in the graphs. Outside the free fermion region, the close encounter weights so generated depend on the configuration and cannot be seen as a local shift of the  $z_i$ .

The approximation will be accurate when close encounters are rare. We have found these regions by deriving the zero temperature phase diagram for isotropic coupling constants. We find that for phase A and phase B (through the symmetry transformations (4.2.5) - (4.2.7)) close encounters are absent in the groundstate and in the lowest excitations (see Fig. 4.6). So we conclude that the phases A and B are described well in the low temperature phase by the free fermion approximation.

We have also calculated the approximate critical surface and given the surface free energies and equilibrium crystal shapes, using the extension of Vdovichenko's method by Calheiros et al.



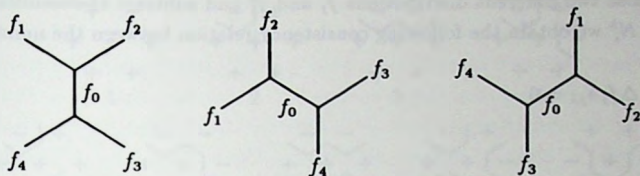


Fig. 4.14. For the vertex-pairs, the fractions  $f_i$  of the bonds that are assigned to it are indicated. A bond is part of five different vertex-pairs and the sum of the fractions of the bond, assigned to each of these vertex-pairs, is 1.

## Appendices

### 4A Consistency relations between the numbers of vertex-pairs

What are the relations between the numbers of vertex-pairs  $n_i(q)$  for an arbitrary configuration of the system? First, the total number of vertex-pairs with orientation  $i$  is given by the total number of sites

$$\sum_{q=1}^8 n_i(q) = N. \quad (4A.1)$$

Next, note that every bond or hole is part of five different vertex-pairs. We assign a fraction  $f_j$  of the bond (hole) to each of them, so that the bond (hole) becomes distributed over these five vertex-pairs. The most general distribution is shown in Fig. 4.14, with the condition that

$$\sum_{j=0}^4 f_j = 1 \quad (4A.2)$$

The total number of bonds  $N_i^b$  with orientation  $i$  for an arbitrary configuration is given by

$$\begin{aligned} N_i^b = & f_0(n_i(3) + n_i(4) + n_i(5) + n_i(6)) + \\ & f_1(n_{i+2}(2) + n_{i+2}(3) + n_{i+2}(5) + n_{i+2}(7)) + \\ & f_2(n_{i+1}(2) + n_{i+1}(4) + n_{i+1}(6) + n_{i+1}(7)) + \\ & f_3(n_{i+2}(2) + n_{i+2}(3) + n_{i+2}(6) + n_{i+2}(8)) + \\ & f_4(n_{i+1}(2) + n_{i+1}(4) + n_{i+1}(5) + n_{i+1}(8)) \end{aligned} \quad (4A.3)$$

If we choose two different distributions  $f_j$  and  $f'_j$  and subtract the resulting expressions for  $N_i^*$  we obtain the following consistency relation between the numbers  $n_i$ :

$$\sum_{j=0}^4 \Delta f_j s_{j,i} = 0 \quad (4A.4)$$

with

$$s_{0,i} = n_i(3) + n_i(4) + n_i(5) + n_i(6) \quad (4A.5)$$

$$s_{1,i} = n_{i+2}(2) + n_{i+2}(3) + n_{i+2}(5) + n_{i+2}(7) \quad (4A.6)$$

$$s_{2,i} = n_{i+1}(2) + n_{i+1}(4) + n_{i+1}(6) + n_{i+1}(7) \quad (4A.7)$$

$$s_{3,i} = n_{i+2}(2) + n_{i+2}(3) + n_{i+2}(6) + n_{i+2}(8) \quad (4A.8)$$

$$s_{4,i} = n_{i+1}(2) + n_{i+1}(4) + n_{i+1}(5) + n_{i+1}(8) \quad (4A.9)$$

and

$$\Delta f_j = f_j - f'_j \quad j = 0, \dots, 4 \quad (4A.10)$$

while the condition (4A.2) becomes

$$\sum_{j=0}^4 \Delta f_j = 0 \quad (4A.11)$$

We can use eq(4A.11) to eliminate one of the variables  $\Delta f_j$  in favour of the others in eq(4A.4) so that the remaining  $\Delta f_j$  are independent and we find the solution

$$s_{0,i} = s_{1,i} = s_{2,i} = s_{3,i} = s_{4,i} \quad (4A.12)$$

or equivalently

$$n_i(5) = n_i(6) \quad (4A.13)$$

$$n_i(7) = n_i(8) \quad (4A.14)$$

$$n_i(2) + n_i(7) = n_{i+1}(3) + n_{i+1}(5) = n_{i+2}(4) + n_{i+2}(5) \quad (4A.15)$$

In (4A.1) and (4A.13) to (4A.15) we have a total of 15 independent relations between the numbers  $n_i(q)$ . With these, the partition sum given by (4.2.3) can be rewritten in the form of (4.2.8) by eliminating  $n_i(1)$ ,  $n_i(3)$  and  $n_i(4)$  in favour of  $n_i(2)$ ,  $n_i(5) + n_i(6)$  and  $n_i(7) + n_i(8)$ , leaving only  $24-15=9$  independent variables:  $a_i$ ,  $b_i$  and  $c_i$ .

In appendix 4B we need the the relations between the numbers of vertex-pairs for the isotropic case where  $a_i = a$ ,  $b_i = b$  and  $c_i = c$  for  $i=1,2,3$ . Summing (4A.1) and

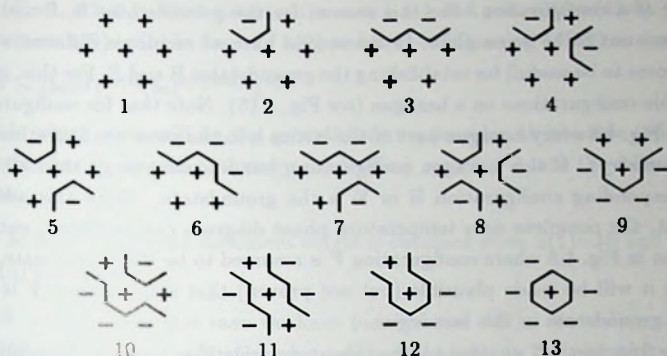


Fig. 4.15. All possible configurations on a hexagon (apart from symmetry).

(4A.13) to (4A.15) over  $i$  we obtain the consistency relations for the isotropic case :

$$\sum_{q=1}^8 n(q) = 3N \quad (4A.16)$$

$$n(3) = n(4) \quad (4A.17)$$

$$n(5) = n(6) \quad (4A.18)$$

$$n(7) = n(8) \quad (4A.19)$$

$$2n(2) + n(7) + n(8) = n(3) + n(4) + n(5) + n(6) \quad (4A.20)$$

## 4B The groundstates

We restrict ourselves to the isotropic case and set  $a_i = a$ ,  $b_i = b$  and  $c_i = c$  (or  $K_i = K$ ,  $L_i = L$  and  $Q_i = Q$ ) for  $i = 1, 2, 3$ . In Fig. 4.6 we show six configurations A to F that are likely candidates for the groundstates. Assuming that these configurations are all the possible groundstates, the Figs. 4.7 and 4.8 give the zero temperature phase diagrams for  $Q > 0$  and  $Q < 0$  respectively. Let us now try to prove the correctness of these phase diagrams. The argumentation consists of three parts. In the first part we try establish the zero temperature phase diagram, using the consistency relations between the numbers of vertex-pairs as derived in appendix 4A. The consistency relations take into account the connectivity properties of the vertex-pairs only to some extent. They are necessary but not sufficient conditions for the

existence of a configuration. For this reason, for the groundstates B, E and F, the prove turns out to be incomplete. In the second part we employ a different strategy which proves to be usefull for establishing the groundstates B and E. For this, consider all possible configurations on a hexagon (see Fig. 4.15). Note that for configuration B and E in Fig. 4.6 every hexagon part of the lattice is in the same configuration (apart from symmetry). If this hexagon configuration has a lower energy then all others, the corresponding configuration B or E is the groundstate. With this additional argument, the complete zero temperature phase diagram can be found, except for the region in Fig. 4.8 where configuration F is assumed to be the groundstate. In the last part it will be made plausible (but not proven) that configuration F is indeed the only groundstate in this last region.

In the first part, all we need are the consistency relations and an expression for the weight of a configuration. In appendix 4A we have derived that for every configuration the numbers of vertex-pairs  $n(q) = \sum_i n_i(q)$  must obey the relations

$$\sum_{q=1}^8 n(q) = 3N \quad (4B.1)$$

and

$$2n(2) + n(7) + n(8) = n(3) + n(4) + n(5) + n(6) \quad (4B.2)$$

Summing them we get

$$n(1) + 3n(2) + 2(n(7) + n(8)) = 3N \quad (4B.3)$$

From the expression for the partition sum given by (4.2.8), together with the definition (4.2.14), we see that the weight  $W$  of a configuration is proportional to

$$W \sim (cx^{1/2})^{2n(2)} b^{n(5)+n(6)} c^{n(7)+n(8)} 1^{n(1)+n(3)+n(4)} \quad (4B.4)$$

For every point of the phase diagram, we will have to look for the values of  $n(2)$ ,  $n(5)+n(6)$ ,  $n(7)+n(8)$  and  $n(1)+n(3)+n(4)$  that will maximize the weight  $W$ , given the restrictions posed by the consistency relations. Since the consistency relations are not sufficient to imply the existence of a configuration, we will end by examining the realizability of the proposed solutions.

Because  $W \sim 1^{n(3)+n(4)} b^{n(5)+n(6)}$ , while for the consistency relations only the total sum  $n(3)+n(4)+n(5)+n(6)$  is relevant and not how the total sum is broken up into  $n(3)+n(4)$  and  $n(5)+n(6)$ , it is favourable to set  $n(3)+n(4)=0$ , if  $b > 1$ , and to set



$n(5)+n(6)=0$ , if  $b < 1$ . First consider the case  $b > 1$  and put  $n(3)+n(4)=0$ . Then we can eliminate  $n(5)+n(6)$  in favor of  $n(2)$  and  $n(7)+n(8)$ , using (4B.2) and we have

$$W \sim (bcx^{\frac{1}{2}})^{2n(2)}(bc)^{n(7)+n(8)}1^{n(1)} \quad (4B.5)$$

To decide which state will be the groundstate we consider all possible orderings of the weights  $bcx^{1/2}$ ,  $bc$  and 1, thereby subdividing case  $b > 1$  into the following four subcases:

- (i)  $1 > bc, bcx^{\frac{1}{2}}$  : Then the maximum weight is obtained when  $n(1)=3N$  and all other  $n(q)$ 's are zero.
- (ii)  $bcx^{\frac{1}{2}} > bc, 1$  : In this case we have to maximize  $n(2)$ . According to (4B.3)  $n(2) \leq N$  and  $n(2)=N$  only when  $n(1)=n(7)+n(8)=0$ . Substituting this into (4B.2) we see that  $n(5)+n(6)=2N$  (remember we put  $n(3)+n(4)=0$ ). The only way to improve on this might be by making  $n(7) + n(8) > 0$  for  $bc > 1$ . But note that increasing  $n(7)+n(8)$  means decreasing  $n(2)$  (see (4B.3)) and at best we can exchange two vertex-pairs of type  $q=2$  for three vertex-pairs of type  $q=7,8$  which would make the weight of the configuration lower. Thus  $n(2)=N$ ,  $n(5)+n(6)=2N$  and all other  $n(q)$ 's zero gives the largest weight  $W$  for this case.
- (iii)  $bc > 1 > bcx^{\frac{1}{2}}$  : In this case we must maximize  $n(7)+n(8)$  and minimize  $n(2)$ . So we have  $n(7)+n(8)=3N/2$  and  $n(2)=0$  (see (4B.3)). Substituting this into (4B.2) we see that  $n(5)+n(6)=3N/2$ . Thus, having  $n(5)+n(6)=n(7)+n(8)=3N/2$  and all other  $n(q)$ 's zero, the weight  $W$  obtains its largest value.
- (iv)  $bc > bcx^{\frac{1}{2}} > 1$  : Again  $n(5)+n(6)=n(7)+n(8)=3N/2$  is a good option. Improvement is possible only by making  $n(2) > 0$  although it makes  $n(7) + n(8) < 3N/2$ . From (4B.3) we see that we can exchange three vertex-pairs of type  $q=7,8$  for two vertex-pairs of type  $q=2$ . If this increases the weight  $W$  [when  $(bcx^{1/2})^4 > (bc)^3$  that is when  $bcx^2 > 1$ ] we should eliminate all vertex-pairs of type  $q=7,8$  in this way, obtaining  $n(2)=N$  and  $n(5)+n(6)=2N$ . Thus, for  $bcx^2 < 1$ , we should take  $n(5)+n(6)=n(7)+n(8)=3N/2$  while for  $bcx^2 > 1$ , it is better to have  $n(2)=N$  and  $n(5)+n(6)=2N$ .

Next consider the case  $b < 1$  and put  $n(5)+n(6)=0$ . Then the weight  $W$  becomes

$$W \sim (cx^{\frac{1}{2}})^{2n(2)}(c)^{n(7)+n(8)}1^{n(1)+n(3)+n(4)} \quad (4B.6)$$

Note that the weight  $W$  has the same form as (4B.5), except that the factors  $b$  are missing, and that the consistency relations are unchanged, except that  $n(5)+n(6)$  is

replaced by  $n(3)+n(4)$ . Thus, analogous to the case  $b > 1$  the weight  $W$  obtains its maximum value when

$$(v) \quad 1 > c, cx^{\frac{1}{2}} : n(1)=3N.$$

$$(vi) \quad cx^{\frac{1}{2}} > c, 1 : n(2)=N \text{ and } n(3)+n(4)=2N.$$

$$(vii) \quad c > 1 > cx^{\frac{1}{2}} : n(3)+n(4)=n(7)+n(8)=3N/2$$

$$(viii) \quad c > cx^{\frac{1}{2}} > 1 : n(3)+n(4)=n(7)+n(8)=3N/2 \text{ for } cx^2 < 1 \text{ and } n(2)=N \text{ and } n(3)+n(4)=2N \text{ for } cx^2 < 1.$$

If all the optimal solutions would correspond to one of the six configurations A to F as given in Fig. 4.6, we would be done. But remember that the consistency relations do not imply the existence of a configuration. So it is not even clear that the solutions found for the above cases (i) - (viii) are actually realizable. Inspecting Fig. 4.6 we see that the solutions for the cases (i) up to (vi) are realized by configuration A,B,C or D. For case (vii) we found that the weight  $W$  reaches its maximum value when  $n(3)+n(4)=n(7)+n(8)=3N/2$ . This turns out not to be possible, as will be proven in the last part of this appendix. There we show that, if we are to avoid vertex-pairs of type  $q=1,2$  [ $n(1)=n(2)=0$  so that, according to (4B.2) and (4B.3),  $n(7)+n(8)=n(3)+n(4)+n(5)+n(6)=3N/2$ ] the maximum for  $n(3)+n(4)$  is only  $N/2$ . So it is not clear which state will be the groundstate here. For case (viii) the groundstate is configuration B if  $cx^2 > 1$  but if  $bx^2 < 1$  we stumble on the same problem as in case (vii).

The dotted line in the Figs. 4.7 and 4.8 mark the regions that belong to case (vii) and case (viii) for  $cx^2 > 1$ , the parts of the phase diagrams for which the groundstates are still unknown. In this second part of our argumentation we will prove the correctness of these parts of the phase diagrams as far as configuration B and E are concerned. Consider all possible configurations on a hexagon (see Fig. 4.15) and write the weight of a configuration of the system as a product of hexagon weights. Each site of the lattice will act as the central site of a hexagon ones. In this way every diamond (or vertex-pair) will be counted twice, so to each hexagon we will assign only half of its energy. There are only 13 different configuration possible on the hexagon (apart from symmetry) as shown in Fig. 4.15. The hexagon energy could be taken equal to the sum of the 6 diamonds that are present in it. Then there is no contribution from the K-interactions between the spins that lie on the boundary of the hexagon. To make the distribution of the total energy over the hexagons adjustable, we prefer to count the contribution of the K-interactions between the boundary spins

hexagon configuration	$\epsilon_h$	groundstate
1	$-(3K+3L+3Q)$	A
2	$-(2-f)K-L$	
3	$-K+L-Q$	E
4	$-(1-2f)K-L+Q$	
5	$-(1-2f)K+L+3Q$	D,F
6	$-fK+L$	
7	$fK+L$	
8	$-3(fK+L)$	C
9	$(1-2f)K+L+Q$	F
10	$K-L-Q$	
11	$K+L-3Q$	B
12	$(2-3f)K-L$	
13	$3(1-2f)K-3L+3Q$	C,D

Table 4.1. Hexagon configurations and their weights.

for a fraction  $f$ , and the contribution of the  $K$ -interactions that involve the central spin of the hexagon for a fraction  $(1-f)$  [ $0 \leq f \leq 1$ ]. The hexagon energy  $\epsilon_h$  is then given by

$$\epsilon_h = -\frac{1}{2} \left( K \sum_{j=1}^6 [f\sigma_j\sigma_{j+1} + (1-f)\sigma_0\sigma_j] + L \sum_{j=1}^6 \sigma_i\sigma_{j+2} + Q \sum_{j=1}^6 \sigma_0\sigma_j\sigma_{j+1}\sigma_{j+2} \right) \quad (4B.7)$$

where  $\sigma_0$  is the central spin and  $\sigma_j$  for  $j = 1, \dots, 6$  are the boundary spins. We have listed the hexagon energies  $\epsilon_h$  in Table 4.1 together with the groundstates in which these hexagons are present.

If we choose  $f=2/3$ , hexagon configuration 3 has the lowest energy in the entire region assigned to configuration E in both the phase diagrams of Figs. 4.7 and 4.8. This proves that it is the correct groundstate for this region. Next consider the two regions where configuration B is assumed to be the groundstate. Both regions are divided into two parts by the dotted lines. We are concerned with the parts where it has not yet been proved that configuration B is the groundstate. If we choose  $f=1/3$  (when  $Q > 0$ ) and  $f=2/5$  (when  $Q < 0$ ) we find that hexagon configuration 11 has the lowest energy for these parts. Thus configuration B is the groundstate in the whole region assigned to it in Figs 4.7 and 4.8.

	5	5	5	·	·	·	·	·	5	5	5	
<i>R</i>	9	9	9	9	·	·	·	·	·	9	9	9
	5	5	5	·	·	·	·	·	·	5	5	5
	5	5	5	·	·	·	·	·	·	5	5	5
	5	5	5	·	·	·	·	·	·	5	5	5
<i>R'</i>	5	13	5	13	·	·	·	·	·	5	13	5
	5	5	5	·	·	·	·	·	·	5	5	5

Fig. 4.16. Two rows *R* and *R'* each of which consists of three layers of overlapping hexagons. The numbers refer to the hexagon configurations in Fig. 4.15.



What remains is whether configuration F is correctly assigned in Fig. 4.8. This we can make plausible but not prove (since configuration F consists of two types of hexagon configurations we cannot use the same arguments as we used for configuration B and E above). If we consider only the configurations that can be constructed out of the last six vertex-pairs of Fig. 4.3 then, amongst these, configuration F is the state with the lowest energy in this last region. For then, only the hexagon configurations 5, 9 and 11 can occur and all possible states are obtained from stacking the rows  $R$  and  $R'$ , shown in Fig. 4.16. Thus only two possible groundstates can be constructed. If row  $R$  has the a lower energy then row  $R'$ , we should use only the rows  $R$  and we obtain configuration F and if rows  $R'$  has the lowest energy we stack only row  $R'$  and we obtain configuration D. In this last region, row  $R$  has the lowest energy so that configuration F is the best candidate for the groundstate. Since configuration F also has a larger energy then configuration B and E here, the first two vertex-pairs are probably not so important in this part of the phase diagram.

Finally, note that  $n(3)+n(4)=0$  for row  $R'$ . Therefore, if  $n(1)=n(2)=0$ ,  $n(3)+n(4)$  reaches its maximum value in configuration F where it is  $N/2$ , as was stated in the first part of our argumentation.

#### 4C The topological theorem

In this appendix we consider to what extent the terms, generated by expanding the rhs of (4.4.1), cancel. We will follow the arguments, given by Burgoyne [16], for the nearest neighbor Ising model on a square lattice. Apart from the difference in lattice (ours is hexagonal) we have the complication that the bend weights  $b_i \neq 1$ . We will not repeat the complete proof by Burgoyne but indicate only where slight modifications are needed.

First it is proved that the terms of the rhs with only single bonds add up to  $\sum I_G$ . Since we work on a hexagonal lattice, there are no crossings (that means no complications with different path interpretations for a crossing as one has for the square lattice) and the statement is trivially true.

Next consider all terms on the rhs which have overlapping bonds. Group together the terms that have the same bonds the same number of times. Consider one such group and choose a  $N$ -fold bond ( $N \geq 2$ ). Remove this  $N$ -fold bond so that each term of the group is a product of closed paths and a set of  $N$  path segments. The terms leading to the same path segments are collected in subgroups. For the nearest neighbor Ising model the terms within each subgroup cancel each other. This is proved

by induction. First it is shown that for a subgroup for which all path segments are *different*, the terms cancel. Second, it is shown that : if the terms within a subgroup cancel, then replacing one path segment (different from all others) by a path segment already present, results in a new subgroup (with less terms because not every way of connecting the path segments gives an existing term) that also cancels.

For the first part of the proof by induction consider a subgroup for which all path segments are different. Every way of connecting the segments (that is each term) corresponds to a permutation  $\pi$  that specifies which of the  $N$  neighbor bonds on one side of the  $N$ -fold bond is connected to which one on the other side. If the permutation is un(even) then the number of crossings at the  $N$ -fold bond is un(even). For the nearest neighbor Ising model the absolute weights of all the terms of the subgroup are equal, while their sign depends on the sign (even or uneven) of the permutation. Because half the permutations are un(even) the sum of the terms is zero. In our case not all the terms have the same absolute weight because  $b_i \neq 1$  (see Fig. 4.9). But when two neighbor bonds, on the same side of the  $N$ -fold bond are parallel (say bond number  $i$  and  $j$ ) then the terms corresponding to the permutations  $\pi$  and  $\pi' = (i, j)\pi$ , cancel. Here  $(i, j)$  is a transposition of  $i$  and  $j$ . When  $N \geq 3$  there are always two parallel neighbor bonds. So, only when  $N = 2$  and the configuration of the neighboring bonds is as in Fig. 4.9 there will be no cancelation.

In the second part of the proof, the cancellation of the terms within a subgroup where some of the segments are equal, is derived from the cancellation of a subgroup where one of those equal segments (say  $q_1$ ) is replaced by one (say  $q_0$ ) that is different from all others. If  $q_0$  is choosen such that the two terminal bonds (the bonds that border on the  $N$ -fold bond) are equal to the terminal bonds of  $q_1$ , this second part of the proof remains valid in our case. Note that the terms that did not cancel in the first part of the proof do not impair the induction process since they are not needed in the second part (because there are no terms with just two equal path segments).

## References

- [1] L. Onsager, *Phys. Rev.* **65**, 117 (1944).
- [2] L. J. de Jongh and A. R. Miedema, *Experiments on simple magnetic model systems*, (Taylor and Francis, London, 1974).
- [3] B. Widom, *J. Chem. Phys.* **84**, 6943 (1986).
- [4] M. Schick and W. Shih, *Phys. Rev. B* **34**, 1797 (1986).

- [5] C. A. Hurst and H. S. Green, *J. Chem. Phys.* **33**, 1059 (1960); C. A. Hurst, *J. Math. Phys.* **7**, 305 (1966).
- [6] C. Fan and F. Y. Wu, *Phys. Rev.* **179**, 560 (1969); *Phys. Rev. B* **2**, 723 (1970).
- [7] R. P. Feynman, *Statistical Mechanics*, (Benjamin/Cummings, Reading, MA, 1972), pp 136-150.
- [8] N. V. Vdovichenko, *Zh. Eksp. Teor. Fiz* **47**, 715 (1964) [*Sov. Phys. JETP* **20**, 477 (1965)].
- [9] G. V. Ryazanov, *Zh. Eksp. Teor. Fiz* **59**, 1000 (1970) [*Sov. Phys. JETP* **32**, 544 (1971)].
- [10] F. Wiegel, *Phys. Lett.* **41A**, 225 (1972).
- [11] F. Calheiros, S. Johannesen and D. Merlini, *J. Phys. A* **20**, 5991 (1987).
- [12] M. Holzer, *Phys. Rev. Lett.* **64**, 653 (1990); *Phys. Rev. B* **42**, 10570 (1990).
- [13] Y. Akutsu and N. Akutsu, *Phys. Rev. Lett.* **64**, 1189 (1990).
- [14] F. Y. Wu, *J. Math. Phys.* **15**, 687 (1974).
- [15] S. Sherman, *J. Math. Phys.* **1**, 202 (1960); *J. Math. Phys.* **4**, 1213 (1963).
- [16] P. N. Burgoyne, *J. Math. Phys.* **4**, 1320 (1963).
- [17] J. E. Sacco and F. Y. Wu, *J. Phys. A* **8**, 1780 (1975).
- [18] C. S. Hsue, K. Y. Lin and F. Y. Wu, *Phys. Rev. B* **12**, 429 (1975).

## Chapter 5

# The Drift Velocity in Reptation Models for Electrophoresis

### 5.1 Introduction

Electrophoresis is a widely used method in biology to separate charged polymers, e.g. DNA molecules, according to length. The polymers are inserted into a gel (itself a neutral polymer network in a solution) and pulled through the gel by an applied electric field. For weak fields and not too long polymers the mobility is inversely proportional to the polymer's length. For longer polymers or larger field strengths, the mobility becomes length independent and the resolution is lost [1].

The motion of the polymers is highly restricted by the polymer network (the gel) in which they are embedded. For dense polymer systems Edwards and Doi [2] envisaged each polymer as confined to a tube, formed by the surrounding polymers. De Gennes [3] assumed that a polymer within a tube moves by diffusion of stored length —local accumulations of the polymer in the form of loops— along the polymer chain (reptation). The tubes themselves are assumed to be static since the motion of the confining network is slow compared to that of a single polymer.

Lerman and Frisch [4] pointed out that these ideas can explain the length separation which is observed in electrophoresis. They extended the scaling arguments of de Gennes to include the self-avoiding walk character of the tubes and found that the drift velocity  $v$  scales with the polymer's length  $N$  as  $v \sim N^{2\nu-2}$ . Here  $\nu$  is the scaling exponent for the average end-to-end distance  $R$  :  $\langle R^2 \rangle \sim N^{2\nu}$ . For dimension  $d = 3$ ,  $\nu \approx 3/5$  and for a random walk  $\nu = 1/2$  in all dimensions.

As the polymer creeps through the gel, it slowly renews the tube by occupying new gel pores at one end of the tube and abandoning tube sections at the other end. The



head of the polymer, that chooses the new tube segments, is biased by the electric field. Thus the tubes become oriented in the field direction. Assuming biased-random-walk configurations for the tubes it follows that  $v \sim (E/N)(1 + cE^2N)$  with  $E$  the electric field strength and  $c$  a constant [5, 6]. The orientation contribution is third order in the field. When the third order term dominates the drift velocity becomes length independent as was observed in experiments.

Longer polymers can still be separated, using a recently developed pulsed field technique [7, 8, 9, 10, 11]. The pulse cycle in this technique consists of a field pulse in one direction followed by a shorter pulse in the reversed direction. When applied to polymers of a given length  $N$ , a minimum in the drift velocity is observed as a function of the cycle duration. The cycle duration  $t_{\min}$  at which the minimum occurs is proportional to  $N$ . An even better length separation is obtained when the field direction is periodically changed by 90 or 120 degrees.

To explain the pulsed field experiments, fluctuations in the tube length are important. Although a consequence of the reptation idea, these fluctuations were discarded in the early models [5] that focused on the effect of tube orientation on the drift velocity. In these models it was assumed that the polymer-as-a-whole slides through the tube under the influence of the total tangential force exerted by the electric field. Without a variable number of length defects, the tube length is fixed. New models were invented to allow the fluctuations in the tube length. The polymer was represented by a bead-spring chain [9] (a Rouse chain with entropic spring constants) or the tube was viewed as a connected chain of gel pores, each capable of housing more than one repton [10, 11]. A repton is a piece of the polymer of the order of the persistence length.

In experiments [12] and in computer simulations of the new models [9, 10, 11, 13], the following cycle was observed in the polymer's motion. Local bunching (a local accumulation of length defects) leads to a partial or complete collapse of the polymer when the trailing end of the polymer catches up with the slower moving bunched part. Out of this collapsed state forms a  $\Lambda$ -shaped configuration as both ends of the polymer move simultaneously in the same direction (the field direction). The polymer, hooked around a gel obstacle, first fully stretches and then starts sliding off the obstacle with the longer end being pulled more strongly than the shorter end. When free from the obstacle, the stretched chain relaxes and the cycle can begin again.

Of course such a cycle of motion would be strongly disrupted by a pulsed field with a comparable cycle duration. Usually the dip in the drift velocity as a function

of the cycle duration is explained as follows [8, 9, 10, 11]. Either, in the collapsed state a polymer is trapped in a nearly zero-velocity state, in which it looks like a ball that constantly unravels and rewinds ( $\Lambda \rightarrow o \rightarrow V \rightarrow o \rightarrow \Lambda \rightarrow \dots$ ). Or more general, an asymmetry in the tube configurations is observed (like hooks at the tail) and a resulting asymmetry in the polymer distribution within the tube, which must be reversed when the field is reversed. The time  $t_{rev}$  after which the steady state behavior is restored is proportional to  $N$ , the same length dependence as for the cycle duration  $t_{min}$  at which the dip in the mobility occurs.

The model investigated in this paper was developed by Rubinstein and Duke [10, 14] to study the effects of the length fluctuations of the tube. It is a strict implementation of the original reptation idea by de Gennes, describing the motion as driven diffusion of stored length along the chain. Space is discretized into cells, such that neighboring cells are ordered in the field direction (see fig. 5.1). The cells represent the gel pores and their size equals the average pore size. The polymer is seen as a string of charged reptons, i.e. pieces of the polymer of the order of the persistence length. Each of the cells that make up the channel (tube) is occupied by at least one repton, expressing the connectivity of the polymer. There is no upper limit to the amount of reptons that may occupy a single cell. More than one repton in a cell means that the polymer has stored some of its length there. The excess reptons can move from cell to cell without mutual tension, according to transition probabilities (biased in the field direction), allowing the stored length to diffuse along the channel. In the interior of the chain the motion of the reptons is confined to the tube. Only through the movements of its endpoints can the polymer retreat from a cell or occupy a new cell. In this way the polymer can renew the channel configuration. The model makes the assumptions that there is no free sliding around gel fibers and that there are no lateral excursions of the chain through the sides of the tube. This limits its validity to low field strengths.

We will extend the model with the additional rule that no more than two reptons may occupy the same cell. This makes the model more realistic because in experiments the average pore size is of the same order as the persistence length. The reptons will hinder one another in their movements (excluded volume effects within a channel) and the mobility of the polymer is reduced. In the language of occupation numbers, introduced in the next section, the Rubinstein-Duke model (RD-model), allowing an arbitrary number of reptons in a cell, displays Bose statistics while the modified version, with 0 or 1 movable reptons per cell, displays Fermi statistics. In the following we will refer to the two versions of the model as the boson and fermion

case or the RD(b) and RD(f)-model.

All the effects mentioned above have been observed in computer simulations of the RD(b)-model [10]. Since the model is probably the simplest realization of reptation it is worth while to try and solve it analytically. Widom et al. [15] have worked out an explicit statistical mechanical formulation of the model. But solving it is difficult due to the endpoint motion (which couples the different channels) and because of the strong correlations which extend from one end of the chain to the other. In order to simplify the mathematics we will study mainly the model with periodic boundary condition. The periodic boundary condition decouples the transport of reptons along the chain from the endpoint motion. The results strongly suggest that it is transport of reptons alone, that determines the drift velocity to linear order in the field and the diffusion constant can be calculated exactly for both versions of the RD-model. The more intriguing properties of the model are a consequence of the endpoint motion and will not be addressed here.

Here follows an outline of this chapter. In the first two sections the model is introduced and the master equation governing the model is given. In the stationary state, the solution is characterized by the constant currents of reptons within the different channels and in the third section an expression for the drift velocity is given in terms of these currents. The full stationary state solution of the master equation for the RD(b)-model and an expansion of the drift velocity to third order in the applied electric field are presented in section 5.4. In section 5.5 the drift velocity for the RD(f)-model is calculated to linear order in the field by taking moments of the master equation. For small fields and long polymers there exists a scaling regime and in section 5.6 the scaling function is computed by a numerical finite-size-scaling analysis for the boson case. In the last section the effect of the periodic boundary condition on the value of the diffusion constant and the behavior of the scaling function is discussed, on the basis of numerical calculations done on both models with free endpoint motion.

## 5.2 The Rubinstein-Duke model

In the RD-model, in arbitrary dimension  $d$ , space is discretized into  $d$ -dimensional cubes (cells) with edge length  $a$ . The electric field is along the direction of the body diagonal of the cubes such that neighboring cells are ordered in the direction of the field. The model is made one-dimensional by projecting the cell positions of the reptons onto the field direction. i.e. a polymer configuration is specified by giving the



projected cell positions  $x_i$  of the reptons which make up the polymer. Alternatively we can specify the configuration of a polymer of  $N$  reptons by its  $(N - 1)$  internal coordinates, which are the differences

$$y_i = (x_{i+1} - x_i)/a' \quad (5.2.1)$$

and its center of mass position

$$x = \frac{1}{N} \sum_{i=1}^N x_i \quad (5.2.2)$$

(see Fig. 5.2). Neighboring reptons lie within the same or in neighboring cells. So, for

$$a' = a/\sqrt{d} \quad (5.2.3)$$

the internal coordinates can only assume the values 1, -1 or 0 depending on whether the next repton is in an upward or downward cell or in the same cell as the previous repton. When there are two or more reptons in a cell, the first and last can move to an adjacent cell that is already occupied by a repton. In this way the reptons will diffuse along the channel already traced out by the polymer. The two reptons at the end of the chain have more options for making a move. When the first (last) cell of the channel is occupied by just one repton, the end repton can only move by retreating into the deeper lying cell of the channel, making the channel shorter. When there are more reptons in the the cell, the end repton can occupy a new cell, not yet part of the channel and can do so by choosing one of the  $d$  upward or  $d$  downward moves. This will make the channel longer. So, it is through the movements of the end reptons that the polymer can renew the cell configuration of the channel.

The transition probabilities  $W(y|y')$  for a transition from state  $y'$  to state  $y$  is  $wB$  when it involves an upward move and  $wB^{-1}$  for a downward move. Here  $w$  is a hopping frequency for the reptons and  $B$  is a bias due to the applied electric field; it is the Boltzmann factor for the change in electric potential energy

$$B = \exp(\epsilon/2) = \exp(eEa/2k_B T) \quad (5.2.4)$$

When there is no move connecting state  $y'$  to state  $y$ ,  $W(y|y')$  is zero.

In the RD(f)-model we restrict the maximum number of reptons that may occupy a cell to two, since the possibility of storing large numbers of reptons in one cell is clearly unphysical. Accordingly all moves that give rise to forbidden configurations are also excluded.



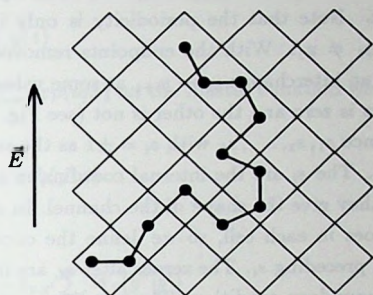
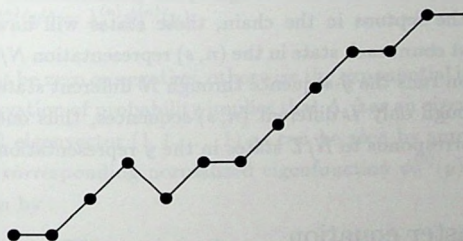


Fig. 5.1. Typical configuration of the chain of reptons on a 2-dimensional lattice. The internal coordinates of the state are given by  $y = (0, 1, 1, -1, 1, 0, 1, 1, 1, 0, 1)$ .



$$\begin{aligned}
 y &= \{ \quad 0 \quad 1 \quad 1 \quad -1 \quad 1 \quad 0 \quad 1 \quad 1 \quad 1 \quad 0 \quad 1 \quad 0 \quad \} \\
 s &= \{ \quad 1 \quad 1 \quad -1 \quad 1 \quad \quad 1 \quad 1 \quad 1 \quad \quad 1 \quad \quad \} \\
 n &= \{ \quad 2 \quad 0 \quad 0 \quad 0 \quad \quad 1 \quad 0 \quad 0 \quad \quad 1 \quad \quad \}
 \end{aligned}$$

Fig. 5.2. The two representations  $y$  and  $(n, s)$  for the configuration of Fig. 5.1

Periodic boundary conditions substantially simplify the problem. We add one extra internal coordinate  $y_N = x_{N+1} - x_N$  and then repeat by identifying  $y_{N+1} = y_1$ ,  $y_{N+2} = y_2$  etc. Note that the periodicity is only in the internal coordinates and in general  $x_{N+1} \neq x_1$ . With the endpoints removed, every move changes the configuration  $y$  by an interchange  $y_i \leftrightarrow y_{i+1}$  at some value of  $i$ , where one of the two internal coordinates is zero and the other is not (see Fig. 5.2). This makes it useful to define the sequence  $s_1, s_2, \dots, s_L$  with  $s_i = \pm 1$  as the subset of  $y_1, \dots, y_N$  which are different from zero. The  $s_i$  are the internal coordinates of the repton pairs lying in neighboring cells, they give the shape of the channel. In addition we need to specify the number of zeroes in each cell, so we define the occupation numbers  $n_i$  as the number of zero  $y$ 's, preceding  $s_i$ . The zeroes after  $s_L$  are included in  $n_1$  in accordance with the periodic boundary condition. The transition rules imply that the sequence  $s_i$  is an invariant of motion, as is the total number of zeroes

$$\sum_{i=1}^L n_i = N - L, \quad (5.2.5)$$

and the dynamics is confined to redistributing the zeroes over the cells.

Because of the way we count  $n_1$ , there are states which are distinct in the  $y$  representation and yet have the same  $(n, s)$  representation. Since these states can be transformed into one another through cyclic permutations, corresponding to a renumbering of the reptons in the chain, these states will have the same weight. Therefore we must count each state in the  $(n, s)$  representation  $N/L$  times. (Repeated cyclic permutation runs the  $y$ -sequence through  $N$  different states while at the same time it runs through only  $L$  different  $(n, s)$ -sequences, thus one state in the  $(n, s)$  representation corresponds to  $N/L$  states in the  $y$  representation.)

### 5.3 The master equation

The master equation for the joint probability  $P(x, y; t)$  in the  $y$  representation is

$$\frac{dP(x, y; t)}{dt} = \sum_{y'} [W(y|y')P(x - \Delta(y, y'), y'; t) - W(y'|y)P(x, y; t)] \quad (5.3.1)$$

with  $\Delta(y, y') = \pm a'/N$  depending on whether going from state  $y'$  to state  $y$  involves an upward (+) or a downward (-) move. For the fermion case the sum over states is more restricted and the matrix  $W(y|y')$  is more sparse than for the boson case.

The dependence on the center of mass position  $x$  is solved by the Fourier transformation

$$P_q(y; t) = \sum_x e^{iqx} P(x, y; t) \quad (5.3.2)$$

Performing the operation  $\sum_x \exp(iqx)$  on the master equation we find for the fourier components

$$\frac{dP_q(y, t)}{dt} = \sum_{y'} \Lambda_q(y, y') P_q(y', t) \quad (5.3.3)$$

with

$$\Lambda_q(y, y') = W_q(y|y') - \delta_{y, y'} \sum_{y''} W_0(y''|y') \quad (5.3.4)$$

where  $\delta$  is the Kronecker-delta and

$$W_q(y|y') = W(y|y') \exp[iq\Delta(y, y')] \quad (5.3.5)$$

The formal solution of (5.3.3) is given by

$$P_q(y, t) = \sum_n A_{n,q} \psi_q^{(n)}(y) \exp(\lambda_q^{(n)} t) \quad (5.3.6)$$

with  $\lambda_q^{(n)}$  and  $\psi_q^{(n)}$  the eigenvalues and eigenfunctions of  $\Lambda_q$ :

$$\sum_{y'} \Lambda_q(y, y') \psi_q^{(n)}(y') = \lambda_q^{(n)} \psi_q^{(n)}(y) \quad (5.3.7)$$

All eigenvalues must be zero or negative, otherwise the exponential in (5.3.6) will grow indefinitely. Conservation of probability implies that  $\Lambda_q$  has an eigenvalue  $\lambda_q^{(0)} = 0$  for  $q = 0$  (with the left eigenvector  $(1, 1, \dots, 1)$  as can be seen by summing (5.3.4) over  $y$  for  $q = 0$ ). The corresponding normalized eigenfunction  $\psi_0^{(0)}(y)$  is the stationary solution  $P_0(y)$  given by

$$\sum_y W(y'|y) P_0(y) = \sum_{y'} W(y|y') P_0(y') \quad (5.3.8)$$

since the other contributions to  $P(x, y; t)$  decay exponentially with time.

When we impose a periodic boundary condition the dynamics is reduced to changes in the cell occupation numbers  $n_i$ . The  $s$ -sequence is invariant i.e. the different channels are not coupled and we have independent solutions for each  $s$ . Therefore we can write

$$P_0(y) = \psi(s) P(n, s) / ([\sum_n P(n, s)] [\sum_s \psi(s)]) \quad (5.3.9)$$

with  $\psi(s)$  an arbitrary positive amplitude and  $P(n, s)$  the solution of the master equation.

The probability for a zero moving from cell  $i$  to cell  $i+1$  is  $wB^{s_i}$  and for the reverse process it is  $wB^{-s_i}$ . Thus, for the RD(b)-model with periodic boundary conditions, the master equation (5.3.8) reads

$$\begin{aligned} \sum_{i=1}^L [\theta(n_i)wB^{s_i} + \theta(n_{i+1})wB^{-s_i}]P(n_1, \dots, n_L) = \\ \sum_{i=1}^L [\theta(n_i)wB^{-s_i}P(n_1, \dots, n_i-1, n_{i+1}+1, \dots, n_L) + \\ \theta(n_{i+1})wB^{s_i}P(n_1, \dots, n_i+1, n_{i+1}-1, \dots, n_L)] \end{aligned} \quad (5.3.10)$$

where the step functions

$$\theta(n_i) = \begin{cases} 0, & n_i = 0 \\ 1, & n_i \geq 1 \end{cases} \quad (5.3.11)$$

make sure that the occupation numbers do not become negative; they select the possible moves. (In the master equations for the periodic chains we suppress the  $s$ -dependence of the probabilities  $P(n, s)$ .)

For the RD(f)-model  $n_i = 0, 1$  and the master equation becomes

$$\begin{aligned} \sum_{i=1}^L [n_i(1-n_{i+1})wB^{s_i} + n_{i+1}(1-n_i)wB^{-s_i}]P(n_1, \dots, n_L) = \\ \sum_{i=1}^L [n_i(1-n_{i+1})wB^{-s_i} + n_{i+1}(1-n_i)wB^{s_i}] \\ P(n_1, \dots, n_{i-1}, n_i \longleftrightarrow n_{i+1}, n_{i+2}, \dots, n_L) \end{aligned} \quad (5.3.12)$$

where the factors  $n_i(1-n_{i+1})$  and  $n_{i+1}(1-n_i)$  select the possible moves i.e. they make sure that there is a zero to move and that the receiving cell is not yet occupied. After a zero has been exchanged between cell  $i$  and cell  $i+1$  the change in the occupation numbers is simply an interchange of the numbers  $n_i$  and  $n_{i+1}$  which we denoted in (5.3.12) by  $n_i \longleftrightarrow n_{i+1}$ .

## 5.4 The drift velocity

The drift velocity  $v$  is defined as

$$v \equiv \frac{d}{dt} \langle x \rangle = \sum_y \sum_x x \frac{dP(x, y; t)}{dt} \quad (5.4.1)$$



If we substitute for  $dP(x, y; t)/dt$  the expression given by the master equation (5.3.1) we find that

$$v = \sum_y v(y) P_0(y; t) \quad (5.4.2)$$

is the average of the velocity

$$v(y) = \sum_{y'} \Delta(y', y) W(y'|y) \quad (5.4.3)$$

in state  $y$ . When the periodic boundary condition is imposed and we restrict ourselves to the stationary state, we may use (5.3.9) and write

$$v = \sum_L \sum_{s_1, \dots, s_L} \psi(s) v(s) / \sum_L \sum_{s_1, \dots, s_L} \psi(s) \equiv \langle v(s) \rangle, \quad (5.4.4)$$

with

$$v(s) = \sum_n v(n, s) P(n, s) / \sum_n P(n, s) \equiv \langle v(n, s) \rangle_n \quad (5.4.5)$$

For the boson case the velocity in state  $(n, s)$  is given by

$$v_b(n, s) = \frac{a'w}{N} \sum_{i=1}^L [\theta(n_i) B^{s_i} - \theta(n_{i+1}) B^{-s_i}] s_i \quad (5.4.6)$$

The first term under the summation gives the contribution of the reptons moving from cell  $i$  to cell  $i + 1$ . The step function checks whether there is a movable repton present in cell  $i$ . When  $s_i = +1$  the move is upwards, contributing a term  $a'wB/N$  to  $v_b(n, s)$ , in accordance with (5.4.3), and when  $s_i = -1$  the move is downwards, contributing a term  $-a'wB^{-1}/N$ . Likewise the second term gives the contribution of the reptons moving from cell  $i + 1$  back to cell  $i$ . If we substitute (5.4.6) into (5.4.5) we find

$$v_b(s) = \frac{a'w}{N} \sum_{i=1}^L J_{b,i}(s) s_i \quad (5.4.7)$$

with

$$J_{b,i}(s) = w[\langle \theta(n_i) \rangle_n B^{s_i} - \langle \theta(n_{i+1}) \rangle_n B^{-s_i}] \quad (5.4.8)$$

$J_{b,i}(s)$  is the net flow of reptons (zeroes) from cell  $i$  to cell  $i + 1$ . It is the constant current of reptons that runs through the periodic chain and thus  $J_{b,i}(s)$  is independent of  $i$  as can be seen as follows. The master equation for the periodic chain has the form

$$\frac{dP}{dt} = \text{gain term} - \text{loss term} \quad (5.4.9)$$

Multiplying  $dP/dt$  by  $n_i$  and summing over  $n$  gives

$$\sum_n n_i \frac{dP}{dt} = \frac{d}{dt} \langle n_i \rangle_n = J_i(s) - J_{i-1}(s) \quad (5.4.10)$$

In the stationary state  $dP/dt = 0$  and  $J_{j-1}(s) = J_j(s) = J(s)$ . Indeed, if we perform the operation  $\sum_n n_j$  on the master equation for the stationary state, i.e taking the first moment of (5.3.10), we find

$$J_{b,i-1}(s) = J_{b,i}(s) \quad (5.4.11)$$

with  $J_{b,i}(s)$  given by (5.4.8). Thus (5.4.7) becomes

$$v(s) = a' \frac{S}{N} J(s) \quad (5.4.12)$$

with

$$S = \sum_{i=1}^L s_i \quad (5.4.13)$$

the end-to-end distance of the polymer in the direction of the electric field.

Similarly we find for the fermion case

$$v_f(n, s) = \frac{a'w}{N} \sum_{i=1}^L [n_i(1 - n_{i+1})B^{s_i} - n_{i+1}(1 - n_i)B^{-s_i}] s_i, \quad (5.4.14)$$

where now the factors  $n(1 - n)$  select the movable reptons. Again the average of the terms in (5.4.14) between [ ] is independent of the cell  $i$  and  $v_f(s)$  is given by (5.4.12) with

$$J_f(s) = w[\langle n_i(1 - n_{i+1}) \rangle_n B^{s_i} - \langle n_{i+1}(1 - n_i) \rangle_n B^{-s_i}] \quad (5.4.15)$$

the expression for the repton current in the fermion case.

## 5.5 The solution of the master equation for the boson case

The master equation for the boson case (5.3.10) can be solved by the ansatz

$$P(n, s) = \prod_{i=1}^L p_i^{n_i} \quad (5.5.1)$$

Inserting this ansatz into the master equation yields

$$\sum_{i=1}^L \theta(n_i) [wB^{s_i} + wB^{-s_{i-1}}] = \sum_{i=1}^L \theta(n_i) [wB^{-s_i} (p_{i+1}/p_i) + wB^{s_{i-1}} (p_{i-1}/p_i)] \quad (5.5.2)$$

which is obviously fulfilled when the parts between [ ] are equal for all  $i$ , that is, when the  $p_i$  satisfy

$$p_{i-1}wB^{s_{i-1}} - p_iwB^{-s_{i-1}} = p_iwB^{s_i} - p_{i+1}wB^{-s_i} \quad (5.5.3)$$

This is the equivalent of (5.4.11), with (5.4.8) [or (5.4.15)] as the current, when there is only one zero hopping through the chain. It allows us to express all the  $p_i$  in terms of  $p_1$  and the value of this constant current, say  $C$ , and by using the periodic boundary condition  $p_{L+1} = p_1$ ,  $p_1$  can also be related to  $C$ . In this way we obtain

$$p_l = \frac{C}{w(B^s - B^{-s})} \sum_k B \sum_i a_{k,i} s_{i+i-1} \quad (5.5.4)$$

with the matrix  $a_{k,i}$  given by

$$a_{k,i} = \begin{cases} 1, & i > k \\ 0, & i = k \\ -1, & i < k \end{cases} \quad (5.5.5)$$

The value of  $C$  can be determined by normalizing the probabilities  $P(n, s)$  but we will choose

$$C = \frac{w}{L}(B^s - B^{-s}) \quad (5.5.6)$$

such that  $p_l = 1$  for zero field ( $B = 1$ ), and work with unnormalized probabilities  $P(n, s)$ .

We return to the calculation of the drift velocity (5.4.12) within a given channel. The averages  $\langle \theta(n_i) \rangle_n$ , in the expression for the current (5.4.8), can now be evaluated. The sum over the occupation numbers must be performed under the constraint (5.2.5) which we remove by introducing, under the sum, the kronecker delta  $\delta_{N-L, \sum_i n_i}$  in the integral representation

$$\delta_{N-L, \sum_i n_i} = \frac{1}{2\pi i} \oint \frac{dz}{z^{N-L+1}} z^{\sum_i n_i} \quad (5.5.7)$$

where the contour runs counter clockwise around  $z = 0$ . Using this representation the summations can be carried out and we find

$$\sum_n \theta(n_i) P(n, s) / \sum_n P(n, s) = p_i Q_{N-1, L}(s) / Q_{N, L}(s) \quad (5.5.8)$$

with  $Q_{N, L}(s)$  given by the constraint sum (see (5.2.5))

$$Q_{N, L}(s) = \sum_n P(n, s) = \sum_n \prod_i p_i^{n_i} \quad (5.5.9)$$

If we think about the  $p_i$  as Boltzmann factors and write them as

$$p_i = e^{-\beta E_i} \quad (5.5.10)$$

with  $E_i$  the "energy level" associated with cell  $i$ , we recognize  $Q_{N,L}$  as the canonical partition sum for an ideal Bose gas of  $N - L$  bosons:

$$Q_{N,L} = \sum_n \exp(-\beta \sum_i E_i n_i). \quad (5.5.11)$$

Another way to lift the restriction (5.2.5) on the possible  $n$  configurations is to use the grand canonical description. Then we obtain for the average

$$\langle \theta(n_i) \rangle_n = \frac{1}{\Xi} \sum_n \theta(n_i) \exp(-\beta \sum_i (E_i - \mu) n_i) = p_i e^{\beta \mu} \quad (5.5.12)$$

with  $\mu$  the chemical potential and  $\Xi$  the grand canonical partition sum, given by

$$\Xi = \sum_n \exp(-\beta \sum_i (E_i - \mu) n_i) = \prod_i \frac{1}{1 - \exp(-\beta(E_i - \mu))} \quad (5.5.13)$$

So we see that the ratio of the two  $Q$ 's in (5.5.8) is equal to the activity  $z(s) = \exp(\beta \mu)$  of the ideal Bose gas

$$z(s) = Q_{N-1,L}(s) / Q_{N,L}(s). \quad (5.5.14)$$

which is fixed by the average number of bosons (zeroes),

$$\langle N - L \rangle = \frac{\partial \ln \Xi}{\partial \beta \mu} = \sum_i \frac{p_i z(s)}{1 - p_i z(s)}, \quad (5.5.15)$$

in the grand canonical description.

The repton current (5.4.8) is the same as the single repton current (5.5.3) with  $p_i$  replaced by  $\langle \theta(n_i) \rangle_n$ . Therefore  $J_b(s)$  is the single repton current (5.5.6) times  $z(s)$ , the  $i$  independent proportionality constant between  $\langle \theta(n_i) \rangle_n$  and  $p_i$ . Using (5.4.12) and (5.4.4) we have for the drift velocity

$$v_b = \frac{a' w}{N} \langle z(s) \frac{S}{L} (B^S - B^{-S}) \rangle, \quad (5.5.16)$$

which is as far as we can get without specifying the amplitudes  $\psi(s)$ .

The natural choice for  $\psi(s)$  is to give equal a priori probabilities to all configurations  $y$ , which is the zero field solution for open chains. (For zero field  $W(y, y')$  is symmetric and the right eigenvector is equal to the left eigenvector which is  $(1, 1, \dots, 1)$ ).



see just below (5.3.7).) Thus  $\psi(s)$  is proportional to the number of  $y$  configurations that correspond to the channel  $s$ . For the boson case this yields

$$\psi_b(s) = \frac{1}{(2d+1)^N} \frac{N}{L} \binom{N-1}{L-1} = \frac{1}{(2d+1)^N} \binom{N}{L} \quad (5.5.17)$$

The factor  $N/L$  accounts for the difference in counting of the  $y$  and  $(n, s)$  configurations, which we mentioned at the end of section 5.2. It is multiplied by the number of ways to distribute  $N - L$  zeroes over  $L$  cells. The first factor normalizes the  $\psi(s)$  such that

$$\sum_L \sum_s \psi(s) = \frac{1}{(2d+1)^N} \sum_L (2d)^L \binom{N}{L} = 1. \quad (5.5.18)$$

In the first equation we used that  $\sum_i 1 = (2d)^L$ , that is, each  $s_i$  can take on the values  $\pm 1$   $d$  times on a  $d$ -dimensional lattice since in each cell one can choose between  $d$  downward and  $d$  upward neighbors. Thus we arrive at the final expression for the drift velocity,

$$v_b = \frac{a'w}{N} \frac{1}{(2d+1)^N} \sum_L \binom{N}{L} \frac{1}{L} \sum_s z(s) S(B^s - B^{-s}) \quad (5.5.19)$$

The average over  $s$  is still a formidable task as  $z(s)$  has an intricate dependence on  $s$ . For small electric fields (see (5.2.4)) we can perform a systematic expansion in powers of  $\epsilon$ . In the appendix 5A we show that to third order in  $\epsilon$ ,  $v_b$  is given by

$$v_b = \frac{a'w}{N} \frac{1}{(2d+1)^N} \sum_L \binom{N}{L} (2d)^L g(N, L, \epsilon) \quad (5.5.20)$$

with

$$g(N, L, \epsilon) = \frac{N-L}{N-1} \left( 1 - \frac{1}{12} \epsilon^2 N \left[ \left(1 - \frac{1}{L}\right) \left(1 - \frac{2}{L}\right) \left(1 - \frac{1}{N}\right) - \frac{1}{2N} \right] \right) \epsilon. \quad (5.5.21)$$

The remaining sum over  $L$  can only be evaluated in closed form for the linear order contribution,

$$v_b = \frac{a'w}{(2d+1)(N-1)} \left( 1 - \frac{1}{(2d+1)^{N-1}} \right) \epsilon + O(\epsilon^3). \quad (5.5.22)$$

However, for the leading term in (5.5.20) one may take only the maximum term  $L = 2dN/(2d+1)$  which yields

$$v_b = \frac{a'w}{(2d+1)N} \left( 1 - \frac{1}{12} \epsilon^2 N + \dots \right) \epsilon. \quad (5.5.23)$$

## 5.6 The diffusion constant

The diffusion constant  $D$  can be obtained from the drift velocity through the Einstein relation,

$$D = \frac{a'}{N} \left( \frac{dv}{d\epsilon} \right)_{\epsilon=0} \quad (5.6.1)$$

which is generally proven in [17]. Using (5.5.22) we find for the boson case that

$$D_b = \frac{(a')^2 w}{(2d+1)N(N-1)} \left( 1 - \frac{1}{(2d+1)^{N-1}} \right) \simeq \frac{w}{(2d+1)} \left( \frac{a'}{N} \right)^2. \quad (5.6.2)$$

For the fermion case the problem with just one movable repton is of course the same as (5.5.3) but the product property (5.5.1) does not apply to the many repton probability. Although an explicit expression for  $P(n, s)$  is lacking, we can still make an expansion for the drift velocity in powers of  $\epsilon$ , by taking moments of the master equation. To obtain  $v$  to linear order in the field, it is enough to take the first moment of the master equation, yielding the repton current (5.4.15). Expanding  $B = 1 + \epsilon/2$  in this expression gives

$$J_f(s) = w [ \langle n_i - n_{i+1} \rangle_n + s_i \langle n_i(1 - n_{i+1}) + n_{i+1}(1 - n_i) \rangle_n \frac{\epsilon}{2} ] \quad (5.6.3)$$

To linear order in the field, we need to calculate the second average only to zeroth order in the field. To this order each state is equally probable and we simply have to count states. For the RD(f)-model the total number of states for a given channel  $\{s_1, \dots, s_L\}$  is  $L!/((N-L)!(2L-N)!)$  which is the number of ways to pick  $N-L$  cells (the ones containing a zero) out of  $L$ . So  $\langle n_i(1 - n_{i+1}) \rangle_n$ , the number of states with one zero in cell  $i$  and none in cell  $i+1$ , divided by the total number of states, is

$$\langle n_i(1 - n_{i+1}) \rangle_n = \frac{\binom{L-2}{N-L-1}}{\binom{L}{N-L}} = \frac{(N-L)(2L-N)}{L(L-1)} \quad (5.6.4)$$

Summing (5.6.3) over  $i$ , the first term drops out and we find to lowest order in  $\epsilon$

$$J_f(s) = w \frac{(N-L)(2L-N)}{L^2(L-1)} S\epsilon \quad (5.6.5)$$

Inserting (5.6.5) into (5.4.12) and using equal a priori probabilities for all configurations  $y$ ,

$$\psi_f(s) \sim \frac{N}{L} \binom{L}{N-L} \quad (5.6.6)$$

in (5.4.4) we find that the diffusion constant (5.6.1) is given by

$$D_f = w \left( \frac{a'}{N} \right)^2 \left[ \frac{\sum_{L=[N/2]}^N \frac{N(N-L)(2L-N)}{L^3(L-1)} \binom{L}{N-L} \sum_{s_1, \dots, s_L} S^2}{\sum_{L=[N/2]}^N \frac{N}{L} \binom{L}{N-L} \sum_{s_1, \dots, s_L} 1} \right] \quad (5.6.7)$$

with

$$[N/2] = \begin{cases} N/2, & N \text{ is even} \\ (N+1)/2, & N \text{ is odd} \end{cases} \quad (5.6.8)$$

The sums over  $s$  are easy to compute

$$\sum_{s_1, \dots, s_L} = (2d)^L \quad \sum_{s_1, \dots, s_L} S^2 = L(2d)^L \quad (5.6.9)$$

and for large  $N$  we can use Stirling's approximation for the factorials and replace the summations over  $L$  by integrations over  $x = L/N$ . This yields

$$D_f \simeq w \left( \frac{a'}{N} \right)^2 \frac{\int_{1/2}^1 dx [(1-x)(2x-1)/x^3] \exp[Ng(x)]}{\int_{1/2}^1 dx x^{-1} \exp[Ng(x)]} \quad (5.6.10)$$

with

$$g(x) = x \ln(x) - (1-x) \ln(1-x) - (2x-1) \ln(2x-1) + x \ln(2d) \quad (5.6.11)$$

When  $N$  is large, the main contribution of the integral comes from a narrow region around  $x_0 = 1/2(1 + \sqrt{d/(d+2)})$  where  $g(x)$  is maximum, ( $g'(x_0) = 0$ ), and

$$D_f \simeq \frac{(1-x_0)(2x_0-1)}{x_0^3} w \left( \frac{a'}{N} \right)^2 = \quad (5.6.12)$$

$$d(2d+3) \left[ 1 + \frac{2}{d(2d+3)^2} \right]^{1/2} - 1 w \left( \frac{a'}{N} \right)^2 \simeq \frac{1}{(2d+3)} w \left( \frac{a'}{N} \right)^2$$

Note that  $D_f < D_b$  because of the restriction on the motion by the fermion exclusion principle. When  $d$  is large the difference between the two diffusion constants becomes small. This is because the configurational entropy of the long channels is larger than that of the short ones (since each cell has  $2d$  neighboring cells). Therefore, the behavior of the chains which are stretched over many cells will dominate and the low density of zeroes will make the difference between the two kinds of statistics unimportant. But the result may be very different when the entropy, due to the many ways that the  $n$  reptons within a cell can be positioned, is taken into account.

This moment method works also for the boson case, but it is essential that one can take moments at fixed channels  $s$ . In appendix 5B we apply the method to the master equation for open chains in the  $y$ -language, which does yield a number of interesting relations, but an explicit expression for the diffusion constant is not obtained. Applying the operation  $\sum_y y_j$  on the master equation gives the drift velocity  $v$  in terms of  $\langle y_1 \rangle_y$  and  $\langle y_1^2 \rangle_y$  (see (5B.9)). Performing the operation  $\sum_y y_j^2$  on the master equation yields an expression for the current of reptons  $J$  along the chain. The current is zero because after the full  $y$ -average as many reptons move to the right as to the left. In one form the relation  $J = 0$  is a relation between  $\langle y_1 \rangle_y$  and  $\langle y_1^2 \rangle_y$ . Thus we can eliminate  $\langle y_1^2 \rangle_y$  in favor of  $\langle y_1 \rangle_y$  and write the drift velocity  $v$  in terms of  $\langle y_1 \rangle_y$ , the orientation of the first link of the polymer chain (see (5B.18)). To obtain the diffusion constant one still needs to calculate the  $1/N$  correction of  $\langle y_1 \rangle_y$ .

## 5.7 The scaling function

In the remainder of this chapter we set  $d = 1$ . Widom et al. [15] have proposed a scaling form for the drift velocity in the limit  $\epsilon \rightarrow 0$ ,  $N \rightarrow \infty$  while keeping  $x = N\epsilon^2$  fixed :

$$v = \frac{aw\epsilon}{3N} f(x) \quad (5.7.1)$$

For the RD(b)-model with periodic boundary condition the expansion of the drift velocity to third order in  $\epsilon$  confirms the scaling hypothesis (see (5.5.23)). An approximate evaluation of the drift velocity for the whole scaling regime [16] also yields a scaling form (5.7.1) with the scaling function

$$f_{\text{approx}}(x) = \int_{-\infty}^{\infty} \frac{d\sigma}{\sqrt{2\pi}} \frac{\sigma \exp(-\sigma^2)(b^\sigma - b^{-\sigma})}{\int_{-\infty}^{\infty} d\mu \exp(-\mu^2/2)(b^\mu - b^{-\mu})} \quad (5.7.2)$$

and  $b = \exp(\sqrt{x/6})$ .

The true scaling function can easily be obtained numerically, starting from the expression for the drift velocity (5.5.19). One should take long polymers and small electric fields to obtain accurate results. To keep the computer time within reasonable limits, we have calculated the drift velocity for chains up to  $N = 30$ . Therefore finite-size effects have to be added to the above scaling form

$$\frac{3Nv_b}{aw\epsilon} = f(x) + g(x)\frac{1}{N} + h(x)\frac{1}{N^2} + \dots \quad (5.7.3)$$



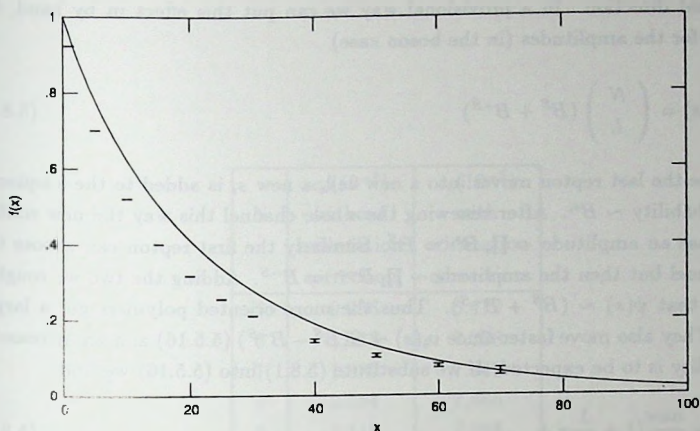


Fig. 5.3. The scaling function  $f(x)$  for the Rubinstein-Duke model with periodic boundary condition and equal probabilities for the channels. The points have been obtained by finite size scaling and the full curve is an approximation.

We computed  $v_b$  for  $N = 5, \dots, 30$  (and matching values for  $\epsilon$ , given  $x$ ). For each three consecutive values of  $N = i, i+1, i+2$  we calculated  $f_i(x), g_i(x)$  and  $h_i(x)$ . Of the thus obtained values  $f_i(x)$   $i = 5, \dots, 28$ ,  $f_{28}(x)$  is our best estimate for  $f(x)$ . The error is estimated from the way the series  $f_i(x)$  converges. In Fig. 5.3 we plot  $f_{\text{approx}}(x)$  given by (5.7.2) together with the numerical values  $f_{28}(x)$ . For the periodic chain with the amplitudes  $\psi_b(s)$  given by (5.5.17), the scaling function is monotonically decreasing, because, as the chain gets longer or the field is larger, the reptons get trapped in the peaks of the  $\Lambda$ -shaped parts of the channel (a long sequence of  $y_i = +1$  followed by a sequence of  $y_i = -1$ ). This probably is an artefact of the model because free sliding around gel fibers is excluded in this local-hopping model [18].

## 5.8 The RD-model with free endpoint motion

Does the imposed periodic boundary condition change the diffusion constant and the scaling function or are the results obtained also correct for the model with free endpoint motion, in the long chain limit? The free endpoint motion couples the different channels and because of the bias due to the field, the polymers are oriented

in the field direction. In a provisional way we can put this effect in by hand, by choosing for the amplitudes (in the boson case)

$$\psi_b(s) = \binom{N}{L} (B^S + B^{-S}) \quad (5.8.1)$$

Each time the last repton moves into a new cell, a new  $s_i$  is added to the  $s$ -sequence with probability  $\sim B^{s_i}$ . After renewing the whole channel this way the new configuration has an amplitude  $\sim \prod_i B^{s_i} = B^S$ . Similarly the first repton can choose the new channel but then the amplitude  $\sim \prod_i B^{-s_i} = B^{-S}$ . Adding the two we roughly estimate that  $\psi(s) \sim (B^S + B^{-S})$ . Thus the more oriented polymers get a larger weight. They also move faster since  $v_b(s) \sim S(B^S - B^{-S})$  (5.5.16) and an increase in the mobility is to be expected. If we substitute (5.8.1) into (5.5.16) we find

$$v_b = \frac{aw\epsilon}{3N} \left(1 + \frac{1}{12}x + \dots\right) \quad (5.8.2)$$

to third order in  $\epsilon$  which should be compared with (5.5.23). Thus for small values of  $x$  the increase in mobility due to the orientation of the polymers is more important than the slowing down due to the  $\Lambda$ -shaped configurations. If for large values of  $x$  the scaling function is dominated by the third order term, the drift velocity becomes independent of  $N$ , as is observed in experiments. The above shows that it might be possible to incorporate the main effects of the endpoint motion by a properly chosen channel statistics.

In Table 5.1 we show how the limiting values  $-1/12$  in (5.5.23) and  $+1/12$  in (5.8.2) for the coefficient  $c_1$  of the linear term in the expansion of the scaling function,  $f(x) = 1 + c_1x + \dots$ , are approached as the chains get longer. Note that in the first column the convergence to the asymptotic value is very slow. But when orientation effects are included in the amplitudes  $\psi_b(s)$  the value  $+1/12$  is reached already for quite small polymers.

The diffusion constant is not affected by the orientation because the field dependence of  $\psi_b(s)$  makes no contribution to the first order term of the drift velocity. But the periodic boundary condition can still affect the diffusion constant because it reduces the mobility of the end reptons. If the end reptons are not allowed to move at all, the drift velocity of the chain must be zero. Of course this is true for any repton in the chain. The drift velocity seems to be limited by the slowest repton and it is probable that for a chain with free endpoints, the mobility is limited by the motion of the internal reptons, because they are more restricted in their movements

N	$c_1(10^{-2})$ without orientation correction	$c_1(10^{-2})$ with orientation correction
5	-0.256	6.472
6	-1.113	7.238
7	-1.887	7.642
8	-2.554	7.865
9	-3.116	7.995
10	-3.590	8.077
20	-5.886	8.281
30	-6.689	8.311
40	-7.096	8.321
50	-7.341	8.326
60	-7.505	8.328
70	-7.623	8.329
80	-7.711	8.330
90	-7.780	8.331
100	-7.835	8.331
200	-8.084	8.333
300	-8.167	8.333
400	-8.208	8.333
500	-8.233	8.333

Table 5.1. The coefficient  $c_1$  as a function of  $N$  for the RD(b)-model with periodic boundary conditions, with and without orientation correction.

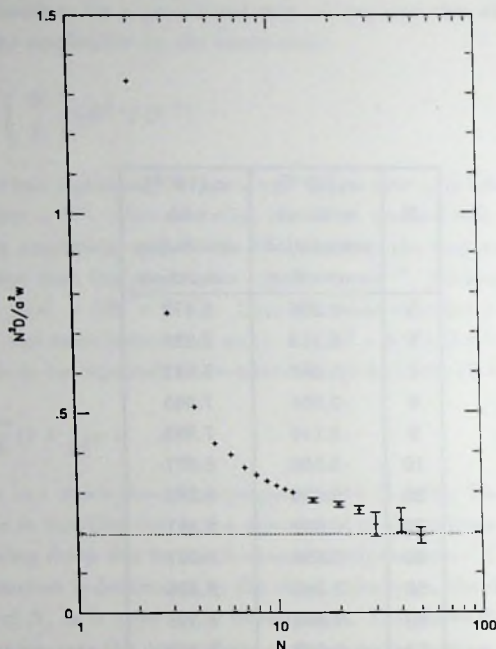


Fig. 5.4. The scaled diffusion coefficient versus the number of reptons for the fermion case with free endpoint motion. The values have been determined by a direct solution of the master equation for chains up to  $N = 12$  and by a Monte Carlo simulation for larger systems. The error bars give the standard deviations and the dotted line is the asymptotic value  $N^2 D / a^2 w = 3\sqrt{3} - 5$  for the periodic chain.

than the endpoints. If so, treating the end reptons as internal reptons, as the periodic boundary condition does, will not diminish the velocity of the polymer and the diffusion constant is the same as for the periodic chain.

To give a more satisfactory answer to the above questions we have computed numerically the drift velocity and diffusion constant for polymers with free endpoint motion. For the short chains ( $N \leq 12$ ) we have used the following iterative method.



number of internal coordinates	$c_1$			
	boson		fermion	
	periodic	open	periodic	open
3		-0.062		-0.021
6	-0.011	-0.060	-0.018	0.114
9	-0.031	0.115	-0.25	0.40

Table 5.2. The coefficient  $c_1$  for open chains as compared to periodic chains.

Because all eigenvalues of  $\Lambda_0$  are zero or negative

$$P_0(y) = \lim_{k \rightarrow \infty} [I + \frac{1}{|\lambda_{\min}|} \Lambda_0(y, y')]^k P_{\text{trial}}(y') \quad (5.8.3)$$

with  $I$  the unit matrix and  $\lambda_{\min}$ , the most negative eigenvalue of  $\Lambda_0$ . For  $P_{\text{trial}}(y)$  we take the zero field solution  $[P_0(y)]_{t=0} = (1, \dots, 1)/3^{N-1}$ . The value for  $\lambda_{\min}$  can easily be obtained by repeatedly applying the matrix  $\Lambda_0$  to  $P_{\text{trial}}(y)$ . Using (5.6.1) and (5.4.2) we have for the diffusion constant

$$D = \lim_{t \rightarrow 0} \frac{a^2 w}{N^2 \epsilon} \sum_{\langle y \rangle} v(y) P_0(y) \quad (5.8.4)$$

and the results for the fermion case are plotted in Fig. 5.4. The values for the longer chains have been obtained by Monte Carlo simulations. Whether  $D = D_{p.b.c.} = 3\sqrt{3} - 5$  for  $N \rightarrow \infty$  cannot really be decided because for  $N \geq 50$  the error bars become too large. The same is true in the boson case for which Widom et al. have carried out the Monte Carlo simulations [15]. But since in both cases the value  $D_{p.b.c.}$  is approached fairly well, it strongly suggests that indeed  $D = D_{p.b.c.}$  for  $N \rightarrow \infty$ . This would mean that the diffusion constant is unaffected by the process of tube renewal and is determined only by the transport of reptons along the chain (for  $N \gg 1$ ).

For small chains the iterative method is accurate enough to calculate the coefficient  $c_1$  of the linear term in the expansion of the scaling function  $f(x) = 1 + c_1 x + \dots$ . In Table 5.2 we give  $c_1$  for different values of  $N$ , in the boson- and fermion case, both with and without periodic boundary conditions. In both cases  $c_1$  is negative for periodic chains and becomes positive for free chains above a certain length. In the fermion case the enhancement of the drift velocity due to the orientation of the polymers seems to be more pronounced. For the free bose chain of length  $N = 10$ ,  $c_1 = 0.115$  which should be compared with  $c_1 = 0.07995$  (see Table 5.1) for the periodic bose chain of length  $N = 9$  with orientation correction included.

## 5.9 Summary

In its most basic results the RD-model is similar to the tube models of Lumpkin, Déjardin and Zimm, and Slater and Noolandi [5]. The form of the drift velocity  $v \sim a\omega\epsilon(1 + c_1\epsilon^2N)/N$  is the same for all three models since it is a consequence of restricting the motion to a tube. Assuming that the tube configuration is random-walk like, a  $1/N$  dependence in linear field order results. The  $N$  independent third order term is a consequence of the stretching (orientation) of the tube in the presence of an electric field, due to the biased way in which the endpoints renew the channel.

The motion of the polymers within the tube on the other hand is quite different in the three models. The RD-model is a strict implementation of the original reptation idea by de Gennes [3], describing the motion as driven diffusion of stored length along the chain. In the other two models, the polymer-as-a-whole slides through the tube (collective motion) under the influence of the total tangential force exerted by the electric field. This sliding motion excludes fluctuations in the tube length, important when the model is extended to the recently developed pulsed-fields techniques [7]. Also the delicate interplay between internal and endpoint motion, present in the RD-model, is not considered.

In the reptation model we distinguish two processes, (1) the transport of reptons from one end of the chain to the other and (2) the motion of the endpoints, acting as the source and sink of reptons, while at the same time renewing the tube. The two processes are strongly correlated because the transport of reptons depends on the shape of the tube, which is determined by the endpoint motion, while the movements of the endpoints depend on the rate at which the length defects diffuse away from the source or arrive at the sink. Yet, we have boldly decoupled this delicate interplay by imposing a periodic boundary condition. This way the transport of reptons in a tube can be studied, isolated from the endpoint motion. In each channel, which are now decoupled, there exists a constant current of reptons  $J$  and the drift velocity in the channel is simply  $a'(S/N)J$ , the effective distance in the field direction per repton times the current. The drift velocity to linear order in the field, averaged over all channels, is compared to that of the full problem, i.e. with endpoint motion. The open-chain value, which has been obtained numerically, comes very close to the periodic-chain value for long polymers. This suggests that it is the transport of reptons along the chain that determines the linear order term of the drift velocity (diffusion constant). For higher orders in the field one must take the endpoint motion into account. We can do that as follows. Because the periodic boundary condition

decouples the channels, one is free to choose the weight given to each channel contribution in the average over channels. Thus carefully choosing the channel statistics one may hope to incorporate the main effects of the endpoint motion. One of these effects is the orientation of the polymer, which contributes to the third order in the field. We have shown that a natural choice yields promising results. Presently we are studying the extent to which a properly chosen channel statistics can yield the correct scaling function.

Also the mutual exclusion of polymers can approximately be separated into two parts. First, the mutual exclusion of the tubes, which can also be incorporated in the channel statistics (see Lerman and Frisch [4]). It will modify the exponent in  $v \sim N^{-1}$ . Second, the excluded volume effect for the reptons moving within a tube. This has been considered in the RD(f)-model. It affects the proportionality constant but not the exponent of the  $N$  dependence in the diffusion constant. The diffusion constant calculated shows a reduction in the mobility, but not much. The boson and fermion case are the two extremes regarding to the amount of polymer that fits into a gel pore. It should give an indication as to how the drift velocity depends on the average pore size.

## Appendices

### 5A Expansion of the drift velocity in power of $\epsilon$

In this appendix we derive formula (5.5.20). For small electric fields ( $B \rightarrow 1$ ) we can perform a systematic expansion of the drift velocity (5.5.19) in powers of  $\epsilon$ . We start by expanding  $z(s)$ . For  $p_l$  we obtain from (5.5.4) and (5.5.6) the series

$$p_l = 1 + \frac{\epsilon}{2L} \sum_{i,k} a_{k,i} s_{i+l-1} + \frac{\epsilon^2}{8L} \sum_{i,j,k} a_{k,i} a_{k,j} s_{i+l-1} s_{j+l-1} + \dots \equiv 1 + \delta p_l \quad (5A.1)$$

and we may write (5.5.9) as

$$Q_{N,L} = \left( \frac{N-1}{L-1} \right) \left\langle \prod_l (1 + \delta p_l)^{n_l} \right\rangle_n, \quad (5A.2)$$

with  $\langle \rangle_n$  the average over all  $n$  satisfying (5.2.5). The product is expanded as

$$\begin{aligned} \prod_l (1 + \delta p_l)^{n_l} &= 1 + \sum_l n_l \delta p_l + \sum_{(l,m)} n_l n_m \delta p_l \delta p_m \\ &+ \frac{1}{2} \sum_l n_l (n_l - 1) \delta p_l^2 + \dots \end{aligned} \quad (5A.3)$$

where  $(l, m)$  stands for a pair  $l \neq m$ . The averages over the  $n_l$  are readily calculated,

$$\begin{aligned} \langle n_l \rangle' &= b_1 = (N - L)/L, \\ \langle n_l n_m \rangle' &= b_2 = (N - L)(N - L - 1)/[L(L + 1)], \quad l \neq m, \\ \langle n_l(n_l - 1) \rangle' &= 2b_2. \end{aligned} \quad (5A.4)$$

Consequently we obtain for  $Q_{N,L}$ ,

$$Q_{N,L} = \binom{N-1}{L-1} \left\{ 1 + b_1 \sum_l \delta p_l + \frac{1}{2} b_2 \left[ \left( \sum_l \delta p_l \right)^2 + \sum_l \delta p_l^2 \right] + \dots \right\}. \quad (5A.5)$$

From (5A.1) and the matrix  $a_{k,i}$  given by (5.5.5) one sees that  $\sum_l \delta p_l$  has no linear term in  $\epsilon$ ,

$$\sum_l \delta p_l = \frac{\epsilon^2}{8L} \sum_{i,j,k,l} a_{k,i} a_{k,j} s_{i+l-1} s_{j+l-1} + \dots \quad (5A.6)$$

So we may ignore its square in (5A.5) to order  $\epsilon^2$ . The other terms yields

$$\sum_l \delta p_l^2 = \frac{\epsilon^2}{4L^2} \sum_{i,j,k,l,m} a_{k,i} a_{m,j} s_{i+l-1} s_{j+l-1} + \dots \quad (5A.7)$$

For the ratio  $z(s)$  we obtain from (5A.5) and (5A.4)

$$z(s) = \binom{N-L}{N-1} \left( 1 - \frac{1}{L} \sum_l \delta p_l - \frac{N-L-1}{L(L+1)} \sum_l \delta p_l^2 + \dots \right), \quad (5A.8)$$

which, with (5A.6) and (5A.7), is accurate to order  $\epsilon^2$ . This must be multiplied by the expansion

$$S(B^S - B^{-S}) = S^2 \epsilon + \frac{1}{24} S^4 \epsilon^3 + \dots, \quad (5A.9)$$

and the sum over  $s$  has to be carried out. Typically we have the sums

$$\sum_s S^4 = L(3L - 2)(2d)^L, \quad (5A.10)$$

$$\sum_s S^2 \left( \sum_{i,j} b_{ij} s_{i+l-1} s_{j+l-1} \right) = \left( (L-2) \sum_i b_{ii} + 2 \sum_{i,j} b_{ij} \right) (2d)^L, \quad (5A.11)$$

where  $b_{ij}$  stands for the terms of either (5A.6) or (5A.7). The diagonal terms  $b_{ii}$  of (5A.6) and (5A.7) yield

$$\frac{1}{L} \sum_{i,k,l} a_{k,i}^2 = L(L-1), \quad (5A.12)$$

$$\frac{1}{L^2} \sum_{i,k,l,m} a_{k,i} a_{m,i} = \frac{1}{3} (L^2 - 1). \quad (5A.13)$$



while the total sum of  $b_{ij}$  over  $i$  and  $j$  gives only a contribution for (5A.6),

$$\frac{1}{L} \sum_{i,j,k,l} a_{k,i} a_{k,j} = \frac{1}{3} L(L^2 - 1). \quad (5A.14)$$

Now all the ingredients for the evaluation of the sum over  $s$  in (5.5.19) are present and we find

$$\begin{aligned} \frac{1}{L} \sum_s z(s) S(B^s - B^{-s}) &= \\ &= (2d)^L \frac{N-L}{N-1} \left( 1 - \frac{1}{12} \epsilon^2 N \left[ \left(1 - \frac{1}{L}\right) \left(1 - \frac{2}{L}\right) \left(1 - \frac{1}{N}\right) - \frac{1}{2N} \right] \right) \epsilon \end{aligned} \quad (5A.15)$$

## 5B Open chains

For an open chain the channel is not an invariant of motion. Therefore we work in the  $y$  representation. The master equation for a chain of  $N$  reptons is given by

$$\begin{aligned} &\left\{ \sum_{i=2}^{N-1} [(1 - y_{i-1}^2) y_i^2 B^{y_i} + y_{i-1}^2 (1 - y_i^2) B^{-y_{i-1}}] + \right. \\ &\quad \left. [(1 - y_1^2) + (1 - y_{N-1}^2)] d(B + B^{-1}) + y_1^2 B^{y_1} + y_{N-1}^2 B^{-y_{N-1}} \right\} P(y) = \\ &\sum_{i=2}^{N-1} [(1 - y_{i-1}^2) y_i^2 B^{-y_i} + y_{i-1}^2 (1 - y_i^2) B^{y_{i-1}}] P(y_{i-1} \leftrightarrow y_i) + \\ &\quad (1 - y_1^2) [BP(y_1 = 1) + B^{-1}P(y_1 = -1)] + \\ &\quad (1 - y_{N-1}^2) [B^{-1}P(y_{N-1} = 1) + BP(y_{N-1} = -1)] + \\ &\quad dy_1^2 B^{-y_1} P(y_1 = 0) + dy_{N-1}^2 B^{y_{N-1}} P(y_{N-1} = 0) \end{aligned} \quad (5B.1)$$

Summing the master equation over  $y$  yield the same expression on both sides of the equality sign, which is a consequence of the conservation of probability. The first moment of the master equation, obtained by applying the operation  $\sum_y y_j$  on (5B.1), gives the the constant velocity of the reptons in the direction of the field

$$v_{j-1} = v_j \quad i = 2, \dots, N-1 \quad (5B.2)$$

with

$$v_1 = \langle y_1 B^{y_1} + d(1 - y_1^2)(B - B^{-1}) \rangle_v \quad (5B.3)$$

$$v_j = \langle (1 - y_{j-1}^2) y_j B^{y_j} - (1 - y_j^2) y_{j-1} B^{-y_{j-1}} \rangle_v \quad (5B.4)$$

for  $j = 2, \dots, N-1$  and

$$v_N = \langle -y_{N-1} B^{-y_{N-1}} + d(1 - y_{N-1}^2)(B - B^{-1}) \rangle_v \quad (5B.5)$$

The total drift velocity (5.4.2) is simply

$$v = \langle v(y) \rangle_v = \frac{a'w}{N} \sum_{j=1}^N v_j = a'wv_1 \quad (5B.6)$$

Since  $y = 0, \pm 1$  we can write

$$yB^y = \frac{1}{2}(B + B^{-1})y[1 + y\delta] \quad (5B.7)$$

with

$$\delta = \frac{B - B^{-1}}{B + B^{-1}} \quad (5B.8)$$

which makes

$$v/a'w = v_1 = \frac{1}{2}(B + B^{-1})[\langle y_1 \rangle_v + \delta\{2d - (2d - 1) \langle y_1^2 \rangle_v\}] \quad (5B.9)$$

We can find another relation between  $\langle y_1 \rangle_v$  and  $\langle y_1^2 \rangle_v$  by performing the operation  $\sum_j y_j^2$  on (5B.1). It yields the constant current of reptons  $J$

$$J_{j-1} = J_j \quad j = 2, \dots, N-1 \quad (5B.10)$$

with

$$J_1 = \langle y_1^2 B^{y_1} - d(1 - y_1^2)(B + B^{-1}) \rangle_v \quad (5B.11)$$

$$J_j = \langle (1 - y_{j-1}^2)y_j^2 B^{y_j} - (1 - y_j^2)y_{j-1}^2 B^{-y_{j-1}} \rangle_v \quad (5B.12)$$

for  $j = 2, \dots, N-1$  and

$$J_N = \langle -y_{N-1}^2 B^{-y_{N-1}} + d(1 - y_{N-1}^2)(B + B^{-1}) \rangle_v \quad (5B.13)$$

The value of this current is zero, because after averaging over all  $y$  as many reptons move to the right as to the left. This can be seen by using the left-right symmetry, that is, draw a vertical line through the middle of Fig. 5.2 and mirror the chain in this line. This symmetry implies that the probability distribution obeys

$$P(y_1, y_2, \dots, y_{N-1}) = P(-y_{N-1}, -y_{N-2}, \dots, -y_1) \quad (5B.14)$$

and thus

$$\langle F(y_i) \rangle_v = \langle F(-y_{N-i}) \rangle_v \quad (5B.15)$$

for any function  $F(y)$ . Applying (5B.15) to  $J_i$  we see that  $J_i = -J_{N-i}$  and therefore

$$J_i = 0 \quad j = 1, \dots, N \quad (5B.16)$$

With the help of (5B.7) we see that

$$J_1 = \frac{1}{2}(B + B^{-1})[\{(2d + 1) \langle y_1^2 \rangle_v - 2d\} + \delta \langle y_1 \rangle_v] = 0 \quad (5B.17)$$

and thus

$$v/a'w = \frac{1}{2}(B + B^{-1})\left[\frac{4d}{2d + 1}\delta + \left(1 + \frac{2d - 1}{2d + 1}\delta^2\right) \langle y_1 \rangle_v\right] \quad (5B.18)$$

The additional relation (5B.17) is not enough to find  $\langle y_1 \rangle_v$ . Yet it is clear from (5B.18) that in order to get the  $1/N$  dependence for the drift velocity, we must have

$$\langle y_1 \rangle_v = \left(-\frac{2d}{2d + 1} + O\left(\frac{1}{N}\right)\right) \epsilon \quad (5B.19)$$

Therefore to obtain the diffusion constant one has to know the  $O(1/N)$  correction of  $\langle y_1 \rangle_v$ .

## References

- [1] H. Hervet and C. P. Bean, *Biopolymers* **26**, 727 (1987) and ref. therein.
- [2] M. Doi and S. F. Edwards, *Theory of polymer dynamics*, (Oxford University, Oxford, 1986)
- [3] P. G. de Gennes, *Scaling Concepts in Polymer Physics*, (Cornell Univ. Press, Ithaca, 1979); *J. Chem. Phys.* **55**, 572 (1971).
- [4] L. S. Lerman and H. L. Frisch, *Biopolymers*, **21**, 995 (1982)
- [5] O. J. Lumpkin, P. Déjardin and B. H. Zimm, *Biopolymers* **24**, 1573 (1985); G. W. Slater and J. Noolandi, *Biopolymers* **25**, 431 (1986);
- [6] M. Jonsson, B. Åkerman, B. Nordén, *Biopolymers* **27**, 381 (1988).
- [7] D. C. Schwartz and C. R. Cantor, *Cell* **37**, 67 (1984); G. F. Carle, M. Frank and M. V. Olson *Science* **232**, 65 (1986).
- [8] J. M. Deutsch, *Phys. Rev. Lett.* **59**, 1255 (1987); *J. Chem. Phys.* **90**, 7436 (1989); T. L. Madden and J. M. Deutsch, *J. Chem. Phys.* **94**, 1584 (1991).
- [9] J. Noolandi, G. W. Slater, H. A. Lim and J. L. Viovy, *Science* **243**, 1456 (1989); H. A. Lim, G. W. Slater and J. Noolandi, *J. Chem. Phys.* **92**, 702 (1990).

- [10] T. A. J. Duke, *Phys. Rev. Lett.* **62**, 2877 (1989); *J. Chem. Phys.* **93**, 9049 (1990); *J. Chem. Phys.* **93**, 9055 (1990).
- [11] B. H. Zimm, *J. Chem. Phys.* **94**, 2187 (1991);
- [12] D. C. Schwartz and M. Koval, *Nature* **338**, 520 (1989); S. B. Smith, P. K. Aldridge and J. B. Callis, *Science* **243**, 203 (1989); J. M. Deutsch and T. L. Madden, *J. Chem. Phys.* **90**, 2476 (1989);
- [14] M. Rubinstein, *Phys. Rev. Lett.* **59**, 1946 (1987); *Proceedings of the International Symposium on New Trends in Physics and Physical Chemistry of Polymers honoring Prof. P. G. de Gennes*, (Plenum Press, New York, 1989).
- [15] B. Widom, J. L. Viovy and A. D. Defontaine, *J. Phys. (Paris) I* **1**, 1759 (1991).
- [16] J. M. J. van Leeuwen and A. Kooiman, *Physica A* **184**, 79 (1992).
- [17] J. M. J. van Leeuwen, *J. Phys. (Paris) I* **1**, 1675 (1991).
- [18] J. M. Deutsch and J. D. Reger, *J. Chem. Phys.* **95**, 2065 (1991).



## Samenvatting

In de statistische mechanica tracht men het macroscopisch (grootschalig) gedrag van een fysiek systeem te verklaren vanuit de microscopische situatie, die wordt gegeven door de bouwstenen (atomen, moleculen, etc.) en hun onderlinge wisselwerking. Het woord "mechanica" verwijst naar de bewegingswetten die de tijdsevolutie van het systeem op microscopisch niveau bepalen. Gelukkig is het volgen van de continue veranderingen op microscopisch niveau niet nodig voor een adequate beschrijving van de macroscopische eigenschappen. In plaats daarvan start men met de basis aanname, dat de waarde van een macroscopische grootheid gelijk is aan zijn gemiddelde waarde, waarbij de middeling zich uitstrekt over alle (voor het systeem toegankelijke) microscopische toestanden. Met "statistisch" wordt dan ook niets anders bedoeld dan de eenvoudigste van alle gebruikte statistische bewerkingen: de middeling. Maar zelfs als het probleem is teruggebracht tot het nemen van gemiddelden, blijft het moeilijk omdat het aantal termen in de middeling zo astronomisch groot is. Alleen als de termen betrekkelijk eenvoudige reeksen vormen is de berekening uiteindelijk uitvoerbaar. Exacte oplossingen beperken zich derhalve tot eenvoudige model systemen, die hooguit recht doen aan de meest essentiële kenmerken van het oorspronkelijke probleem.

In dit proefschrift worden twee onderwerpen bestudeerd aan de hand van dergelijke model systemen. Het eerste onderwerp betreft de grenslaag tussen twee coëxisterende fasen. Een klassiek voorbeeld hiervan is de grenslaag in een vloeistof-damp systeem. In de grenslaag varieert de dichtheid continu van de vloeistof- naar de damp waarde omdat een abrupte overgang in de dichtheid wordt vervaagd door thermische fluctuaties in de dichtheid, soortgelijk aan die welke zich voordoen in de bulkfasen. Op deze wijze ontstaat een intrinsiek dichtheidsprofiel met een eindige breedte. Een verdere uitsmering van dit profiel over een veel bredere laag is het resultaat van de golvende bewegingen van het intrinsieke profiel (de capillaire golven). Het zijn de eindigheid van het grensoppervlak en de onderdrukking van de capillaire golven door de zwaartekracht, die voorkomen dat de golven met lange golflengten leiden tot een divergentie in de dikte van de grenslaag.

Een eenvoudig model voor het vloeistof-damp systeem is het Ising model. Dit is een roostermodel met op iedere rooster punt een spin die slechts twee standen kan aannemen, op of neer. De spins wisselwerken alleen met hun naaste burens. Voor temperaturen beneden de kritieke temperatuur gaan de spins bij voorkeur parallel staan (spontane magnetisatie). De twee coëxisterende fasen zijn derhalve, een fase waarin de spins gemiddeld omhoog wijzen (positieve magnetisatie) en een fase waarin de spins gemiddeld omlaag wijzen (negatieve magnetisatie). In hoofdstuk 2 wordt het model opgelost voor een 1-dimensionale keten van spins in de aanwezigheid van een lineair variërend magnetisch veld. Dit veld is analoog aan het zwaartekrachtsveld in het vloeistof-damp systeem. In een 1-dimensionale keten vindt geen spontane fase scheiding plaats, maar wordt deze geïnduceerd door het lineair variërend veld. Voor hoge temperaturen en kleine gradienten in het magnetisch veld, volgt de lokale magnetisatie nauwkeurig de variatie in de sterkte van het veld (locaal veld gedrag). Naarmate de temperatuur daalt en/of de veld gradient toeneemt, wordt het gedrag steeds minder lokaal t.g.v. de capillaire golven, die hier slechts de verschuivingen zijn van het grenspunt tussen de twee fasen. De resultaten worden vergeleken met de theorie van Fisk en Widom die een goede benadering blijkt te geven, behalve daar waar de oplossing gedomineerd wordt door de capillaire golven.

In hogere dimensies is het Ising model, in aanwezigheid van een lineair variërend magnetisch veld, niet oplosbaar en een verdere vereenvoudiging is noodzakelijk. Deze vereenvoudiging wordt gezocht in een beschrijving van de grenslaag, los van de twee bulkfasen. In principe is dit mogelijk door de microscopische details uit te integreren tot op een lengte schaal, groter dan de gemiddelde omvang van de bulk fluctuaties. Dit leidt tot een capillaire-golf theorie waarin alleen de golfbewegingen van de grenslaag reesteren. De microscopische details van het probleem komen nu nog slechts tot uiting via twee parameters in de capillaire-golf hamiltoniaan. Dat zijn de stijfheid (die voor een isotroop systeem gelijk is aan de oppervlakte spanning) en de minimaal toegestane golflengte, die van de orde van de bulk correlatie lengte is. Het afleiden van een uitdrukking van deze twee parameters uit de microscopische interacties, staat gelijk aan het oplossen van het volledige probleem en is dus al even moeilijk.

Een spin model op een rooster waarin alleen de capillaire-golf fluctuaties in rekening worden gebracht, maar dan op iedere lengte schaal, dus ook op microscopisch niveau, is het SOS model. Voor dit model kan de connectie tussen de macroscopische eigenschappen en de microscopische detail volledig worden uitgewerkt. In hoofdstuk 3 wordt een algemeen SOS model bestudeerd. Het blijkt dat op macroscopisch niveau de microscopische details alleen tot uitdrukking komen in de stijfheid.

Het 2D-Ising model zonder magnetisch veld is wel oplosbaar. De oplossing methode van Vdovichenko leidt zelfs tot een ontkoppeling van de bulk- en grenslaag bijdragen aan de vrije energie. Dit maakt het mogelijk de oppervlakte spanning van de grenslaag op eenvoudige wijze te berekenen. In hoofdstuk 4 gebruiken we deze methode om de vrije energie en de oppervlakte spanning uit te rekenen voor een Ising model met naaste- en volgende-buur interacties. De oplossing is exact onder gegeven restricties (de vrije fermionen oplossing) en is een redelijke benadering voor een veel groter bereik van de koppelingsconstanten.

In het laatste hoofdstuk wordt een geheel ander onderwerp bestudeerd, namelijk, reptatie modellen voor electrophorese. Electrophorese is een veel gebruikte techniek in de biologie voor het scheiden van uniform geladen polymeren (zoals DNA moleculen) naar lengte. De DNA moleculen worden door een electrisch veld door een gel (een netwerk van neutrale polymeren) heen getrokken. Voor zwakke velden en niet al te lange polymeren is de mobiliteit omgekeerd evenredig met de lengte van de polymeren. Voor langere polymeren en/of een sterker electrisch veld wordt de mobiliteit onafhankelijk van de lengte en gaat de resolutie verloren.

Dit zeer complexe systeem wordt tot een betrekkelijk eenvoudig model gereduceerd op grond van de volgende overwegingen. De kluwe van polymeren die de gel vormt zit vol met kleine poriën. Een DNA molecuul in de gel strekt zich uit over een aantal van deze poriën die tesamen een kanaal vormen. De bewegingsvrijheid van het lange molecuul is in hoge mate beperkt tot bewegingen in de lengte richting van het kanaal. Het molecuul kan zich gedeeltelijk ophopen in één of meer van de poriën. Deze stukjes opgeslagen lengte (lussen in het DNA molecuul) kunnen door thermische beweging door het kanaal diffunderen, bij voorkeur in de richting van het veld. Deze vorm van voortbewegen wordt reptatie genoemd vanwege de gelijkenis met de verplaatsingswijze van sommige soorten reptielen zoals slangen.

In het model wordt de ruimte opgedeeld in een regelmatig rooster van cellen die de poriën representeren. Het DNA molecuul wordt voorgesteld als een streng van geladen reptonen. Reptonen zijn stukjes van het DNA molecuul van een zodanige lengte dat het molecuul op deze schaal volledig flexibel is. De reptonen die één DNA molecuul vormen, liggen in een serie aaneengesloten cellen (het kanaal). Twee opeenvolgende reptonen bevinden zich in dezelfde cel of in twee aangrenzende cellen, hetgeen de connectiviteit van het polymeer tot uitdrukking brengt. Meerdere reptonen in een cel betekent dat het polymeer lengte heeft opgeslagen in de cel in de vorm van lussen. Deze extra reptonen kunnen van cel naar cel springen, met overgangswaarschijnlijkheden waarin de voorkeursrichting t.g.v. het veld tot uitdrukking

komt. Verder zijn er de volgende twee restricties op de beweging van het molecuul. De connectiviteit moet behouden blijven en voor de interne reptonen (alle behalve de twee eind reptonen) is de bewegingsvrijheid beperkt tot het kanaal. Alleen via de beweging van de eind reptonen kan het kanaal langzaam worden vernieuwd, doordat nieuwe cellen worden bezet en oude cellen worden verlaten.

Dit leidt tot de bovengenoemde lengte afhankelijkheid van de mobiliteit. Het verlies aan resolutie voor langere polymeren en/of een sterker elektrisch veld is het gevolg van de orientatie van de moleculen in het veld. In het laatste hoofdstuk wordt aangetoond dat de mobiliteit van de polymeren tot op eerste orde in het veld, onafhankelijk is van de processen die het kanaal vernieuwen. Dit maakt een exacte berekening van de mobiliteit tot op laagste orde in het veld mogelijk.



## Curriculum vitae

Alle betrouwbare bronnen vermelden dat ik op 16 april 1963 te Barendrecht werd geboren. Na een gestaagde opmars via MAVO, HAVO en Atheneum kon ik in 1982 beginnen met de Natuurkunde studie aan de Rijksuniversiteit te Leiden (R.U.L.). De studie werd in 1986 afgesloten met een experimentele stage in de werkgroep "Moleculen in Aangeslagen Toestand". In deze groep heb ik deelgenomen aan een lopend onderzoek aan de triplet toestand van pyridine d.m.v. electro spin echo experimenten o.l.v. dr. E. J. J. Groenen. Afgestudeerd ben ik op een vergelijkend onderzoek naar de gevoeligheid en tijdsresolutie van twee typen trilholten: een Loop-Gap-Resonator en een Reënant Cavity. Daarop volgend heb ik ruim anderhalf jaar gewerkt als Assistent In Opleiding in dienst van de R.U.L. in de vakgroep "Gecondenseerde Materie" met dr. R. C. Thiel als mijn directe begeleider. Door middel van Mössbauer spectroscopie heb ik daar onderzoek gedaan naar de vibratie spectra van ruthenium clusters. Per 1 januari 1989 trad ik in dienst van de stichting Fundamenteel Onderzoek Materie, om bij prof.dr. J.M.J. van Leeuwen aan het Instituut-Lorentz van de R.U.L. te beginnen aan een promotie onderzoek die geleid heeft tot dit proefschrift.

## List of publications

- One-dimensional interfaces, G. L. M. Dassen, A. Kooiman and J. M. J. van Leeuwen, *Physica A* **159**, 91 (1989).
- Interfacial profiles in the rough phase, G. L. M. Dassen, A. Kooiman, N. Jan and J. M. J. van Leeuwen, *Phys. Rev. B* **41**, 4593 (1990).
- Finite-size effects and capillary waves in solid-on-solid models, A. Kooiman, J. M. J. van Leeuwen and R. K. P. Zia, *Physica A* **170** 124 (1990).
- Free fermion approximation for the Ising model with further-neighbor interactions on a triangular lattice, A. Kooiman and J. M. J. van Leeuwen, *J. Stat. Phys.* **69**, 247 (1992).
- The drift velocity in the Rubinstein-Duke model for electrophoresis, J. M. J. van Leeuwen and A. Kooiman, *Physica A* **184**, 79 (1992).
- Reptation models for electrophoresis, A. Kooiman and J. M. J. van Leeuwen, to appear in *J. Chem. Phys.*



# Stellingen

1. De verklaring die Noolandi et al. geven voor het geobserveerde minimum in de mobiliteit als functie van de polymeerlengte (in constant-veld electrophorese experimenten) berust op de beperktheid van hun model, waarin alleen de collectieve beweging van het polymeer in beschouwing wordt genomen.

*J. Noolandi et al., Phys. Rev. Lett. 58 (1987) 2428*

2. Als men de effecten van de vrije eindpuntbeweging van de polymeren in het Rubinstein-Duke model in rekening wil brengen d.m.v. een goed gekozen waarschijnlijkheidsverdeling over de kanalen (in een berekening met periodieke randvoorwaarden) is een orientatiecorrectie alleen onvoldoende.

*Hoofdstuk 5 van dit proefschrift*

3. Reptatie modellen voor electrophorese waarin de reptonen met elkaar verbonden zijn d.m.v. veren met een entropische oorsprong, zijn niet in overeenstemming met de experimentele situatie, waarin de gemiddelde porie grootte in de gel van de orde van de persistentielengte is.

*H. Lim et al., J. Chem. Phys. 92 (1990) 709*

*B. H. Zimm, J. Chem. Phys. 94 (1991) 2187*

4. De universele verklaring van de rechten van de mens zou men beter kunnen herformuleren als een universele verklaring van de plichten van de mens.
5. Speculatieve psychologische theorieën horen niet thuis in het onderwijspakket van een beroepsopleiding.
6. De marge tussen nog te goed zijn om in aanmerking te komen voor plaatsing in een bejaardentehuis of te slecht, is wel erg klein.



7. De voortvarendheid waarmee videocamera bezittend Nederland de kinderjaren van haar kroost vastlegt, belooft een gouden toekomst voor psychologisch onderzoek.
8. De verbijsterende ontdekking van vele kinderen dat Sinterklaas eigenlijk de buurman is, speelt mogelijk een grote rol bij de ontkerkelijking in Nederland.
9. Het komt de leesbaarheid van de nederlandse wet ten goede als de typografische weergave daarvan een afspiegeling vormt van de structuur van de wet.
10. Een holistische wereld zal nooit worden begrepen.
11. De diffusie constante die in hoofdstuk 5 van dit proefschrift wordt afgeleid voor het Rubinstein-Duke model is onafhankelijk van de richting van het elektrisch veld t.o.v. de roosterassen.
12. Het real-space renormalisatieschema van Migdal voor het Ising model, waarin koppelingen worden verschoven, kan men interpreteren als bestaande uit een gedeeltelijke ontkoppeling van de spins gecombineerd met een beperking op de toegelaten configuraties. De toestandsom wordt zodoende benaderd door het maken van twee elkaar grotendeels compenserende fouten.

*T. W. Burkhardt, in Real-Space Renormalization, Vol. 30, uit Topics in Current Physics, T. W. Burkhardt en J. M. J. van Leeuwen, eds. (Springer-Verlag, Berlin, 1982).*

André Kooiman, maart 1993.

RIJKSUNIVERSITEIT TE LEIDEN  
BIBLIOTHEEK INSTITUUT-LORENTZ

Postbus 9506 - 2300 RA Leiden  
Nederland